THE ELASTIC AND PLASTIC BEHAVIOUR OF CELLULAR MATERIALS

by

Lorna Jane Gibson

A dissertation submitted to the
University of Cambridge for the
Degree of Doctor of Philosophy

Churchill College

August 1981

ACKNOWLEDGEMENTS

I am most deeply grateful to Professor M.F. Ashby for his
guidance, encouragement and good humour throughout the course of
my stay in Cambridge. Professor K.E. Easterling of the University
of Luleå in Sweden worked with Professor Ashby and myself studying
the mechanics of cork: his enthusiasm and assistance are sincerely
appreciated. I am also grateful to Dr. P. Echlin for enlightening
discussions on cork and to Dr. W.C. Nixon for providing the deforma-
tion stage and for help with scanning electron microscopy during
the cork project. The case study on the selection of materials for
packaging applications developed from a Part II project done in this
Department by Mr. W. Nixon. I am grateful to him for his comments
and interest. I would like to thank Dr. C.R. Calladine for his help
in analyzing elastic buckling problems. I was also able to discuss
many of my ideas with other research students in the Engineering Depart-
ment: I am indebted to them for their comments and suggestions.

The technicians of the Engineering Department provided invaluable
technical assistance. I would especially like to thank Mr. J. Godlonton,
Mr. B. Butler, Mr. R. Denston and Mr. R. Brand for their sound advice
and assistance, which were always available. Sheila Owen in the Drawing
Office prepared the drawings for reports and publications throughout my
stay, for which I am grateful.

Several companies generously supplied me with specimens. Foam
samples came from: Bulstrode Plastics and Chemical Co. Ltd.; Messrs. Coolag
Ltd.; Dunlopillo Division of Dunlop Ltd.; Frelen Ltd.; Harrison and Jones
(Flexible Foam) Ltd.; and Kay Metzeler Ltd. Mr. George Woodley of Ciba
Geigy gave me samples of Aeroweb. I am grateful to all of these suppliers.

The thesis was typed by Trish Shepherd. I greatly appreciate the speed and skill with which she did this.

PREFACE

The work described in this dissertation was carried out in the Engineering Department of the University of Cambridge, during the period October, 1978 to August, 1981. Except for commonly understood and accepted ideas or where specific reference is made to the work of others, the contents of this dissertation are my original work and do not include the outcome of work done in collaboration. No part of this dissertation has been submitted, in part or in whole, for any degree or other qualification at any other university.

ABSTRACT

Cellular materials are widespread. Some, like wood and bone, occur in nature, while others, like polymeric foams, are manmade. Because of their cellular structure, they have unusual mechanical properties: they can be stiff, yet light, and they are capable of absorbing large deflections and thus large amounts of energy. Yet their mechanical behaviour has hardly been studied: no comprehensive attempt to relate mechanical properties to structure exists. In this thesis, we have attempted to do this.

We first model a cellular material as a simple, two-dimensional array of hexagonal cells and identify and analyze the mechanisms by which it deforms. From this we calculate the elastic moduli and the elastic and plastic collapse stresses for ideal two-dimensional cellular materials. The results (which we have experimentally verified) show that each of these properties depends on three parameters: a solid cell wall material property, a geometric constant, and the relative density of the cellular material raised to the power two or three.

We then examine three-dimensional cellular materials. Because their geometry is irregular and very complicated, no exact analysis of their behaviour is possible. But, with our understanding of two-dimensional cellular materials and how they deform, we can use dimensional arguments to analyze three-dimensional cellular materials. The results of this analysis agree well with experimental data.

Finally, we have applied our understanding of cellular materials to two case studies. In the first, we have examined the structure of cork, a quasi-two-dimensional cellular material, and explained some of its mechanical properties. The second case study analyzes the problem of material selection in packaging.

TABLE OF CONTENTS Page

TABLE OF CONTENTS (cont.)   Page

NOTATION

Symbols which have more than one meaning are listed along with the chapter for which each definition holds. Within a particular chapter, each symbol has only one meaning.

a = one half the crack length (mm) (Ch. 5)

a = amplitude of a corrugation in a cork cell (mm) (Ch. 7)

A = shape anisotropy of a cellular material (-) (Ch. 5)

A = cross-sectional area of a packaged object (mm^2) (Ch. 8)

b = width of a member in a cellular material (mm)

C = force (N) (Ch. 3)

C = constant (-) (Ch. 2, 5, 6)

C = damping coefficient of a packaging material (kg sec^{-1}) (Ch. 8)

D = specific damping energy (J m^{-3})

E = Young's modulus of a cellular material (MN m^{-2})

E_s = Young's modulus of cell wall material (MN m^{-2})

E_1 = Young's modulus in the X_1 direction for a cellular material (MN m^{-2})

E_2 = Young's modulus in the X_2 direction for a cellular material (MN m^{-2})

$f(y)$ = restoring spring force for model of a packaging material (N)

F = force (N)

g = acceleration due to gravity (9.8 m sec^{-2})

G = shear modulus of a cellular material (MN m^{-2})

G_s = shear modulus of cell wall material (MN m^{-2})

G_{cs} = toughness of cell wall material (kJ m^{-2})

h = length of vertical member in a cellular material (mm) (Ch. 3, 4, 5)

h = height from which packaged object falls (m) (Ch. 8)

h_o = midspan deflection of buckled column (mm)

I = second moment of area (mm^4)

K = rotational spring stiffness (Nm radian^{-1}) (Ch. 3)

K = constant (-) (Ch. 5)

K = spring constant for model of a packaging material (Nm^{-1}) (Ch. 8)

K_o = constant stress response constant for model of a packaging material (N)

ℓ = length of an inclined member of the two-dimensional model of a cellular material (mm) Ch. 3)

ℓ = length of a member in a three-dimensional cellular material (mm) (Ch. 5)

ℓ = length of a member of a cork cell (μm) (Ch. 7)

M = moment (Nm) (Ch. 3, 5)

M = mass of a packaged object (kg) (Ch. 8)

M_p = fully plastic moment (Nm)

n = Euler buckling load end constraint factor (-) (Ch. 3, 5, 6)

n = creep constant (-) (Appendix 5B)

n = power (-) (Ch. 5, 6)

N = number of cells per unit volume (mm^{-3})

P = force (N)

P_{cr} = Euler buckling load for a column (N)

Q = foam property

Q_S = cell wall property

S = thickness of packaging material (mm)

$S_{ijk\ell}$ = $ijk\ell$ element of compliance tensor (m^2 N^{-1})

t = cell wall thickness (mm) (Ch. 3, 4, 5, 6, 7)

t = time (sec.) (Ch. 8)

t_e = thickness of cell edge (mm)

t_f = thickness of cell face (mm)

U = strain energy per unit volume (J/m^3)

U_M = strain energy of bending (J)

U_{MAX} = maximum strain energy per unit volume in a cycle of load $(J\ m^{-3})$

U_S = shear deflection (mm)

V = volume of a cell (mm^3)

V_c = volume of a unit cell (mm^3)

V_s = volume of solid per unit cell (mm^3)

V_o = velocity of packaged object on impact $(m\ sec^{-1})$

w = force/length $(N\ m^{-1})$

W = force (N)

W_E = elastic strain energy (J)

W_V = viscous strain energy (J)

X_i = coordinate axes (m)

y = coordinate of deflection normal to beam (m) (Ch. 3)

y = position coordinate (m) (Ch. 8)

z = depth of a cork cell (μm)

α^2 = factor relating (edge length)^2 to area of pentagonal dodecahedron (-)

β = factor relating length of a column with rotational springs at its ends to length of a pinned column (-) (Ch. 3)

β = constant used in calculating volume of a pentagonal do-decahedron (-) (Ch. 5)

β^* = value of β that satisfies equation 3.10 (-) (Ch. 3)

γ = shear strain (-)

δ = deflection (mm)

δ_a = axial deformation (mm)

δ_s = shear deflection (mm)

Δ = log decrement of peak amplitude (-)

$\dot{\varepsilon}$ = strain rate (sec^{-1})

$\dot{\varepsilon}_o$ = strain rate creep parameter (sec^{-1})

ε_{ij} = ij element of strain tensor (−)

ε_2^* = value of ε_2 when buckling begins (−)

η = loss coefficient (−)

θ = angle between the inclined member and the horizontal in two-dimensional model of cellular material (degrees)

θ^* = value of θ when buckling begins (degrees)

λ = length of pinned column for elastic line buckling analysis (mm) (Ch. 3)

λ = corrugation wavelength in cork cells (μm) (Ch. 7)

ν = Poisson's ratio of cellular material (−)

ν_s = Poisson's ratio of cell wall material (−)

ν_1 = Poisson's ratio for loading in the X_1 direction for a cellular material (−)

ν_2 = Poisson's ratio for loading in the X_2 direction for a cellular material (−)

ρ = density of cellular material (kg/m^3)

ρ_s = density of cell wall material (kg/m^3)

σ_f = tensile failure stress of cork (MN/m^2)

σ_{fs} = fracture stress of the cell wall material (MN m^{-2})

$\sigma_{k\ell}$ = kℓ element of the stress tensor (MN m^{-2})

σ_{max} = maximum stress exerted by packaging on packaged object (MN m^{-2})

σ_o = creep parameter (MN m^{-2})

σ_y = yield stress of cell wall material (MN m^{-2})

σ_{bf}^* = stress in cellular material at which brittle fracture occurs (MN m^{-2})

$\sigma_{e\ell}^*$ = elastic buckling stress of a cellular material (MN m^{-2})

σ_{pl}^* = plastic collapse stress for a cellular material (MN m^{-2})

$(\sigma_1^*)_{pl}$ = plastic collapse stress for a cellular material loaded in the X_1 direction (MN m^{-2})

$(\sigma_2^*)_{pl}$ = plastic collapse stress for a cellular material loaded in the X_2 direction (MN m^{-2})

τ = shear stress ($MN\ m^{-2}$) (Ch. 3)

τ = period of oscillation of packaged object (sec.) (Ch. 8)

ϕ = angle of rotation (degrees) (Ch. 3)

ϕ = volume of polymer in the cell face: volume of polymer in cell edges (-) (Ch. 5)

ϕ = cushion factor (-) (Ch. 8)

ω = frequency of vibration of packaged object (sec^{-1})

CHAPTER 1

INTRODUCTION

Cellular materials, consisting either of hollow parallel cells in a two-dimensional array or of an interconnected three-dimensional network, are widespread. They occur in nature as, among other things, wood and cork. Man has made use of the exceptional properties of these cellular materials for centuries: wood is the world's oldest structural material and is still the most widely used; and cork was used by the Romans much as we still use it today: for sealing wine bottles, for the soles of shoes and for floats. In the last fifty years, man has produced his own cellular materials: first with polymeric foams and more recently with foamed metals, ceramics and glasses.

These materials have been used and developed because of their remarkable properties. They can be stiff yet light: wood is weight for weight as stiff as mild steel. Some have exceptional energy absorbing characteristics: polymeric foams are used for packaging and metal foams may be incorporated into car bumpers for this reason. They are capable of accommodating large elastic deformations: elastomeric polymeric foams can be compressed comfortably in cushions. They act as good insulators of heat, sound and vibration: cork is an excellent insulator of all three.

In several of these applications, the mechanical properties of the cellular material are of central importance. Yet the basic processes which determine these properties have hardly been studied. Some progress has been made in identifying mechanisms of deformation and failure in cellular structures, but no comprehensive attempt to relate mechanical properties to structure exists. It is the aim of this study to do this and explain why cellular materials behave mechanically as they do.

1.1 Analysis of the Mechanics of Cellular Materials

Cellular materials commonly assume one of two basic geometries. They can be a simple two-dimensional array of parallel hollow cells (e.g. wood) or a connected network of struts or plates in three dimensions (e.g. open and closed cell polymeric foams). These three-dimensional structures are complicated; too much so to analyse exactly the forces acting on each member and the resulting deformations. But the two-dimensional cellular materials are simpler and they can be modelled as an array of honeycomb-like hexagonal cells. The mechanical behaviour of this model can be determined exactly using the techniques of structural analysis: this analysis works very well for idealized two-dimensional cellular materials; we find that it also gives a good description of the mechanical properties of quasi two-dimensional cellular materials, such as cork.

Both two- and three-dimensional cellular materials respond to load by the same mechanisms. Both deform in a linear elastic way by bending of the cell members and collapse either by elastic buckling or the formation of plastic hinges in the members. Because of this, we can extend our understanding of two-dimensional cellular materials to the more complex three-dimensional ones by using dimensional arguments. The experimental evidence of ourselves and of other workers shows this type of analysis to be adequate.

1.2 Outline of this Study

The mechanisms of deformation in cellular materials and the current analyses of these mechanisms available in the literature are discussed in Chapter 2. Chapters 3 and 4 deal with two-dimensional cellular materials: the theory for their behaviour is developed in Chapter 3

and the experimental work and discussion are contained in Chapter 4.
Similarly, Chapters 5 and 6 discuss the theoretical and experimental
work on three-dimensional cellular materials. Two case studies, apply-
ing the theory that has been developed are presented in Chapters 7 and 8:
one is on the mechanics of cork while the other discusses the use of foams
in packaging. Finally, the conclusions of the study are stated in Chapter 9.

CHAPTER 2

MECHANISMS OF DEFORMATION IN CELLULAR MATERIALS: PREVIOUS WORK

To analyse the mechanical behaviour of cellular materials properly, we must first understand the mechanisms by which they deform. In the study reported in this thesis, these mechanisms have been identified both by making model two-dimensional foams and examining the way in which they deform and by the microscopic study of real three-dimensional foams. As a result, we can now state that the mechanism of *linear-elastic* deformation is predominantly that of bending of the cell walls and edges, with small contributions from shear and axial deformation; that the mechanism of *collapse of flexible foams* is that of a co-operative elastic buckling of the cell wall; and that the mechanism of *collapse of rigid foams* is that of the plastic bending of the cell walls.

The difficulty in reviewing previous work in this field is that many workers, not examining their foams microscopically, have failed to identify the correct mechanism of deformation and have (correctly) analysed one which is inappropriate or wrong. Thus several papers calculate linear elastic behaviour from axial extension of the cell walls, although this contribution to deformation is, in reality, a minor one. Others analyse the collapse of rigid foams by an elastic buckling calculation, whereas rigid foams actually collapse plastically.

In this review, papers relating to the three modes of deformation already mentioned (linear elastic behaviour, elastic collapse and plastic collapse) will be discussed first for two- and then for three-dimensional cellular materials.

2.1 Two-Dimensional Cellular Materials

There is very little previous work on the mechanics of two-dimensional cellular materials. The work that has been done has concentrated on the across-plane shear behaviour of aluminium honeycomb sheet which is used as the core of sandwich panels in aircraft. (For example, see Kelsey et al., 1958). It appears that the only work to date on the in-plane mechanics of two-dimensional cellular solids is that of Abd El-Sayed et al. (1979). They calculated the in-plane Young's moduli and Poisson's ratios for honeycomb sheet by estimating the bending and axial displacements of a cell when subjected to forces in two orthogonal directions. Although the method is correct, there are slight errors in their results. They analysed the elasto-plastic behaviour using a standard equation relating displacement to the applied load, the extent of plasticity at a section, the ratio of maximum applied bending moment to the fully plastic bending moment and the geometrical and material properties of the beam. Once plastic hinges form, the overall behaviour is plastic; Abd El-Sayed et al. have also analysed this. Their experimental findings are in good agreement with the theory they developed.

2.2 Three-Dimensional Cellular Materials

Linear elastic behaviour

The linear elastic moduli of cellular materials reflect principally the bending of the cell members. Several attempts have been made to deduce the moduli from this bending.

Ko (1965) has calculated the bending, shearing and axial deformations of rhombic and trapezo-rhombic dodecahedra and arrived at expressions

for the relative Young's modulus, E/E_s, and Poisson's ratio, ν, as a function of relative density, ρ/ρ_s, for both polyhedra. But to explain his experiments, he had to suppose that real foams are a mixture of 67 % trapezo-rhombic dodecahedra and 33 % rhombic dodeca-hedra. Although the analysis of the bending of the polyhedra members is sound, it seems unrealistic to model the structure as a combination of two different polyhedra.

Chan and Nakamura (1969) derived expressions for E/E_s and ν for open and closed cell foams based on the bending deflection of an initially bent column or plate loaded axially. This method breaks down if the columns or plates are initially straight: then they are loaded axially and no bending occurs. This method ignores the standard beam bending of members loaded perpendicular to their length. This derivation does not, then, analyse the actual mechanism of deformation for the linear elastic behaviour of foams.

Menges and Knipschild (1975) noticed from microscopic examination that the faces of closed cell foams have very little stiffness and strength and concluded that the faces do not contribute significantly to the stiffness or strength of the foam. They then treated open and closed cell foams identically. Their analysis of the bending and axial deformation of the cell edges gave:

$$E/E_s = \frac{C_1 \, (\rho/\rho_s)^2}{\rho/\rho_s + C_2}$$

where C_1 and C_2 are constants, to be determined by experiment. Their experimental results for rigid, closed cell polyurethane are in good agreement with this expression.

Barma et al. (1978) have derived an expression for the Young's modulus of rigid polyurethane foams by modelling these foams as pentagonal dodecahedra with open faces and with some initial curvature in the cell edges. Like Chan and Nakamura (1969) they calculated the bending deflection of the initially curved cell edges under an axial load and then related this to the axial displacement. They also neglected the bending of members loaded perpendicularly to their length. Again, this derivation does not analyse the actual mechanism of deformation for the linear elastic behaviour of cellular materials.

In addition to the bending of the cell members during linear elastic behaviour, there are also contributions to deformation from axial extension or compression and shear. Gent and Thomas (1959, 1963) and Lederman (1971) have derived expressions for E/E_s and ν based on the axial deformation of the cell members. But axial deformation only becomes important at high relative densities: at low relative densities it is negligible compared to the bending deformations. These two models, then, are not applicable to low density foams.

Non-linear elastic behaviour

Non-linear elastic behaviour in cellular solids is the result of some members buckling elastically. Realising this, Gent and Thomas (1959) found an expression for the post-buckling stress-strain behaviour of open celled foams based on the product of the Euler buckling load of a column and an empirically determined function of the strain in the member. They did not derive a specific expression relating the elastic collapse stress to relative density.

Several investigators studying the collapse of *rigid* foams have sought to explain and model their observations by an elastic collapse calculation. (Matonis, 1964; Chan and Nakamura, 1969; Patel and Finnie, 1970; Menges and Knipschild, 1975 and Barma et al., 1978)*. We think this is wrong: the base polymers of rigid foams have well defined plastic yield points and these foams behave plastically during collapse. But the idea behind their calculations has relevance for *elastomeric* foams. It is developed further in Chapters 3 and 5.

Plastic Collapse Behaviour

Cellular materials made from solids with a plastic yield point, such as rigid polymeric foams and metallic foams, may collapse either elastically or plastically, depending on which mode occurs at a lower stress. When plastic collapse occurs, it is by the formation of plastic hinges at the section of maximum bending moment in the member. There appears to have been little work done on analysing this mode of collapse for three-dimensional foams: the only papers available on the plastic behaviour of foams are those of Shaw and Sata (1966) and Wilsea et al. (1975).

Shaw and Sata (1966) have compared the plastic behaviour of polystyrene to that of fully dense solids. One of their observations was that the Meyer hardness of a foam is about equal to its yield stress, while in solids the hardness is about three times the yield stress. Wilsea et al. (1975) investigated this further by analysing the stress acting beneath the indenter. Neither of these papers suggests any way of relating the density of a foam to its yield stress.

---

*These authors have all calculated a collapse stress based on some form of elastic buckling: Matonis (1964) used the critical load of an axially loaded plate; Chan and Nakamura (1969) analysed the buckling of initially bent plates and columns; Patel and Finnie (1970) estimated the collapse stress from the buckling of a bar supported along its length by an elastic foundation; Menges and Knipschild (1975) calculated the buckling load of a restrained column; and Barma et al. (1978) based their calculation on the buckling of an initially bent column.

2.3 Conclusions

No comprehensive treatment of the elastic and plastic behaviour of cellular materials exists. Most of the work done to date has centred on calculating linear-elastic moduli and elastic collapse stresses. But often these analyses have been based on an incorrect mechanism of deformation. To understand the mechanical behaviour of cellular materials properly, the correct mechanism of deformation must be identified and analysed, relating it to the cell wall properties and the cell geometry. In this study we have first examined simple, two-dimensional cellular materials to gain an understanding of the mechanisms of deformation. We then apply this understanding to the more complex three-dimensional cellular materials. Finally, we present two case studies in which the theory developed for two- and three-dimensional cellular solids is applied.

CHAPTER 2: REFERENCES

Abd El-Sayed, F.K., Jones, R. and Burgess, I.W. (1979) Composites, 10, 209.

Barma, P., Rhodes, M.B. and Salovey, R. (1978) J. of Applied Physics, 49, 4985.

Chan, R. and Nakamura, M. (1969) J. of Cellular Plastics, 5, 112.

Gent, A.N. and Thomas, A.G. (1959) J. of Applied Polymer Science, 1, 107.

Gent, A.N. and Thomas, A.G. (1963) Rubber Chemistry and Technology, 36, 597.

Kelsey, S., Gellatly, R.A. and Clark, B.W. (1958) Aircraft Engineering, 30, 294.

Ko, W.L. (1965) J. of Cellular Plastics, 1, 45.

Lederman, J.M. (1971) J. of Applied Polymer Science 15, 693.

Matonis, V.A. (1964) SPE Journal Sept., 1024.

Menges, G. and Knipschild, F. (1975) Polymer Engineering Science, 15, 623.

Patel, M.R. and Finnie, I. (1970) J. of Materials, 5, 909.

Shaw, M.C. and Sata, T. (1966) Int. J. Mech. Sci., 8, 469.

Wilsea, M., Johnson, K.L. and Ashby, M.F. (1975) Int. J. Mech. Sci., 17, 457.

CHAPTER 3

TWO-DIMENSIONAL CELLULAR MATERIALS: THEORETICAL ANALYSIS

We model two-dimensional cellular materials as a honeycomb-like array of hexagons as shown in Fig. 3.1. We have studied the mechanisms of deformation of silicon rubber and aluminium models with a range of such geometries: we find that beam bending is the primary mechanism of deformation in linear-elastic regime; that elastic buckling governs the non-linear elastic behaviour; and that the formation of plastic hinges causes plastic collapse. The model structure can be analysed using these mechanisms of deformation to give the linear-elastic moduli and the elastic and plastic collapse stresses, and the way in which they depend on cell shape and density. In this chapter we have done this, making the assumption that the strains are small, and neglecting shear and axial deformation of the members. The appendices at the end of the chapter give more detailed analyses in which large strains and shear and axial deformation are included. We have also assumed a constant strain rate.

3.1 Linear Elastic Behaviour

The number of independent moduli

The linear-elastic behaviour of a solid is completely described by a set of n elastic constants. The number n depends on the dimensionality and symmetry of the structure.

In a general deformation of a linear elastic material, the strains are related to the stresses by:

$$\varepsilon_{ij} = S_{ijk\ell} \, \sigma_{k\ell}$$
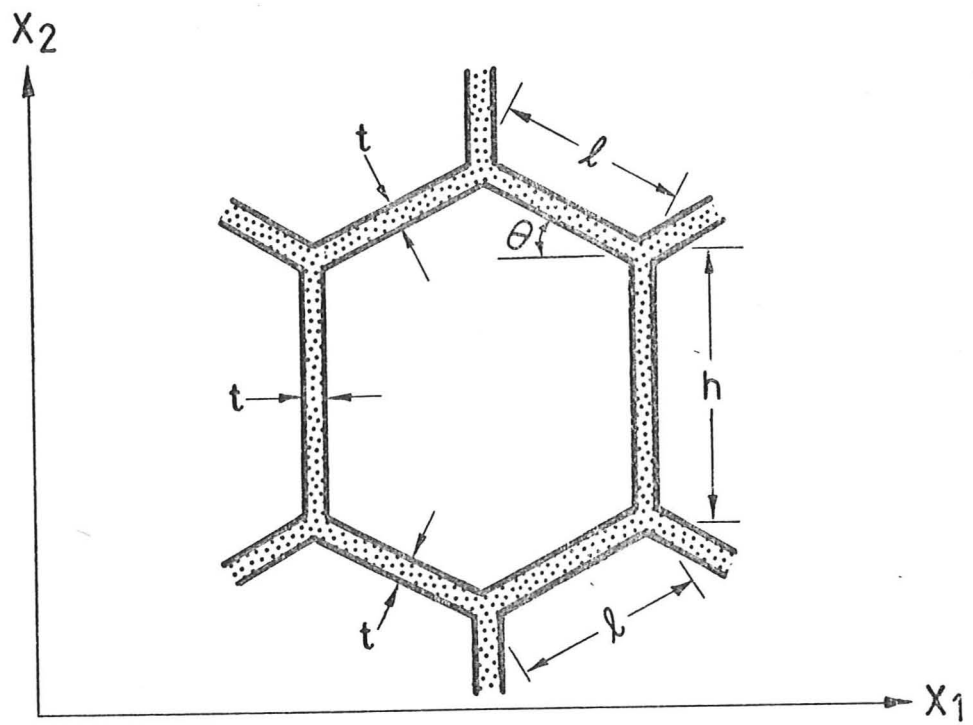
Fig. 3.1   Unit cell of two-dimensional model of a cellular
material.

where $S_{ijk\ell}$, ε_{ij} and $\sigma_{k\ell}$ are the compliance, the strain and
the stress tensors respectively. Symmetry and energy considera-
tions reduce the 81 components of the compliance tensor to 21.
The cellular model of Fig. 3.1 is orthotropic; it has three orth-
ogonal axes of symmetry such that a rotation of 180° about any
one of these axes leaves the structure unchanged. Such materials
have only nine independent elastic constants, listed below. A com-
plete description of a general (anisotropic) three-dimensional foam
or cellular structure requires these nine constants.

$$
\begin{matrix}
S_{1111} & S_{1122} & S_{1133} & - & - & - \\
S_{1122} & S_{2222} & S_{2233} & - & - & - \\
S_{1133} & S_{2233} & S_{3333} & - & - & - \\
- & - & - & S_{2323} & - & - \\
- & - & - & - & S_{1313} & - \\
- & - & - & - & - & S_{1212}
\end{matrix}
$$

In the case of the two-dimensional model of cellular materials,
the stiffness along the X_3 direction is very great,   as is the

resistance to the shears ε_{32} and ε_{31} so that:

$$S_{3333} = S_{2323} = S_{1313} = 0$$

Further, the contraction in the X_3 direction when a stress σ_1 or σ_2 is applied is negligible, so that:

$$S_{3311} = S_{3322} = 0$$

There remain four independent elastic constants. The compliance matrix now becomes:

$$
\begin{array}{|cccccc|}
\hline
S_{1111} & S_{1122} & - & - & - & - \\
S_{1122} & S_{2222} & - & - & - & - \\
- & - & - & - & - & - \\
- & - & - & - & - & - \\
- & - & - & - & - & - \\
- & - & - & - & - & S_{1212} \\
\hline
\end{array}
$$

These four constants can be written in terms of two Young's moduli, one Poisson's ratio and one shear modulus, which completely describe a two-dimensional cellular structure. Axial loading under a stress σ_{11} results in the strain:

$$\varepsilon_{11} = S_{1111} \, \sigma_{11}$$

from which

$$E_1 = \frac{1}{S_{1111}} \qquad (3.1)$$

For loading in the X_2 direction:

$$E_2 = \frac{1}{S_{2222}} \qquad (3.2)$$

Poisson's ratio for loading in the X_1 direction is:

$$\nu_1 = -\frac{\varepsilon_{22}}{\varepsilon_{11}} = \frac{S_{1122}}{S_{1111}} \qquad (3.3)$$

That for loading in the X_2 direction is:

$$\nu_2 = -\frac{\varepsilon_{11}}{\varepsilon_{22}} = \frac{S_{1122}}{S_{2222}} \qquad (3.4)$$

These four moduli are obviously related by the expression:

$$E_1 \, \nu_2 = E_2 \, \nu_1 \qquad (3.5)$$

The final independent constant is the shear modulus G:

$$G = \frac{1}{S_{1212}} \qquad (3.6)$$

We now calculate all four indepentent moduli.

Formulae used in calculating elastic properties

For the unit cell shown in Fig. 3.1, the volume of solid per cell is:

$$V_s = (2\ell + h) \, bt$$

The volume of a cell is:

$$V_c = 2\ell \cos\theta \, (h + \ell \sin\theta) \, b$$

The relative density, ρ/ρ_s, is therefore:

$$\frac{\rho}{\rho_s} = \frac{(2 + h/\ell) \, t/\ell}{2 \cos\theta \, (h/\ell + \sin\theta)} \tag{3.7}$$

which, for regular hexagons, becomes:

$$\frac{\rho}{\rho_s} = \frac{2}{\sqrt{3}} \frac{t}{\ell} \tag{3.8}$$

The following standard beam formulae, neglecting shear deformations, have been used in the derivations of the elastic constants. E_s is the Young's modulus of the material of which the beam is made and I is the second moment of area of the beam. For a beam of rectangular cross-section bt,

$$I = bt^3/12 \tag{3.9}$$

The end deflection of a cantilever beam of length ℓ loaded at the end by a force F (Fig. 3.2a) is:
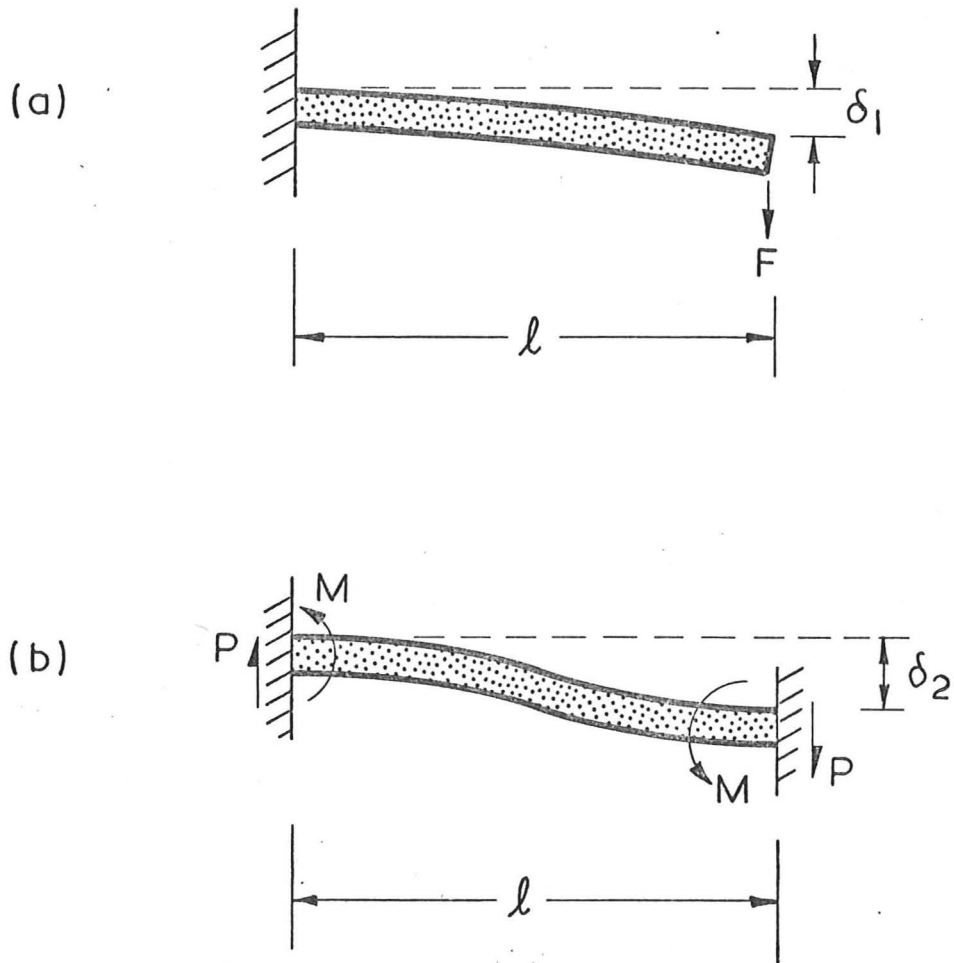
$$\delta_1 = F\ell^3/3E_s I \tag{3.10}$$

Fig. 3.2   Beam formula.

The end deflection of a beam of length ℓ fixed at both ends to which equal but opposite loads P are applied each end (Fig. 3.2b) is:

$$\delta_2 = P\ell^3/12E_SI = M\ell^2/6E_SI \qquad (3.11)$$

In deriving the linear-elastic moduli we have neglected shear and axial deformations of the cell members and have assumed that the strains are small. In Appendix 3A we derive the moduli including the contribution of shear and axial deformations; Appendix 3B gives the equations for stress-strain behaviour at large strains.

The calculation of Young's Moduli and Poisson's Ratios

(a) Loading in the X_1 direction

Consider the linear-elastic response of the structure shown in Fig. 3.3a when subjected to a stress σ_{11}. The forces acting on the cell walls of length ℓ and depth b are shown in Fig. 3.3c. By symmetry, the force C acting on the walls of length h lie in the plane of the wall; and there is no rotation of the joints. Since (for reasons of equilibrium) no net force acts across any plane through the structure which lies normal to the X_2 axis, we have:

$$C = 0$$

$$M = \frac{P\ell \sin\theta}{2} \qquad (3.12)$$

where $\qquad P = \sigma_{11} (h + \ell \sin\theta) b$

The wall deflects by:

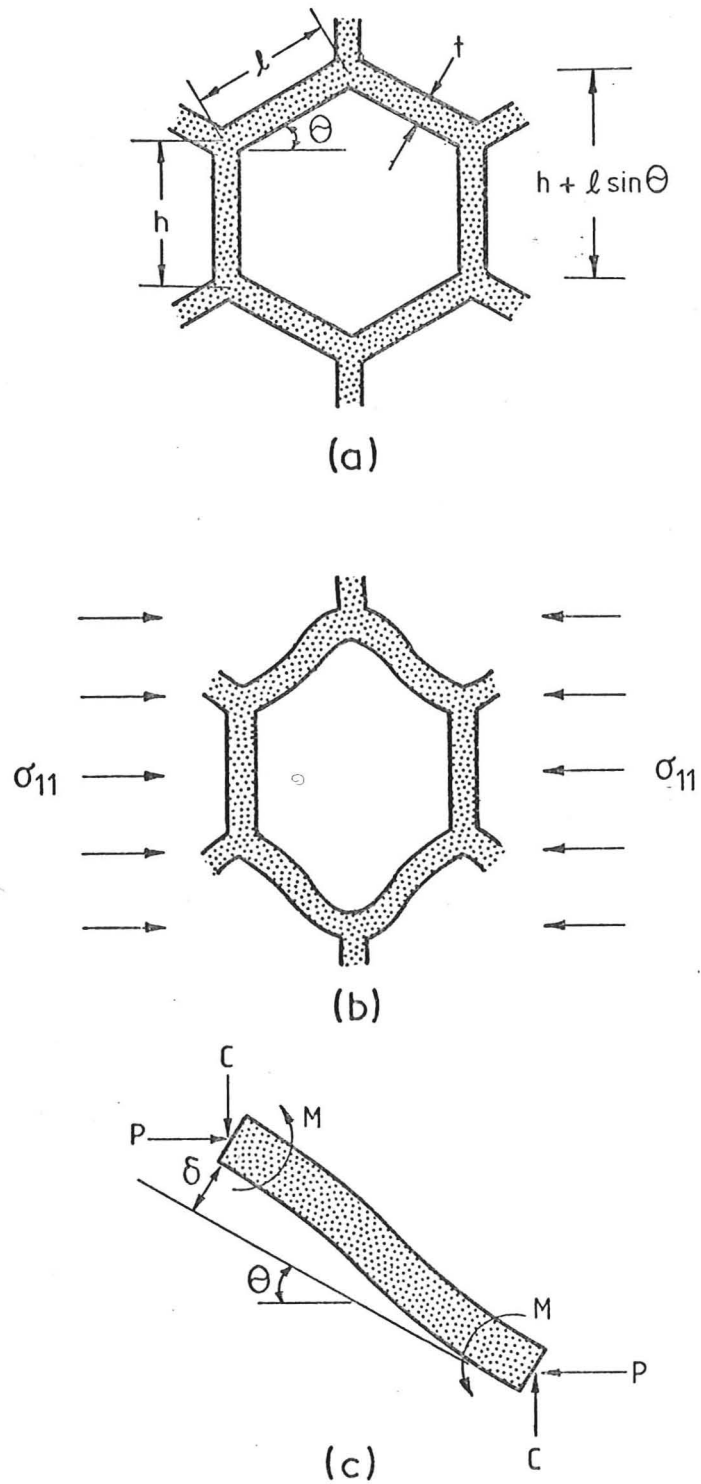$$\delta = \frac{P\ell^3 \sin\theta}{12E_SI} \qquad (3.13)$$

(a)

(b)

(c)

Fig. 3.3   Cell deformation under σ_{11}.

Of this, a component $\delta \sin\theta$ is parallel to the X_1 axis, giving a strain:

$$\varepsilon_{11} = \frac{\delta \sin\theta}{\ell \cos\theta}$$

$$= \frac{\sigma_{11}(h + \ell \sin\theta) \, b\ell^2 \sin^2\theta}{12 E_s I \cos\theta}$$

for which Young's modulus parallel to X_1 is:

$$\boxed{E_1 = \frac{12 E_s I \cos\theta}{(h + \ell \sin\theta) \, b \, \ell^2 \sin^2\theta}} \qquad (3.14)$$

For regular hexagonal cells this becomes:

$$E_1 = \frac{4}{\sqrt{3}} \frac{t^3}{\ell^3} E_s \qquad (3.15)$$

The strain parallel to the X_2 axis is:

$$\varepsilon_{22} = - \frac{\delta \cos\theta}{(h + \ell \sin\theta)}$$

from which Poisson's ratio for loading in the X_1 direction is:

$$\boxed{\nu_1 = - \frac{\varepsilon_{22}}{\varepsilon_{11}} = \frac{\ell \cos^2\theta}{(h + \ell \sin\theta) \sin\theta}} \qquad (3.16)$$

For regular hexagonal cells this reduces to $\nu_1 = 1$.

(b) Loading in the X_2 direction

The forces acting on the cell wall of length ℓ and depth b are shown in Fig. 3.4. As before, symmetry requires that the forces in the walls of length h lie in the plane of the walls; and there is no rotation of the joints. By equilibrium:
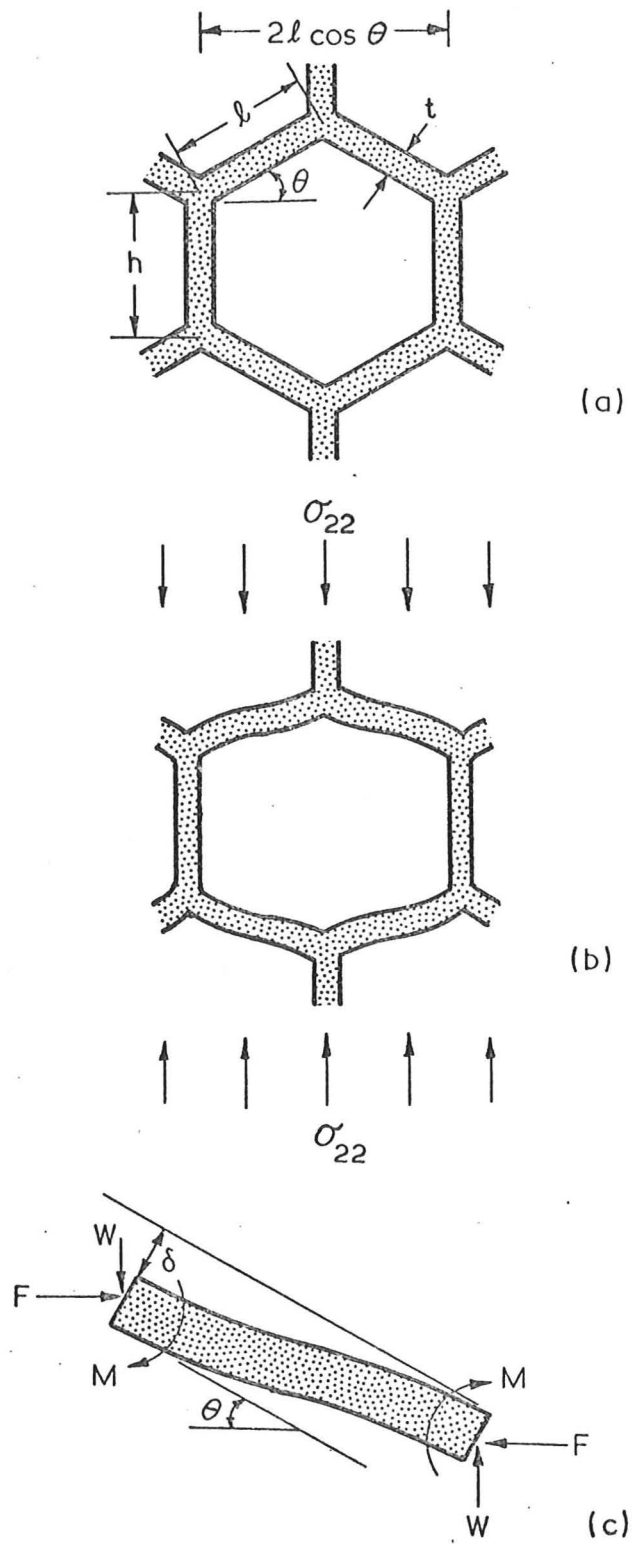
Fig. 3.4   Cell deformation under σ_{22}.

$$F = 0$$

$$W = \sigma_{22} \, \ell b \, \cos\theta$$

$$M = \frac{W\ell \, \cos\theta}{2}$$

The wall deflects by:

$$\delta = \frac{W\ell^3 \, \cos\theta}{12E_S I}$$

Of this, a component $\delta \cos\theta$ is parallel to the X_2 axis, giving a strain:

$$\varepsilon_{22} = \frac{\delta \, \cos\theta}{(h + \ell \, \sin\theta)}$$

$$= \frac{\sigma_{22} \, b\ell^4 \, \cos^3\theta}{12E_S I \, (h + \ell \, \sin\theta)}$$

from which Young's modulus parallel to the X_2 axis is:

$$\boxed{E_2 = \frac{12E_S I \, (h + \ell \, \sin\theta)}{b\ell^4 \, \cos^3\theta}} \qquad (3.17)$$

For regular hexagonal cells this becomes:

$$E_2 = \frac{4}{\sqrt{3}} \frac{t^3}{\ell^3} E_S \qquad (3.18)$$

(This is identical with the result for loading in the X_1 direction.)

The strain parallel to the X_1 axis is:

$$\varepsilon_{11} = -\frac{\delta \, \sin\theta}{\ell \, \cos\theta}$$

from which Poisson's ratio for loading in the X_2 direction becomes:

$$\boxed{\nu_2 = -\frac{\varepsilon_{11}}{\varepsilon_{22}} = \frac{(h + \ell \, \sin\theta) \, \sin\theta}{\ell \, \cos^2\theta}} \qquad (3.19)$$

(c) *The reciprocal theorem*

We showed previously that E_1, ν_1, E_2, and ν_2 must obey the reciprocal theorem:

$$E_1 \, \nu_2 = E_2 \, \nu_1$$

The results of the last two sections for E_1, E_2, ν_1, and ν_2 satisfy the constraint imposed by the reciprocal theorem, namely,

$$E_1 \, \nu_2 = E_2 \, \nu_1 = \frac{12 E_s I}{\ell^3 b \, \sin\theta \, \cos\theta} \qquad (3.20)$$

The shear modulus

Consider the elastic deformation of the cellular structure when a shear stress is applied such that the forces acting on it are as shown in Fig. 3.5. By symmetry, there is no relative motion of the points A,B and C and the forces acting on the members are as shown in Fig. 3.5c. Summing moments at B, we find the moment applied to the members AB and BC is:

$$M = \frac{Fh}{4}$$

All the joints rotate through an angle ϕ as shown in Fig. 3.5d. Then, since there is no deflection of B with respect to A, we have (using eqn. (3.11)):

$$\phi\ell = \frac{Fh}{4} \cdot \frac{\ell^2}{6 E_s I}$$

giving

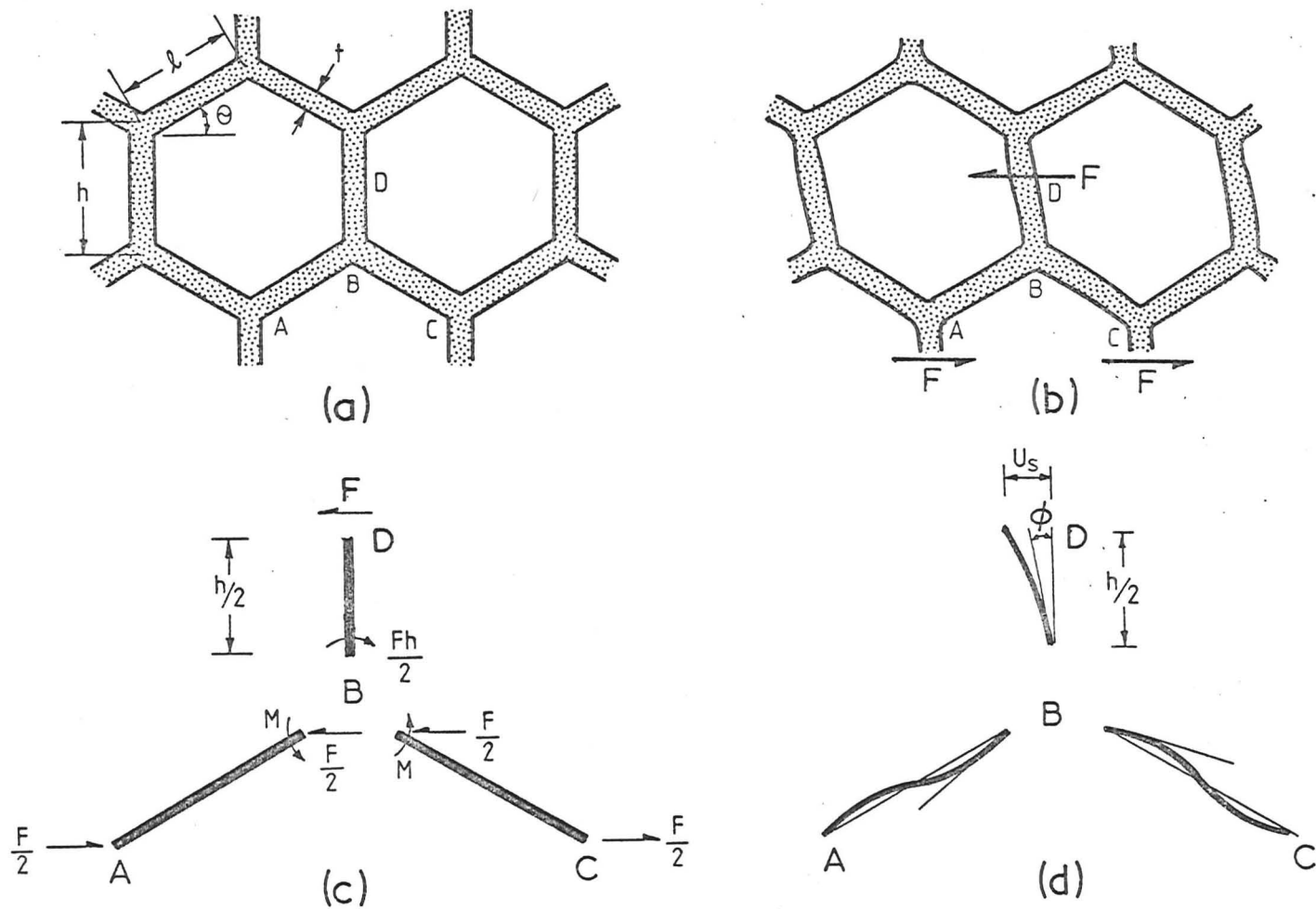$$\phi = \frac{Fh\ell}{24 E_s I}$$

Fig. 3.5   Cell deformation under shear stress.

The shearing deflection (U_s) of the point D with respect to B is (using eqn. (3.10)):

$$U_s = \phi \frac{h}{2} + \frac{F}{3E_sI} \left(\frac{h}{2}\right)^3$$

$$= \frac{Fh^2}{48E_sI} (\ell + 2h)$$

The shear strain, γ, is given by:

$$\gamma = \frac{2U_s}{(h + \ell \sin\theta)}$$

$$= \frac{Fh^2}{24E_sI} \frac{(\ell + 2h)}{(h + \ell \sin\theta)}$$

The distant shear stress, τ, is:

$$\tau = \frac{F}{2\ell b \cos\theta}$$

Hence the shear modulus is:

$$\boxed{G = \frac{12E_sI (h + \ell \sin\theta)}{bh^2\ell \cos\theta (\ell + 2h)}} \qquad (3.21)$$

For a regular structure, this becomes:

$$G = \frac{1}{\sqrt{3}} \frac{t^3}{\ell^3} E_s \qquad (3.22)$$

3.2 Non-Linear Elastic Behaviour

Cellular materials collapse elastically by the elastic buckling of the cell wall members. The cell walls buckle in a cooperative way, allowing further large deformations at almost constant load. In this section we analyse this buckling for the two-dimensional model.

Buckling mode and basic equations

The elastic buckling load of a column of length ℓ under an end load F is given by the Euler formula:

$$F = \frac{n^2 \, \pi^2 \, E_S \, I}{\ell^2} \tag{3.23}$$

where n is an end constraint factor.

In experiments on elastic models, described later, we have observed the buckling mode illustrated by Fig. 3.6. By symmetry, all joints rotate through the angle $\pm \phi$; and the midpoint D of the beam BE is a point of inflection and thus carries zero bending moment.

For equilibrium of the beam AB we have:

$$\frac{P\ell \, \cos\theta}{2} = M_1 - M_2 \tag{3.24}$$

The curvature of the beam is given by:

$$\frac{d^2 y}{dx^2} = - \frac{M}{E_S I} \tag{3.25}$$

Relating the end slope of the beam AB to the moments acting on it, we obtain:

$$M_1 + M_2 = \frac{4 E_S I \phi}{\ell} \tag{3.26}$$

The beam BE can then be considered as a column with rotational springs of stiffness $K = \dfrac{M}{\phi} = \dfrac{4 E_S I}{\ell}$ at each end.
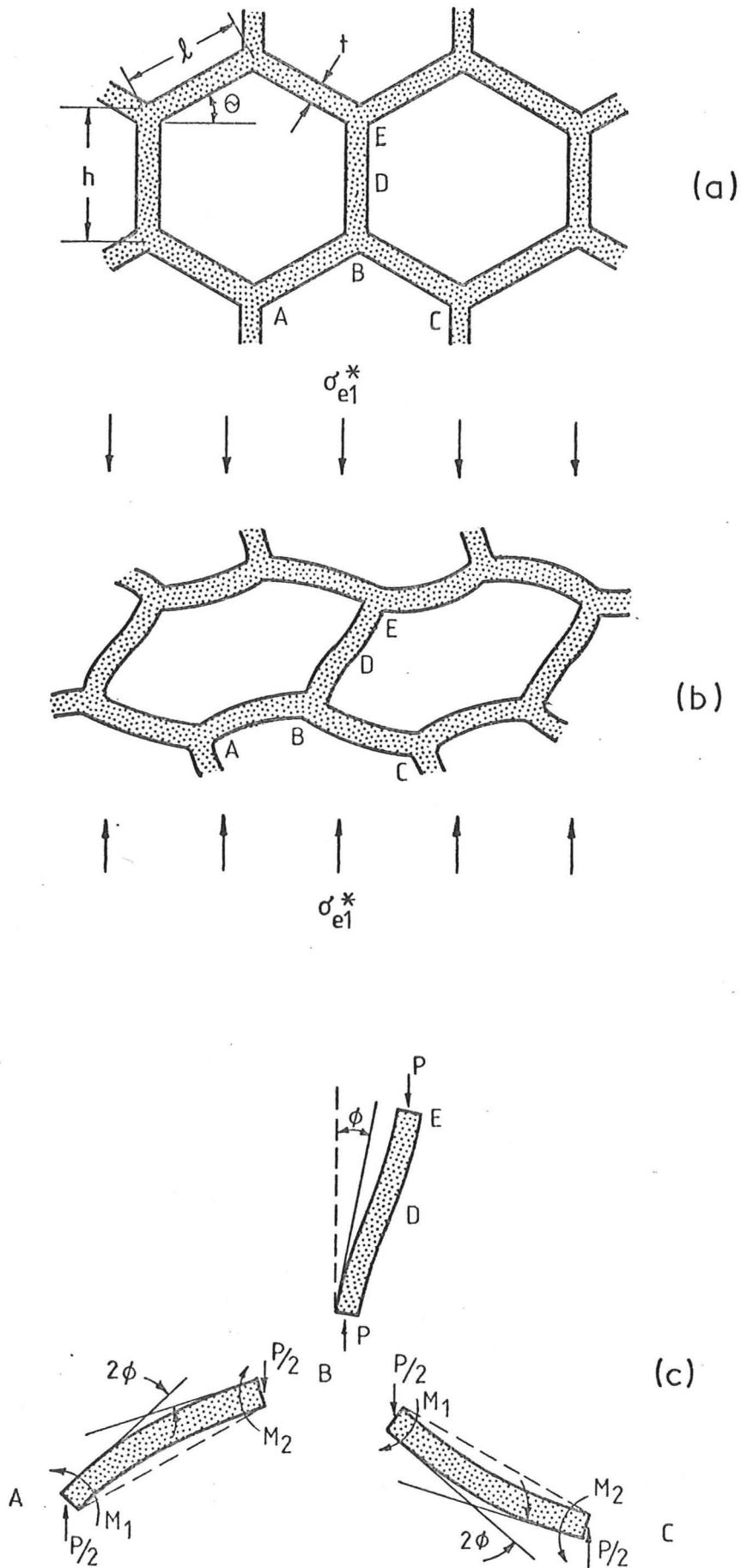
Fig. 3.6   Cell deformation under elastic buckling.

Elastic line method of analysis

Consider a column of length λ pinned at both ends and subjected to its critical Euler buckling load:

$$P_{cr} = \frac{\pi^2 E_S I}{\lambda^2} \tag{3.27}$$

as in Fig. 3.7. The deflected shape of such a column is described by:

$$y = h_o \sin \frac{\pi x}{\lambda} \tag{3.28}$$

where h_o is the midspan deflection. Our column, BE, can be considered to be part of this pinned column of length λ. To determine the part, we match the rotational stiffness at the ends of the column BE to that of the column of length λ at the point $x = L$.

At $x = L$ the moment is M

$$M = P h_o \sin \left(\frac{\pi L}{\lambda}\right) = \frac{\pi^2 E_S I}{\lambda^2} h_o \sin \left(\frac{\pi L}{\lambda}\right) \tag{3.29}$$

the rotation is ϕ

$$\phi = \frac{dy}{dx}\bigg|_{x=L} = \frac{h_o \pi}{\lambda} \cos \frac{\pi L}{\lambda} \tag{3.30}$$

and the rotational spring stiffness is K

$$K = \frac{M}{\phi} = \frac{\pi E_S I}{\lambda} \tan \left(\frac{\pi L}{\lambda}\right) \tag{3.31}$$

Thus a column of length L, held at the base by a rotational spring of stiffness K, buckles at the load (eqn. (3.23)) of:
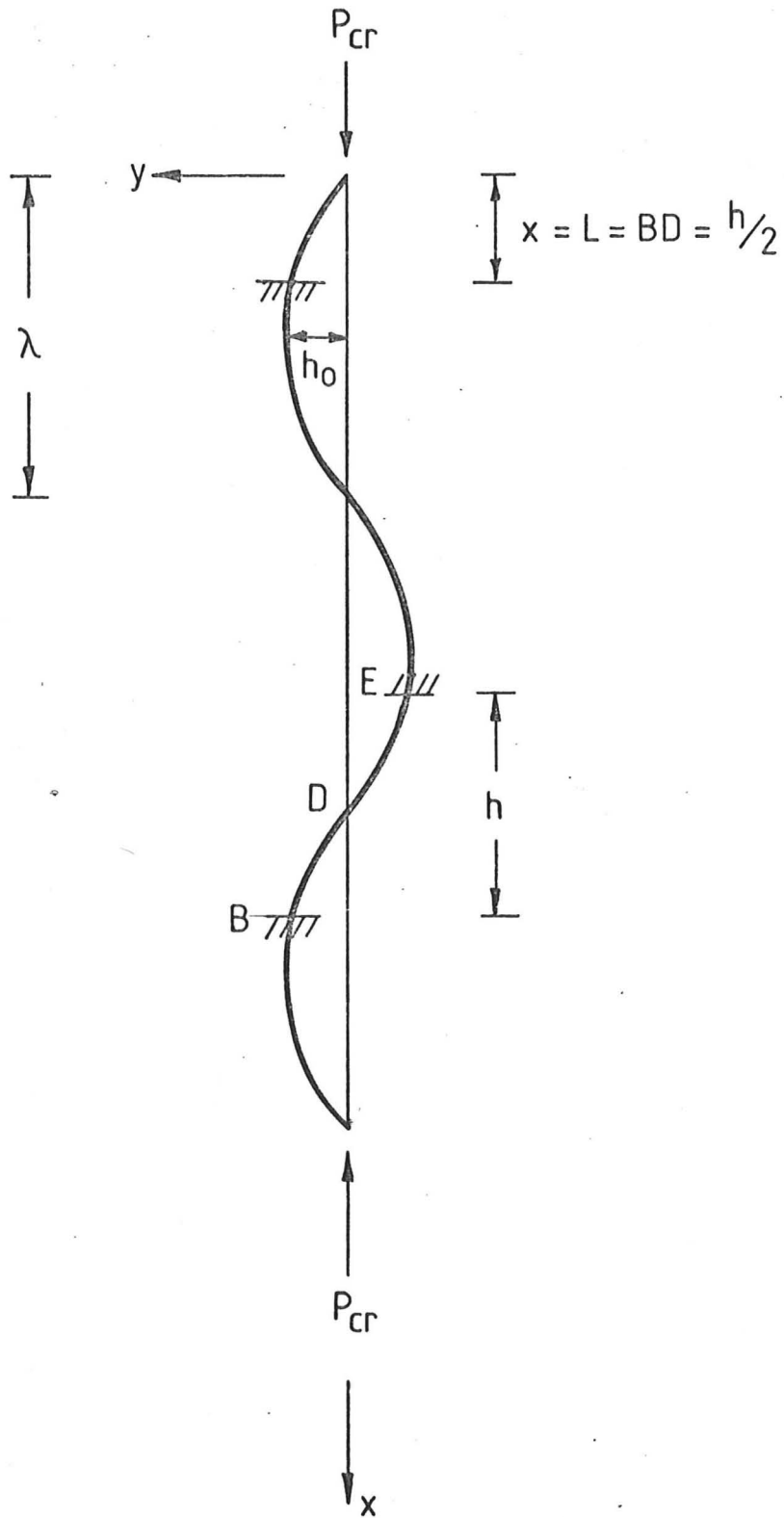
Fig. 3.7   Elastic line method of buckling analysis.

$$P = \frac{\pi^2 E_S I}{\lambda^2}$$

By relating λ to L and K, we can find the critical load for the column.

Let $$\beta = \pi L / \lambda$$

then $$K = \frac{\beta E_S I}{L} \tan\beta$$

or $$\tan\beta = \frac{KL}{E_S I} \frac{1}{\beta}$$

For hexagonal cells, $L = h/2$ and $K = M/\phi = 4E_S I/\ell$, giving:

$$\tan\beta = \frac{2h}{\ell\beta} \qquad (3.32)$$

The solution $\beta = \beta^*$ is found graphically, by plotting $\tan\beta$ and $(\frac{2h}{\ell\beta})$ against β. This gives a relation between λ and L, which can be used to determine the elastic buckling load for a two-dimensional cellular material. Noting that $\lambda = \frac{\pi h}{2\beta^*}$, we obtain the critical buckling load:

$$P_{cr} = \frac{\pi^2 E_S I}{\lambda^2} = \frac{E_S b t^3 \beta^{*2}}{3h^2} \qquad (3.33)$$

The critical buckling stress is given by:

$$\boxed{\sigma_{el}^* = \frac{P_{cr}}{2\ell b \cos\theta} = \frac{E_s t^3 \beta^{*2}}{6\ell h^2 \cos\theta}} \qquad (3.34)$$

Values for β^* for several h/ℓ are given in Table 3.1.

Table 3.1: Solutions for β^* for buckling equation

h/ℓ	β^*
1.0	$.343\pi$
1.5	$.380\pi$
2.0	$.403\pi$

For regular hexagons, this reduces to:

$$\sigma_{e1}^* = 0.22 \, E_s \, \left(\frac{t}{\ell}\right)^3$$

Eqn. (3.34) neglects the small effect of the change in cell wall angle, θ, during linear-elastic deformation. The solution for the elastic buckling stress including this effect is given in Appendix 3C.

The strain at which elastic buckling occurs is given by σ_{e1}^*/E_2, which is approximately 10 % for regular hexagons.

Other buckling modes

Other possible modes of buckling were examined. It was found that all of the other modes examined violated equilibrium requirements and thus the mode for which σ_{e1}^* has been derived is the only one which is likely to occur.

3.3 Plastic Behaviour

If the cell wall material in a cellular structure has a plastic yield point, the structure can collapse plastically if the bending moment in a member reaches the fully plastic moment. This determines the plastic collapse stress, σ_{pl}^*, of the foam. As with elastic collapse, the structure now suffers large strains at almost constant load, thereby absorbing a large amount of energy.

The subsequent calculations use the standard equation for the fully-plastic moment of a beam of rectangular cross-section, bt,

$$M_p = \frac{\sigma_y \, b t^2}{4} \tag{3.35}$$

where σ_y is the yield strength of the cell wall material.

Plastic collapse on loading in the X_1 *direction*

An upper bound on the plastic collapse stress is given by equating the work done by the force:

$$P = \sigma_1 \ (h + \ell \ \sin\theta) \ b$$

during a plastic rotation ϕ of the four plastic hinges A B C D to the plastic work done at the hinges as shown in Fig. 3.8, giving:

$$4 \ M_p \ \phi \geq 2 \ \sigma_1 \ b \ (h + \ell \ \sin\theta) \ \phi\ell \ \sin\theta$$

from which: $\qquad (\sigma_1^*)_{pl} \leq \dfrac{\sigma_y \ t^2}{2\ell \ (h + \ell \ \sin\theta) \ \sin\theta}$ $\qquad\qquad$ (3.36)

A lower bound is given by equating the maximum moment in the beam to M_p. This maximum moment (Fig. 3.8) is:

$$M_{max} = \sigma_1 \ (h + \ell \ \sin\theta) \, b \frac{\ell \ \sin\theta}{2}$$

from which $\qquad \boxed{(\sigma_1^*)_{pl} \geq \dfrac{\sigma_y \ t^2}{2\ell \ (h + \ell \ \sin\theta) \ \sin\theta}}$ $\qquad$ (3.37)

The two results are identical, and thus define the exact solution to the problem. This does not, however, imply that other mechanisms do not occur in practice.

For the regular cellular structure, this becomes:

$$\sigma_{pl}^* = \tfrac{2}{3} \frac{t^2}{\ell^2} \ \sigma_y$$ $\qquad\qquad$ (3.38)

Plastic collapse on loading in the X_2 *direction*

We proceed as in the last section, using Fig. 3.9. The upper bound on the plastic collapse stress is given by the work equation:
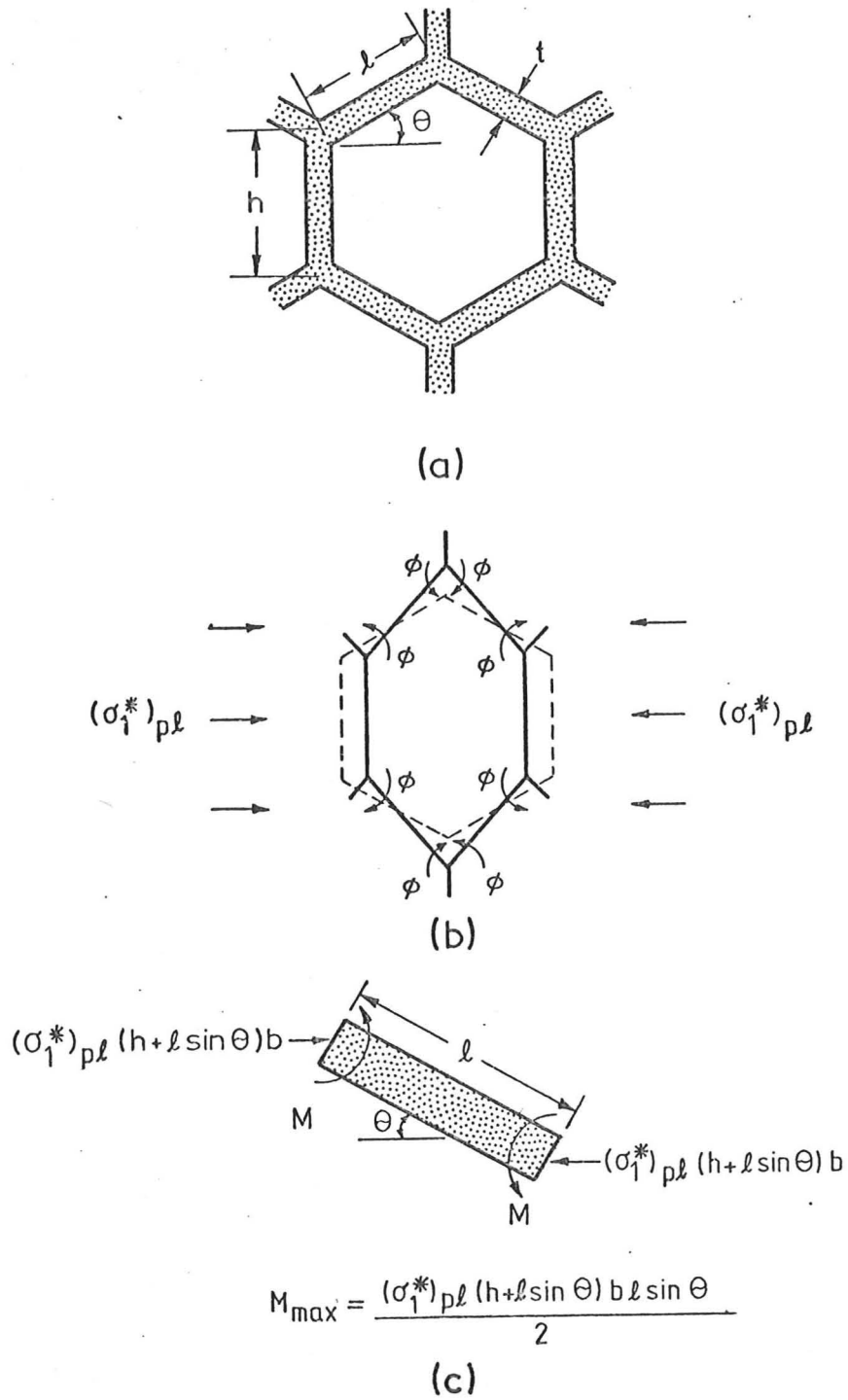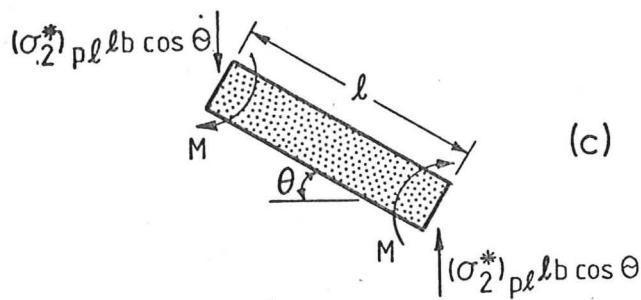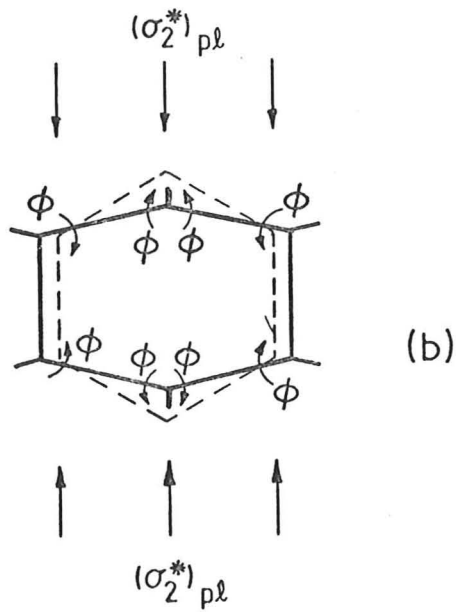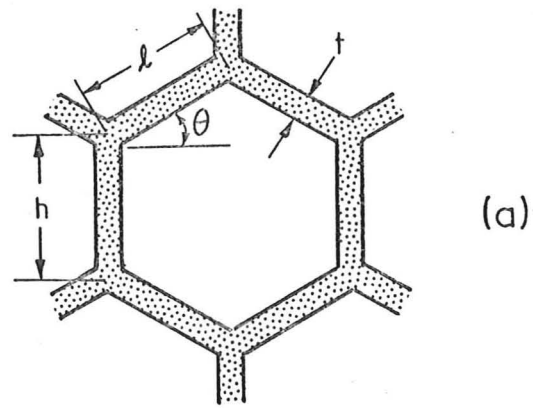
(a)

(b)

$$(\sigma_1^*)_{p\ell}(h+\ell\sin\Theta)b \rightarrow$$

$$M_{max} = \frac{(\sigma_1^*)_{p\ell}(h+\ell\sin\Theta)\,b\,\ell\sin\Theta}{2}$$

(c)

Fig. 3.8   Plastic collapse under σ_{11}.

$(\sigma_2^*)_{pl}$

$(\sigma_2^*)_{pl}$

(a)

(b)

(c)

$$M_{max} = \frac{(\sigma_2^*)_{pl} \, l^2 \, b \cos^2 \theta}{2}$$

Fig. 3.9   Plastic collapse under σ_{22}.

$$4 M_p \phi \geq 2 \sigma_2 \phi \ell^2 b \cos^2\theta$$

from which

$$(\sigma_2^*)_{p1} \leq \frac{\sigma_y t^2}{2\ell^2 \cos^2\theta} \tag{3.39}$$

The maximum bending moment in the beam of length ℓ (Fig. 3.9) is:

$$M_{max} = \frac{\sigma_2 b\ell^2 \cos^2\theta}{2}$$

Equating this to the fully plastic moment of the beam gives the lower bound:

$$\boxed{(\sigma_2^*)_{p1} \geq \frac{\sigma_y t^2}{2\ell^2 \cos^2\theta}} \tag{3.40}$$

As before, the two results are identical and therefore equal to the exact solution – even though the actual arrangement of the plastic hinges need not be identical with that suggested here. For the regular cellular structure, this becomes:

$$\sigma_{p1}^* = \frac{2}{3} \frac{t^2}{\ell^2} \sigma_y \tag{3.41}$$

The two collapse stresses $(\sigma_1^*)_{p1}$ and $(\sigma_2^*)_{p1}$ are identical for the regular structure; we shall term it σ_{p1}^*.

We note that the strain at which plastic collapse occurs is given (for regular hexagons) by:

$$\frac{\sigma_{p1}^*}{E} = \frac{\sigma_y}{3E_S (\rho/\rho_s)} \tag{3.42}$$

This is the strain at which yielding occurs. Note that, for low density foams $(\rho/\rho_s = 10^{-2})$ this strain can be of order 10 %.

3.4 Conclusions

In this chapter we have derived expressions for the linear-
elastic moduli and the elastic and plastic collapse stresses for
idealised two-dimensional cellular materials. We have found that
these properties can be related to the cell wall properties $(E_s$
and $\sigma_y)$, the cell shape $(\theta$ and $h/\ell)$ and density (t/ℓ) by
simple expressions. In the next chapter, we present the results
of tests on two-dimensional cellular materials and find that these
expressions predict the measured behaviour well. The analysis of
this chapter appears to be correct: it is then reasonable to extend
this analysis to three-dimensional cellular materials. We do this in
Chapter 5.

APPENDIX 3A: SMALL STRAIN CALCULATION OF THE MODULI, INCLUDING AXIAL

AND SHEAR DEFORMATIONS

In this appendix, we recalculate the moduli E_1, E_2, ν_1 and ν_2 including the axial and shear deformation of the beams making up the cell walls. At small strains, and for $\rho/\rho_s \ll 1$, they reduce to those given in the text of Chapter 3.

Loading in the X_1 direction, small strains, including shear and axial deformations

From Fig. 3.3, we have:

$$\delta = \frac{P\ell^3 \sin\theta}{12E_s I}$$

From Timoshenko and Goodier (1970), we find that we can write the shear deflection of the member as:

$$\delta_s = \frac{P\ell^3 \sin\theta}{12E_s I} (2.4 + 1.5 \nu_s)(t/\ell)^2$$

An axial load of $P \cos\theta$ acts on the member and hence the axial deflection is:

$$\delta_a = \frac{P\ell \cos\theta}{E_s t b}$$

The total deflection in the X_1 direction is then:

$$\delta_1 = \delta \sin\theta + \delta_s \sin\theta + \delta_a \cos\theta$$

Hence,

$$\varepsilon_{11} = \frac{\delta_1}{\ell \cos\theta}$$

$$= \frac{P\ell^3 \sin^2\theta}{12E_S I \, \ell \cos\theta} \, (1 + (2.4 + 1.5 \, \nu_S)(t/\ell)^2 + \cot^2\theta \, (t/\ell)^2)$$

$$= \frac{\sigma_{11} \, b \, (h + \ell \sin\theta) \, \ell^2 \sin^2\theta}{12E_S I \cos\theta} \, (1 + (2.4 + 1.5 \, \nu_S + \cot^2\theta) \, t^2/\ell^2)$$

And

$$E_1 = \frac{\sigma_{11}}{\varepsilon_{11}} = \frac{12E_S I \cos\theta}{(h + \ell \sin\theta) \, b \, \ell^2 \sin^2\theta} \, \frac{1}{1 + (2.4 + 1.5 \, \nu_S + \cot^2\theta)(t/\ell)^2}$$

The strain in the X_2 direction is:

$$\varepsilon_{22} = -\frac{\delta_2}{h + \ell \sin\theta} = -\frac{(\delta \cos\theta + \delta_S \cos\theta - \delta_a \sin\theta)}{h + \ell \sin\theta}$$

$$= \frac{-P\ell^3 \sin\theta \cos\theta}{12E_S I \, (h + \ell \sin\theta)} \, (1 + (2.4 + 1.5 \, \nu_S - 1) \, t^2/\ell^2)$$

giving:

$$\nu_1 = -\frac{\varepsilon_{22}}{\varepsilon_{11}} = \frac{\ell \cos^2\theta}{(h + \ell \sin\theta) \sin\theta} \, \frac{1 + (1.4 + 1.5 \, \nu_S)(t/\ell)^2}{1 + (2.4 + 1.5 \, \nu_S + \cot^2\theta)(t/\ell)^2}$$

Loading in the X_2 direction, small strains including shear and axial

deformations

Reconsidering Fig. 3.4, we find the bending deflection of the inclined member is, as before,

$$\delta = \frac{W\ell^3 \cos\theta}{12E_S I}$$

The shear deflection of this member is then (from Timoshenko and Goodier (1970)):

$$\delta_s = \frac{W\ell^3 \cos\theta}{12E_S I} (2.4 + 1.5 \ v_S) \ t^2/\ell^2$$

The axial deflection of the inclined member is:

$$\delta_a \text{ inclined} = \frac{W\ell \sin\theta}{E_S tb}$$

The axial deflection of the upright member is:

$$\delta_a \text{ upright} = \frac{2Wh}{btE}$$

The total deflection in the X_2 direction is then:

$$\delta_2 = \delta \cos\theta + \delta_s \cos\theta + \delta_a \text{ inclined} \sin\theta + \delta_a \text{ upright}$$

$$= \frac{W\ell^3 \cos^2\theta}{12E_S I} \left[1 + (2.4 + 1.5 \ v_S) \frac{t^2}{\ell^2} + \tan^2\theta \frac{t^2}{\ell^2} + \frac{2 \ (h/\ell)}{\cos^2\theta} \frac{t^2}{\ell^2} \right]$$

and $$\varepsilon_{22} = \delta_2/(h + \ell \sin\theta)$$

This gives:

$$E_2 = \frac{\sigma_{22}}{\varepsilon_{22}}$$

$$= \frac{\sigma_{22} (h + \ell \sin\theta) \, 12E_S I}{W\ell^3 \cos^2\theta \left[1 + (2.4 + 1.5 \, \nu_S + \tan^2\theta + \frac{2 \, (h/\ell)}{\cos^2\theta}) \frac{t^2}{\ell^2}\right]}$$

$$= \frac{12E_S I \, (h + \ell \sin\theta)}{b \, \ell^4 \cos^3\theta \left[1 + (2.4 + 1.5 \, \nu_S + \tan^2\theta + \frac{2 \, (h/\ell)}{\cos^2\theta}) \frac{t^2}{\ell^2}\right]}$$

The strain in the X_1 direction is:

$$\varepsilon_{11} = -\frac{\delta_1}{\ell \cos\theta} = -\frac{(\delta \sin\theta + \delta_s \sin\theta - \delta_a \text{ inclined } \cos\theta)}{\ell \cos\theta}$$

$$= -\frac{W\ell^2 \sin\theta}{12E_S I} \left[1 + (2.4 + 1.5 \, \nu_S - 1) \frac{t^2}{\ell^2}\right]$$

Therefore:

$$\nu_2 = -\frac{\varepsilon_{11}}{\varepsilon_{22}}$$

$$= \frac{\sin\theta \, (h + \ell \sin\theta)}{\ell \cos^2\theta} \, \frac{1 + (1.4 + 1.5 \, \nu_S) \, (t/\ell)^2}{1 + (2.4 + 1.5 \, \nu_S + \tan^2\theta + \frac{2 \, (h/\ell)}{\cos^2\theta})(t/\ell)^2}$$

This gives:

$$E_2 = \frac{\sigma_{22}}{\varepsilon_{22}}$$

$$= \frac{\sigma_{22} \ (h + \ell \sin\theta) \ 12 E_S I}{W\ell^3 \ \cos^2\theta \left[1 + (2.4 + 1.5 \ \nu_S + \tan^2\theta + \frac{2 \ (h/\ell)}{\cos^2\theta}) \ \frac{t^2}{\ell^2}\right]}$$

$$= \frac{12 E_S I \ (h + \ell \sin\theta)}{b \ \ell^4 \ \cos^3\theta \left[1 + (2.4 + 1.5 \ \nu_S + \tan^2\theta + \frac{2 \ (h/\ell)}{\cos^2\theta}) \ \frac{t^2}{\ell^2}\right]}$$

The strain in the X_1 direction is:

$$\varepsilon_{11} = - \frac{\delta_1}{\ell \ \cos\theta} = - \frac{(\delta \ \sin\theta + \delta_s \ \sin\theta - \delta_{a \ \text{inclined}} \ \cos\theta)}{\ell \ \cos\theta}$$

$$= - \frac{W\ell^2 \ \sin\theta}{12 E_S I} \left[1 + (2.4 + 1.5 \ \nu_S - 1) \ \frac{t^2}{\ell^2}\right]$$

Therefore:

$$\nu_2 = - \frac{\varepsilon_{11}}{\varepsilon_{22}}$$

$$= \frac{\sin\theta \ (h + \ell \sin\theta)}{\ell \ \cos^2\theta} \ \frac{1 + (1.4 + 1.5 \ \nu_S) \ (t/\ell)^2}{1 + (2.4 + 1.5 \ \nu_S + \tan^2\theta + \frac{2 \ (h/\ell)}{\cos^2\theta})(t/\ell)^2}$$

APPENDIX 3B: LARGE STRAIN CALCULATION OF THE MODULI

Loading in the X_1 direction, large strain approximation

As the load on a cell is increased the angle θ changes (Fig. 3B.1). From Fig. 3B.1 it can be seen that:

$$\delta\theta = -\frac{\delta}{\ell}$$

Previously, we had:

$$\varepsilon_{11} = \frac{\delta \sin\theta}{\ell \cos\theta}$$

Hence

$$\delta\theta = -\varepsilon_{11} \frac{\cos\theta}{\sin\theta}$$

For a constant angle θ, we derived the following expression relating σ_{11} to ε_{11}

$$\varepsilon_{11} = \frac{\sigma_{11} (h + \ell \sin\theta) b \ell^2 \sin^2\theta}{12 E_S I \cos\theta}$$

Letting

$$\theta = \theta + \delta\theta \quad \text{and} \quad h = \ell$$

we obtain:

$$\varepsilon_{11} = \frac{\sigma_{11} b \ell^3}{12 E_S I} \frac{(1 + \sin(\theta + \delta\theta)) \sin^2(\theta + \delta\theta)}{\cos(\theta + \delta\theta)}$$

Using the identities for $\sin(\alpha + \beta)$ and $\cos(\alpha + \beta)$ and assuming $\cos\delta\theta = 1$ and $\sin\delta\theta = \delta\theta$ for small $\delta\theta$ we obtain:

$$\varepsilon_{11} = \frac{\sigma_{11} \ell^3}{12 E_S I} \frac{(\sin\theta - \varepsilon_{11} \frac{\cos^2\theta}{\sin\theta})^2 + (\sin\theta - \varepsilon_{11} \frac{\cos^2\theta}{\sin\theta})^3}{\cos\theta (1 + \varepsilon_{11})}$$
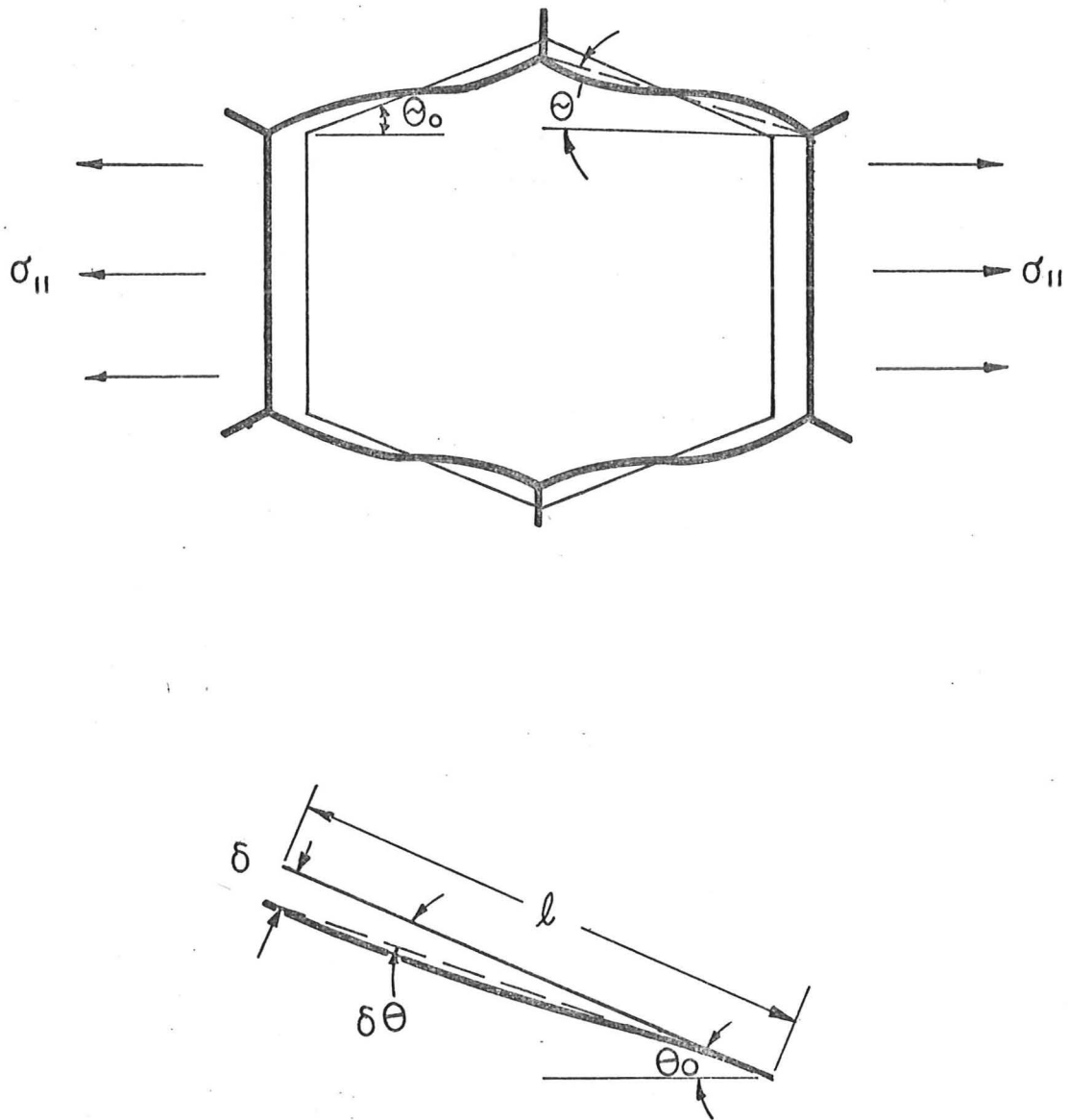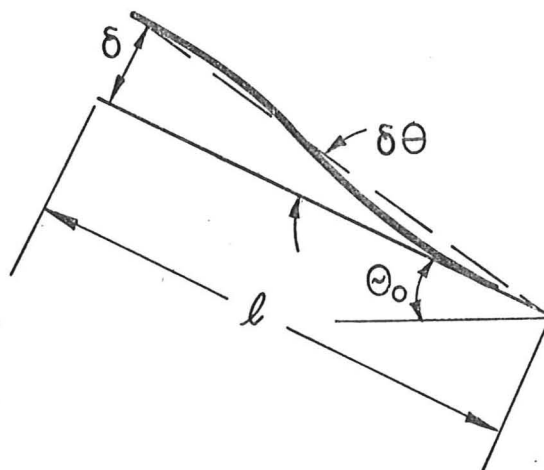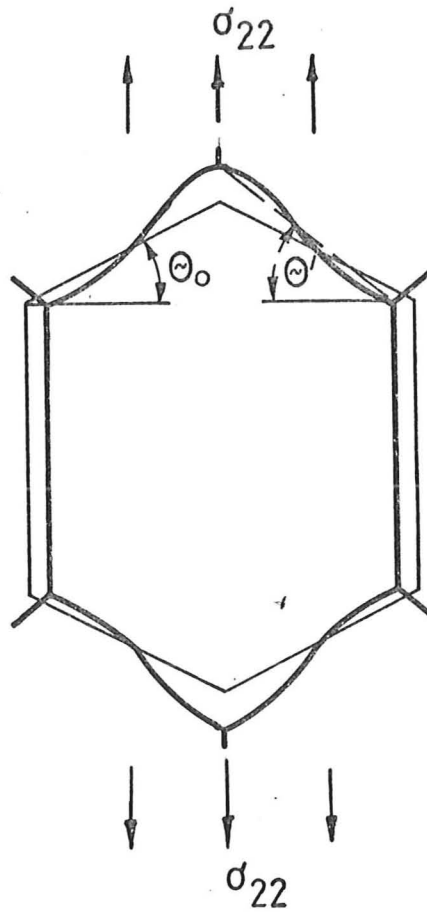
Fig. 3B.1   Large strain approximation - loading in X_1 direction.

or

$$\frac{\sigma_{11} \ell^3}{12E_S I} = \frac{\varepsilon_{11} (1 + \varepsilon_{11})(\cos\theta)}{(\sin\theta - \varepsilon_{11} \frac{\cos^2\theta}{\sin\theta})^2 + (\sin\theta - \varepsilon_{11} \frac{\cos^2\theta}{\sin\theta})^3}$$

A graph of this relationship for $\theta_o = -30°$, $30°$, $45°$, and $60°$ is shown in Fig. 3B.2.

Loading in the X_2 direction, large strain approximation

From Fig. 3B.3 it can be seen that:

$$\delta\theta = \frac{\delta}{\ell}$$

and for $h = \ell$:

$$\varepsilon_{22} = \frac{\delta \cos\theta}{\ell (1 + \sin\theta)}$$

so

$$\delta\theta = \varepsilon_{22} \frac{(1 + \sin\theta)}{\cos\theta}$$

From the previous derivation for E_2, we have:

$$\varepsilon_{22} = \frac{\sigma_{22} b \ell^3 \cos^3\theta}{12E_S I (1 + \sin\theta)}$$

or

$$\frac{\sigma_{22} b \ell^3}{12E_S I} = \frac{\varepsilon_{22} (1 + \sin\theta)}{\cos^3\theta}$$

Substituting $\theta = \theta + \delta\theta$, and noting that for small $\delta\theta$ $\cos\delta\theta \sim 1$ and $\sin\delta\theta \sim \delta\theta$, we obtain:
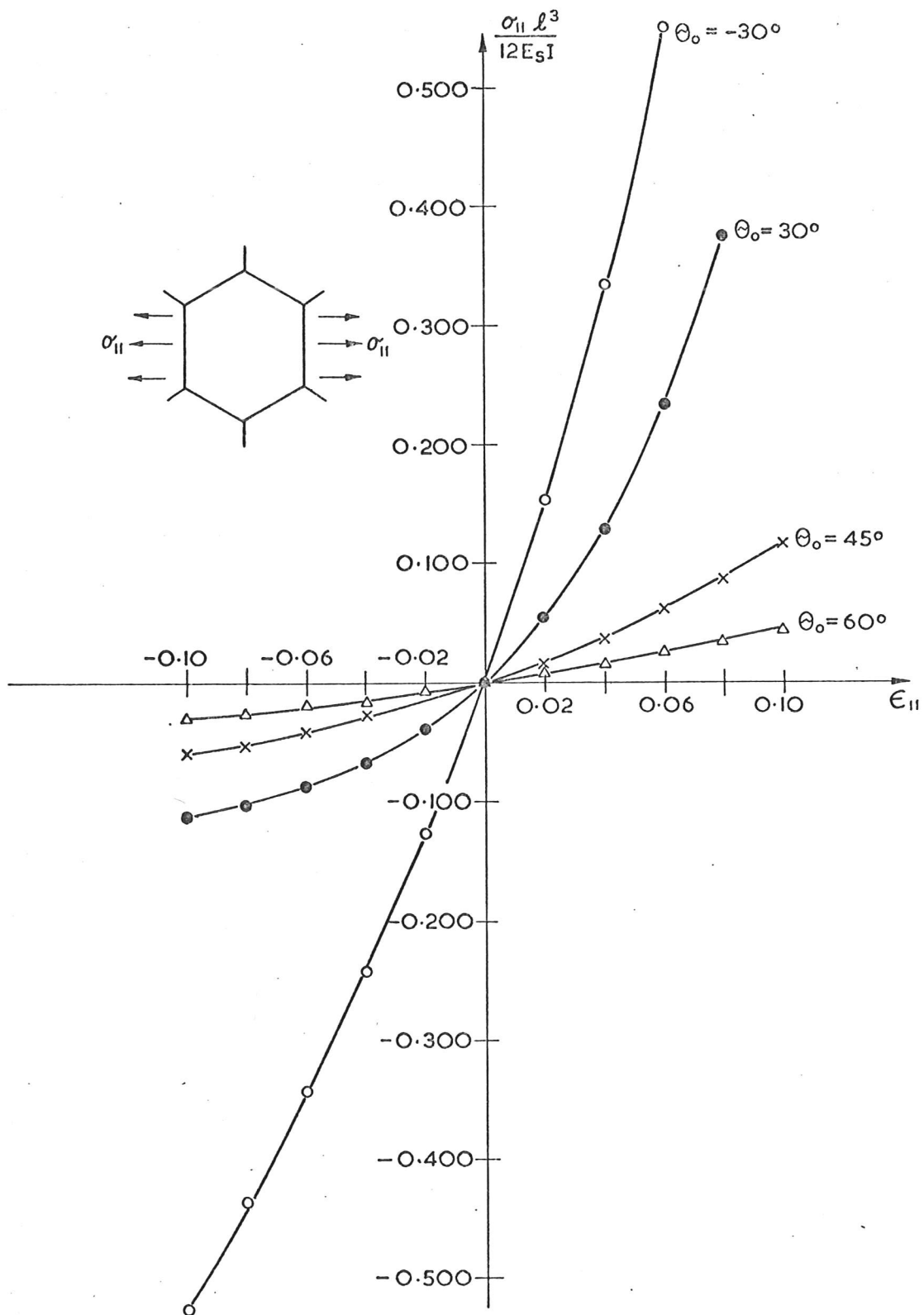
Fig. 3B.2   Stress—strain curve for large strain approximation — loading in X_1 direction.

Fig. 3B.3   Large strain approximation - loading in
X_2 direction.

$$\frac{\sigma_{22} \ell^3}{12E_S I} = \frac{\varepsilon_{22} (1 + \sin\theta)(1 + \varepsilon_{22})}{(\cos\theta - \varepsilon_{22} (1 + \sin\theta) \tan\theta)^3}$$

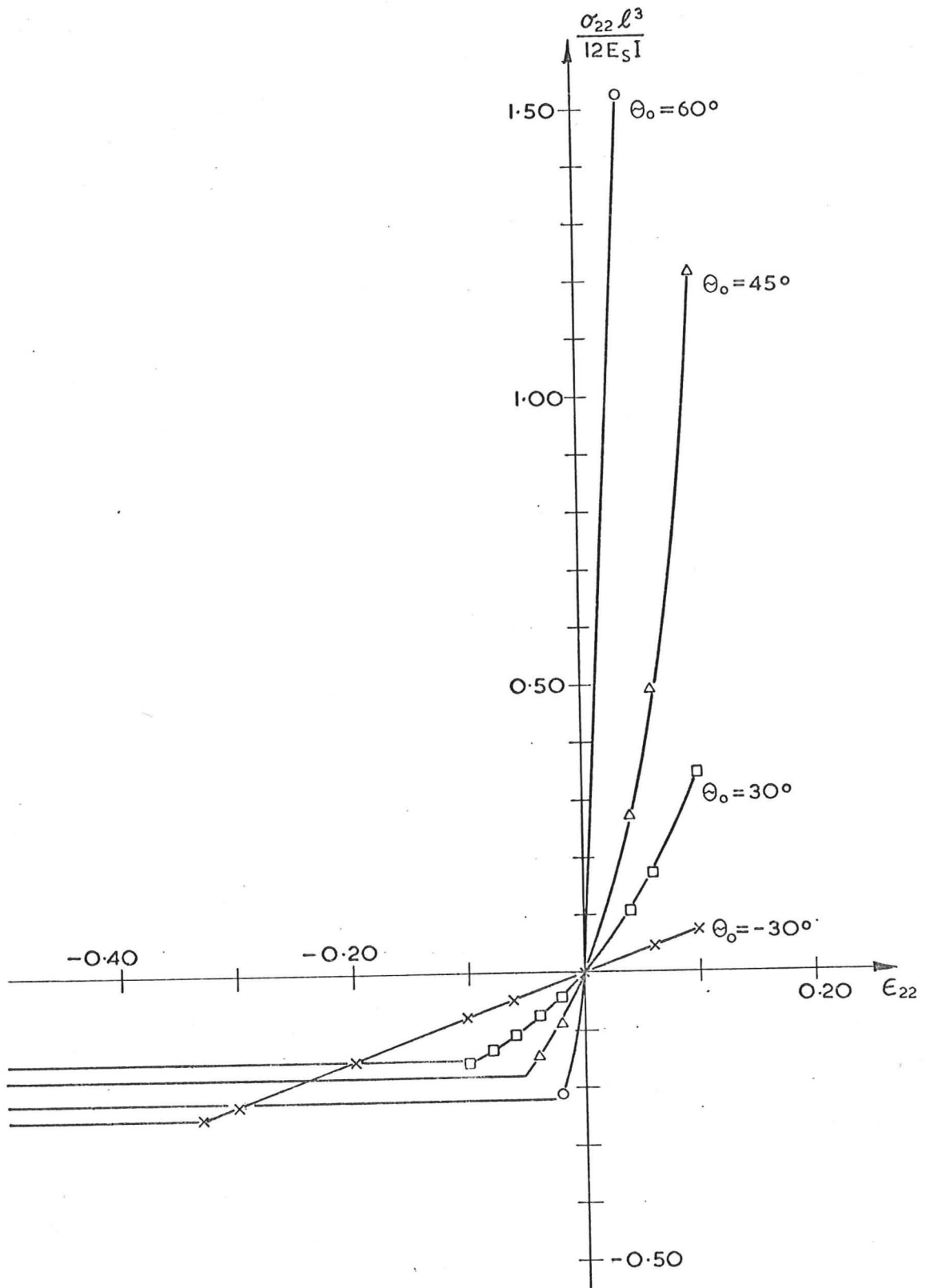This relationship is shown in Fig. 3B.4.

Fig. 3B.4   Stress-strain curve for large strain approximation -
loading in X_2 direction.

APPENDIX 3C: ELASTIC BUCKLING INCLUDING CHANGE OF CELL SHAPE PRIOR
TO BUCKLING

The angle θ changes during elastic deformation. Let θ^* denote the value of θ when buckling begins. θ^* can be found by equating the cell strain at buckling to σ^*_{el}/E_2

$$\varepsilon^*_2 = \frac{h + \ell \sin\theta - (h + \ell \sin\theta^*)}{h + \ell \sin\theta} = \frac{\sin\theta - \sin\theta^*}{h/\ell + \sin\theta}$$

$$\varepsilon^*_2 = \frac{\sigma^*_{el}}{E_2} = \frac{\beta^{*2} E_S t^3}{6h^2 \ell \cos\theta^*} \frac{\ell^3 \cos^3\theta}{E_S t^3 (h/\ell + \sin\theta)}$$

This leads to:

$$\frac{\beta^{*2} \cos^3\theta}{6 (h/\ell)^2} = \cos\theta^* (\sin\theta - \sin\theta^*)$$

which can be solved by trial and error. The equation for the elastic buckling stress is then:

$$\boxed{\sigma^*_{el} = \frac{\beta^{*2} E_S t^3}{6h^2 \ell \cos\theta^*}}$$

CHAPTER 3: REFERENCES

Timoshenko, S.P. and Goodier, J.N. (1970) "Theory of Elasticity", Third Ed.
McGraw-Hill Book Company, p.121.

CHAPTER 4

TWO-DIMENSIONAL CELLULAR MATERIALS:
EXPERIMENTAL METHOD, RESULTS AND DISCUSSION

Silicon rubber models of two-dimensional cells were made, vary-ing the cell wall thickness and size (and thus the density), and the cell shape. They allow a complete test of the theory for the linear and non-linear elastic behaviour, developed in Sections 3.1 and 3.2.

Metal honeycombs ("Aerowebs") of different densities, cell sizes and shape were also tested, allowing the theory of plastic collapse developed in Section 3.3 to be tested. The results are presented below.

4.1 The Models

The models were made with ICI Silcoset 105 silicon rubber in the geometries given in Table 4.1. Models 1-4 vary θ for constant t/ℓ and h/ℓ. Models 5-7 vary h/ℓ for constant t/ℓ and θ, and models 8-10 vary t/ℓ for constant h/ℓ and θ values. The models were made by pouring a degassed mixture of silicon rubber and hardener into a mould which consisted of a perspex base with machined brass formers (irregular hexagons) screwed onto it at appropriate spacings to produce the correct wall thickness.

Aluminium honeycombs ("Aerowebs") made of aluminium foil joined by strips of epoxy and expanded to give hexagons of various angles θ, were obtained from Ciba Geigy. It is not possible to vary h/ℓ for commercial Aerowebs, so punch and die jigs were machined to stamp out strips of copper which, when joined, gave hexagonal cells with various values of h/ℓ. Table 4.2 shows the nominal geometries. Ten specimens of each geometry were tes-ted: five loaded in the X_1 direction, five in the X_2 direction.

TABLE 4.1:   Geometry of Rubber Models

MODEL	1	2	3	4	5	6	7	8	9	10
t/ℓ	.21	.21	.21	.21	.21	.21	.21	.21	.176	.134
h/ℓ	2.0	2.0	2.0	2.0	1.0	1.5	2.0	1.0	1.0	1.0
θ	-30°	0°	30°	45°	30°	30°	30°	30°	30°	30°
UNIT CELL										

TABLE 4.2:   Nominal Geometry of Metal Models

MODEL	$(t/\ell)_1$	$(t/\ell)_2$	$(t/\ell)_3$	θ_1	θ_2	θ_3	$(h/\ell)_1$	$(h/\ell)_2$	$(h/\ell)_3$
t/ℓ	.0088	.0120	.0177	.0119	.0119	.0119	.0243	.0243	.0243
θ	42°	42°	42°	28°	44°	68°	30°	30°	30°
h/ℓ	.74	.74	.74	.73	.73	.73	1.0	1.5	2.0
UNIT CELL									

4.2 Linear Elastic Behaviour

The moduli E_1 and E_2 were measured from the slope of the load-deflection curve for loading in the X_1 and X_2 directions respectively. The two Poisson's ratios ν_1 and ν_2 were calculated from measurements of displacements in the X_1 and X_2 directions using targets on the models and a travelling microscope. The shear modulus G, was measured by loading the models along their diagonal in a special jig, and calculating the modulus from the slope of the resulting load-deflection curve.

Fig. 4.1 shows typical compression stress-strain curves for a rubber model and an Aeroweb specimen. Both curves show a well defined linear elastic region with slope E, followed by an almost horizontal plateau. This plateau is caused by the cells collapsing: in the rubber model they buckle elastically; in the Aeroweb plastic hinges form. Finally, when the cells have collapsed completely, the stress rises steeply.

Theoretical and experimental values of E_1 and E_2 for the rubber models are plotted in Figs. 4.2 and 4.3. Errors bars of width one standard deviation, show how scatter in measuring cell wall thickness, t, height, h, angle θ and so on, affect the calculations. The error in the experimental value of the Young's moduli was too small to show on these figures. Agreement between theory and experiment is good except for model 1 with $\theta = -30^\circ$.

The way in which E_1 and E_2 vary with density, t/ℓ, cell aspect ratio, h/ℓ, and cell angle, θ, are shown in Figs. 4.4 to 4.6. It is clear that the changes predicted by the theory are borne out in practice.
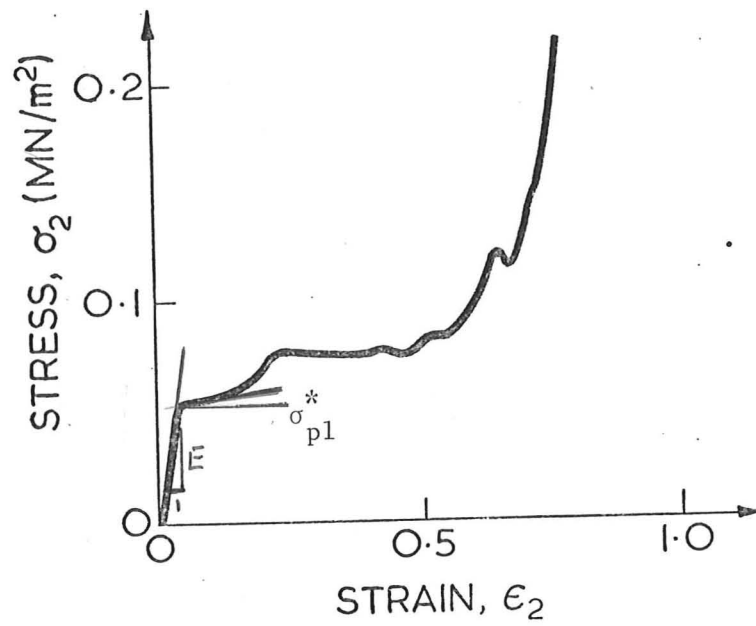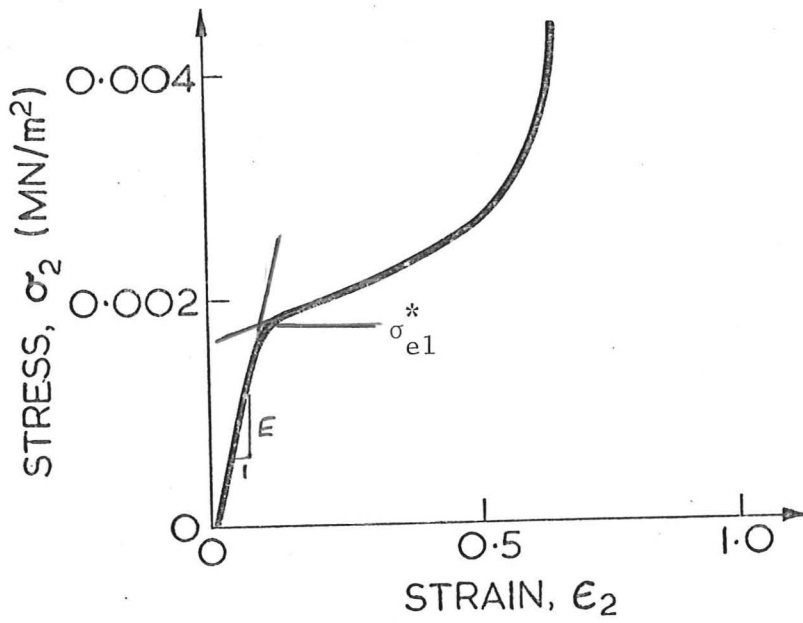
Fig. 4.1   Stress-strain curve for (a) rubber model,
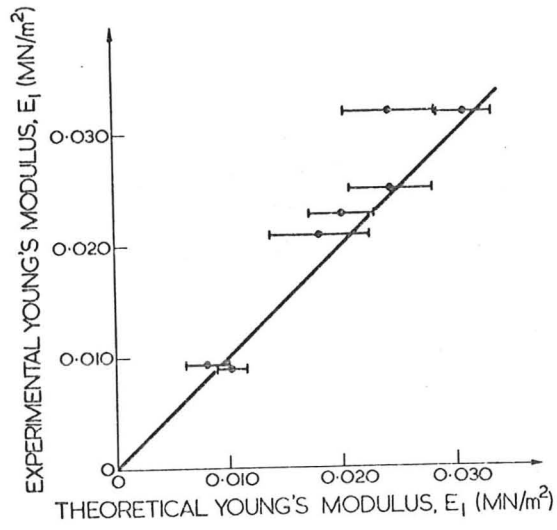(b) Aeroweb.

Fig. 4.2   Theoretical and experimental values of E_1 for rubber models.
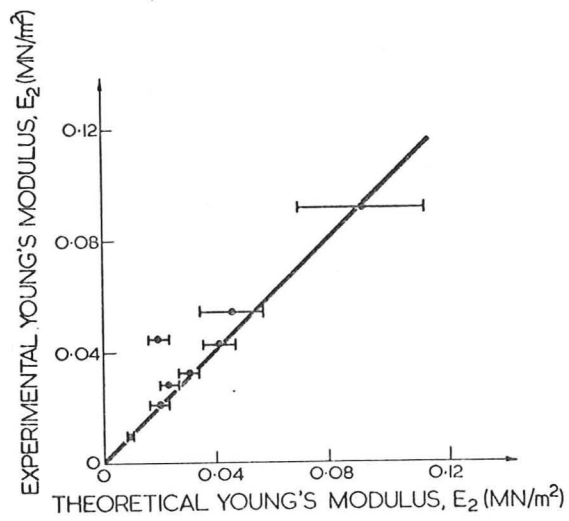

Fig. 4.3   Theoretical and experimental values of E_2 for rubber models.
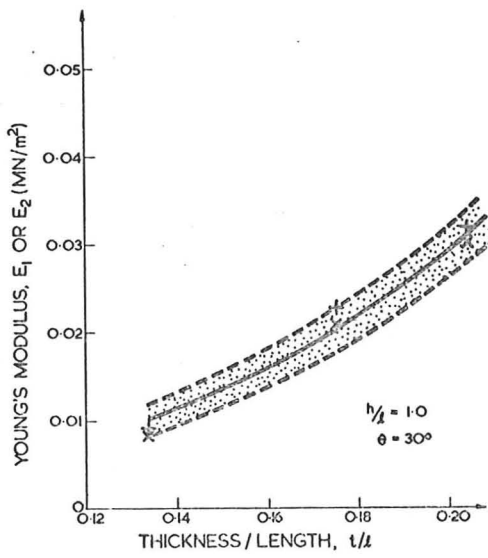
Fig. 4.4 E_1 and E_2 as a function of t/ℓ for rubber models.

Fig. 4.5 E_1 and E_2 as a function of h/ℓ for rubber models.
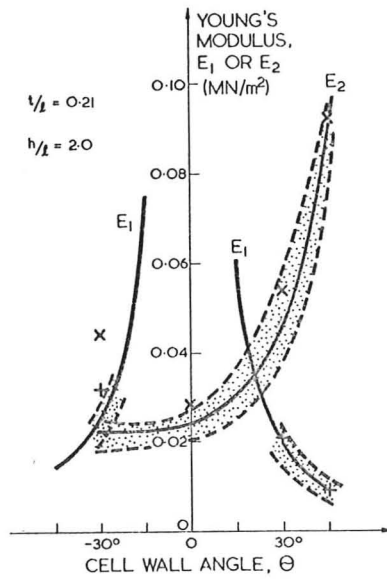
Fig. 4.6 E_1 and E_2 as a function of θ for rubber models.
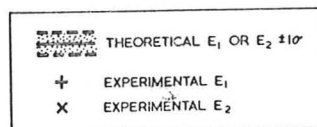
The moduli of the metal models are compared with theoretical values in Figs. 4.7 and 4.8. The dependence on t/ℓ and on θ is shown in Figs. 4.9 to 4.12. The errors are a little larger because the geometry of these models is less regular than that of the rubber models. Agreement is again good.

Theoretical and experimental values of ν_1 and ν_2 are plotted in Figs. 4.13 to 4.17. Since Poisson's ratio is a function of the geometry of the unit cell only and since this is known very accurately, the error in the theoretically predicted value of ν is small. However, the experimental error is large. Poisson's ratio was measured experimentally by attaching targets onto the walls of the rubber models and measuring the displacement of the targets under load. Plots of strain in the load direction against strain in the lateral direction were then made and ν was calculated using a linear regression analysis. The scatter in this strain data was large, and so the error in the experimentally measured value of ν is large. There is good agreement between the experimental and theoretical values of ν_1 and ν_2 with the exception of ν_1 for model 10 and ν_2 for model 6.

Theoretical and experimental values of shear modulus are plotted in Figs. 4.18 to 4.21. As with Young's modulus one standard deviation error bars are plotted for the experimentally measured values. The experimental values of shear modulus are slightly higher than is expected from the theory, perhaps because of the stiffening effect of the shear jig.
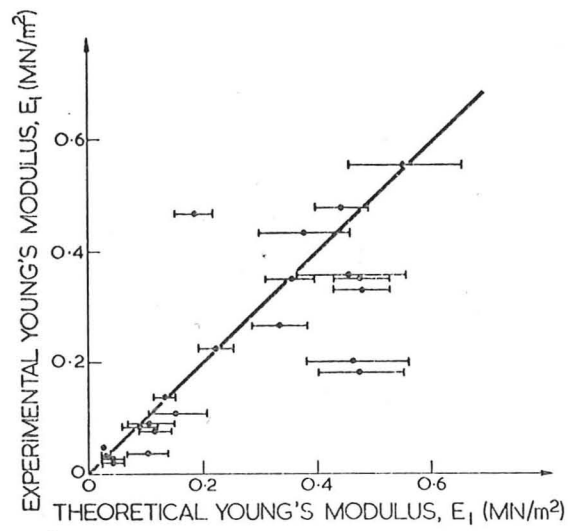
Fig. 4.7   Theoretical and experimental values of E_1 for metal models.
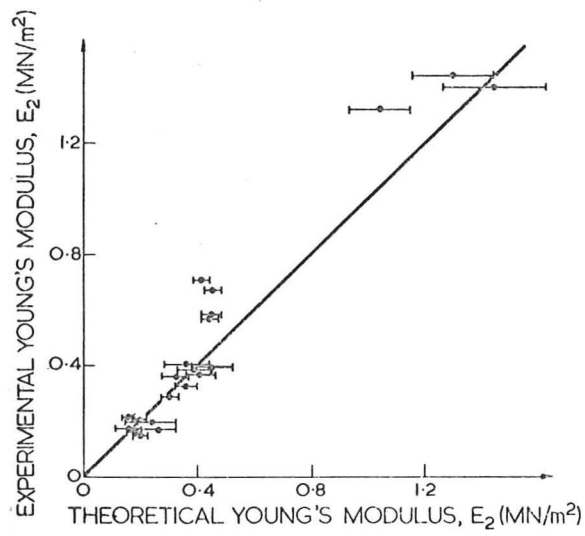
Fig. 4.8   Theoretical and experimental values of E_2 for metal models.

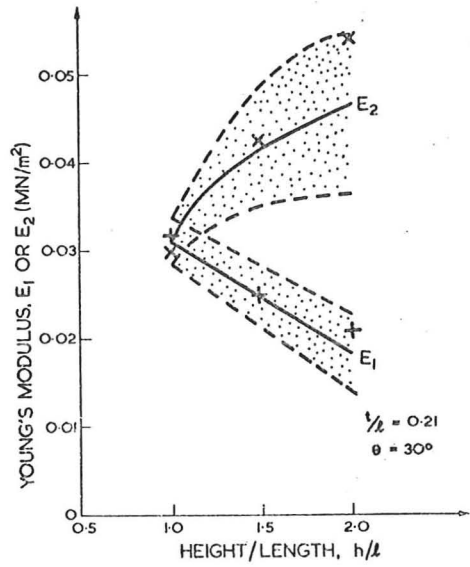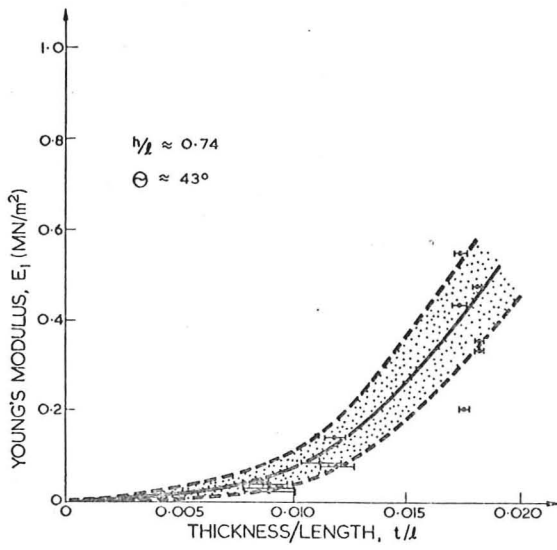Fig. 4.9 E_1 as a function of t/ℓ for metal models.
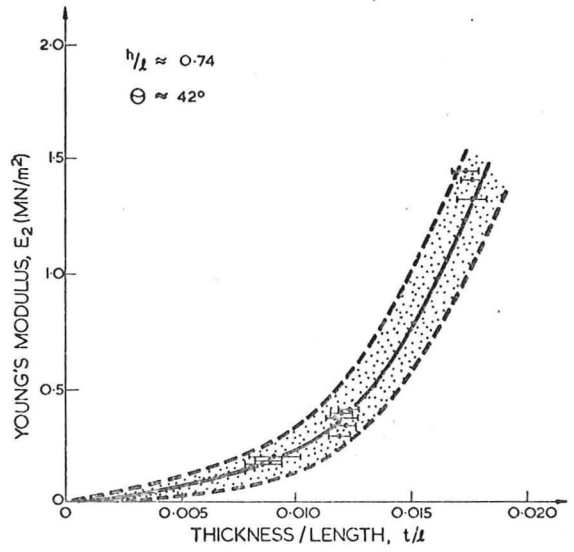
Fig. 4.10 E_2 as a function of t/ℓ for metal models.
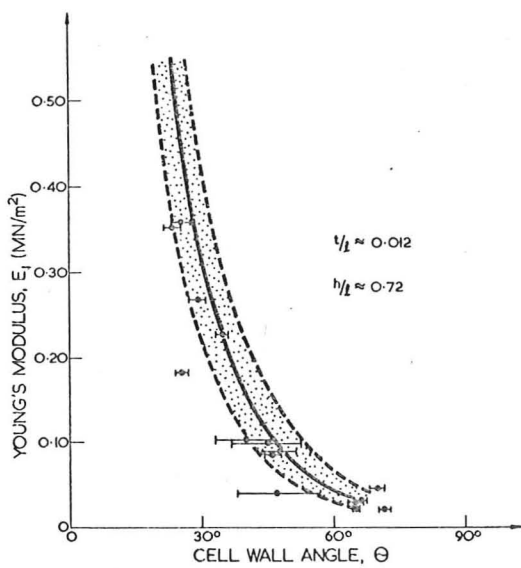
Fig. 4.11 E_1 as a function of θ for metal models.
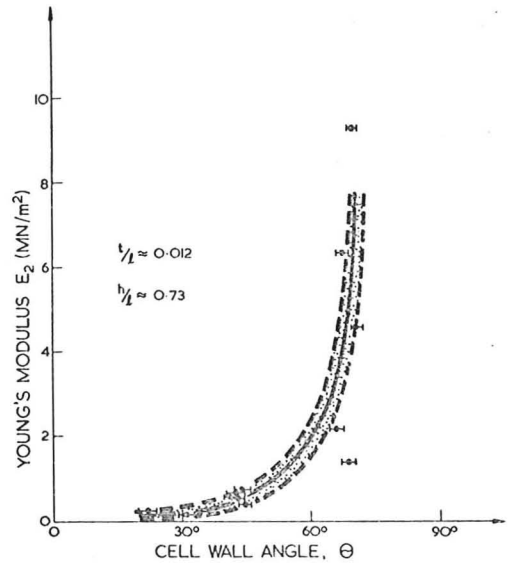
Fig. 4.12 E_2 as a function of θ for metal models.

THEORETICAL E_1 OR $E_2 \pm 1\sigma$

EXPERIMENTAL E_1 OR $E_2 \pm 1\sigma$
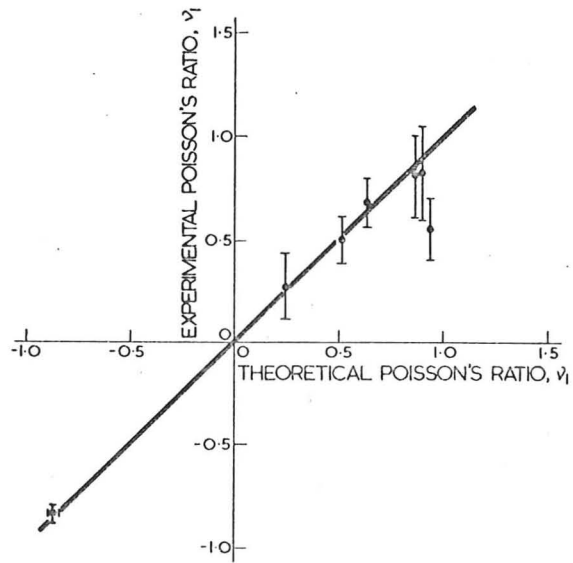
Fig. 4.13   Theoretical and experimental values of ν_1 for rubber models.
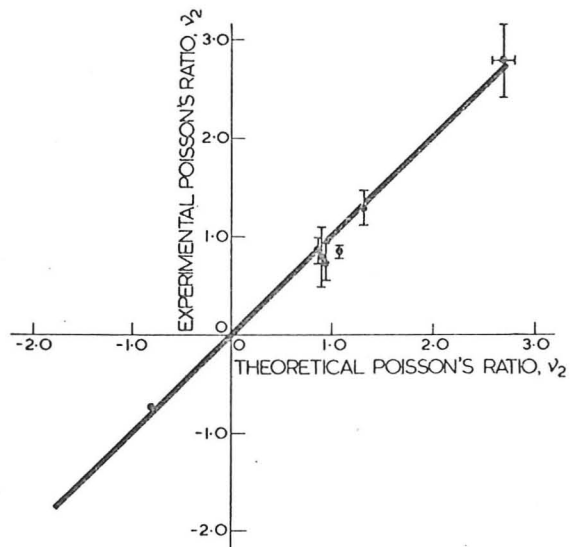
Fig. 4.14   Theoretical and experimental values of ν_2 for rubber models.
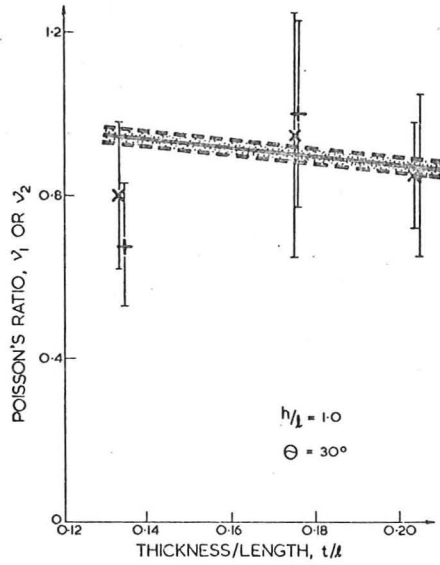
Fig. 4.15 ν_1 and ν_1 as a function of t/ℓ for rubber models.
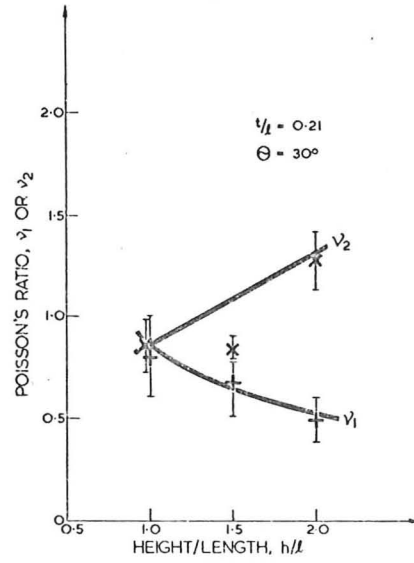
Fig. 4.16 ν_1 and ν_2 as a function of h/ℓ for rubber models.
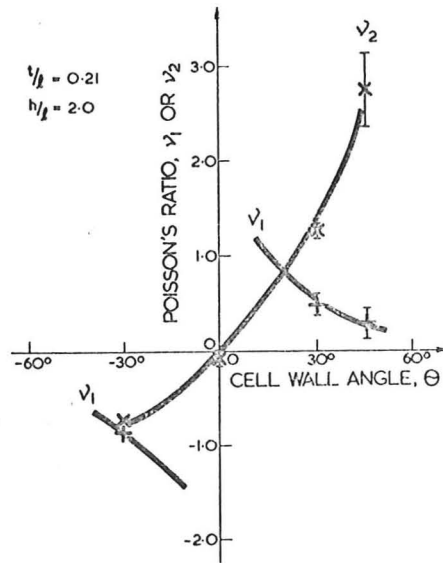
Fig. 4.17 ν_1 and ν_2 as a function of θ for rubber models.
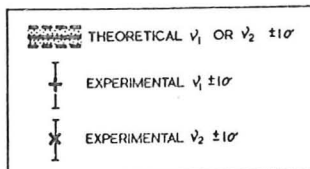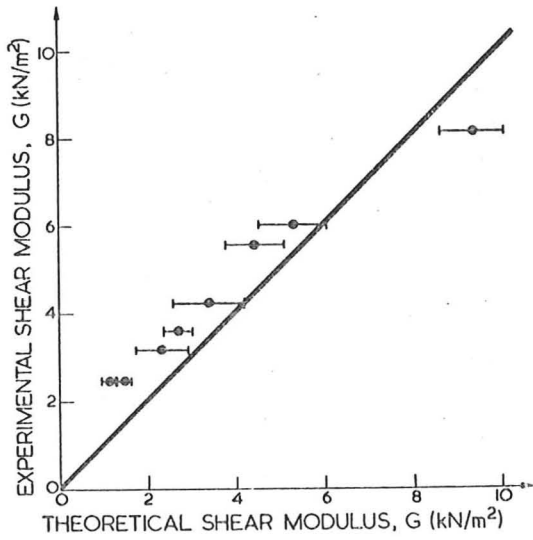
Fig. 4.18   Theoretical and experimental values of G for rubber models.
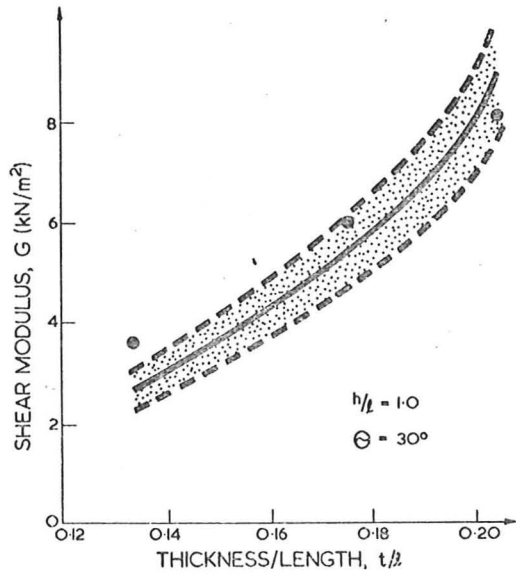
Fig. 4.19   G as a function of t/ℓ for rubber models.
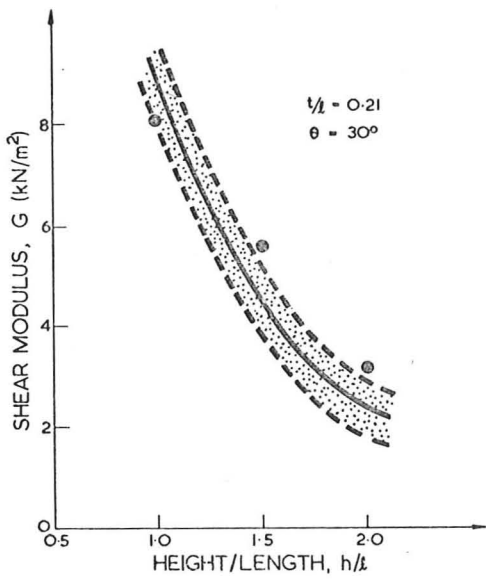
Fig. 4.20   G as a function of h/ℓ for rubber models.

Fig. 4.21   G as a function of θ for rubber models.

THEORETICAL G ±1σ

EXPERIMENTAL G
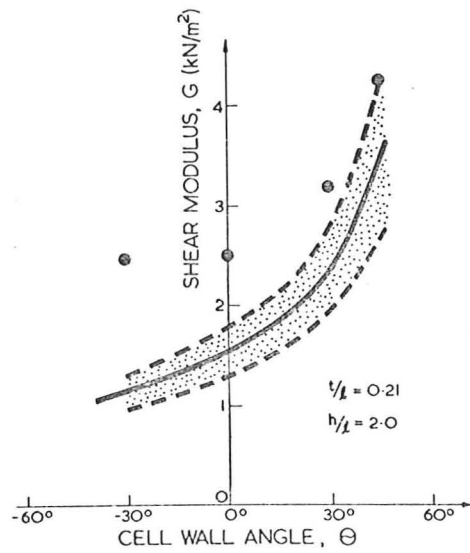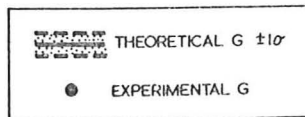
4.3 Non-Linear Elastic Behaviour

The elastic buckling stress, σ^{*}_{el}, was measured for the rubber models in the way shown in Fig. 4.1 The results are plotted, as a function of cell geometry, in Figs. 4.22 to 4.25. Agreement is good.

4.4 Plastic Collapse

The metal models were compressed until they showed permanent plastic deformation (the stress-strain curve resembles that shown in Fig. 4.1), and the collapse stresses $(\sigma^{*}_1)_{pl}$ and $(\sigma^{*}_2)_{pl}$ were calculated from the plateau load. The results are compared with the theory of Section 3.3 in Figs. 4.26 and 4.27. The stresses $(\sigma^{*}_1)_{pl}$ and $(\sigma^{*}_2)_{pl}$ are shown as a function of t/ℓ, h/ℓ and θ in Figs. 4.28 to 4.32. Agreement is less good than for the rubber models, but still satisfactory.

Photographs of deformed cellular structures

Photographs of deformed rubber models and metal models are shown in Figs. 4.33 and 4.34.

4.5 Discussion and Summary of the Study of Two-Dimensional Cellular Materials

Theory

The results of the calculations of Chapter 3 are summarised in Tables 4.3 and 4.4, in two forms. The first lists the results in terms of the cell geometry (t, ℓ, h, θ). The second lists them in terms of the relative density and cell shape $(\rho/\rho_s, h/\ell, \theta)$. The results can be written as:
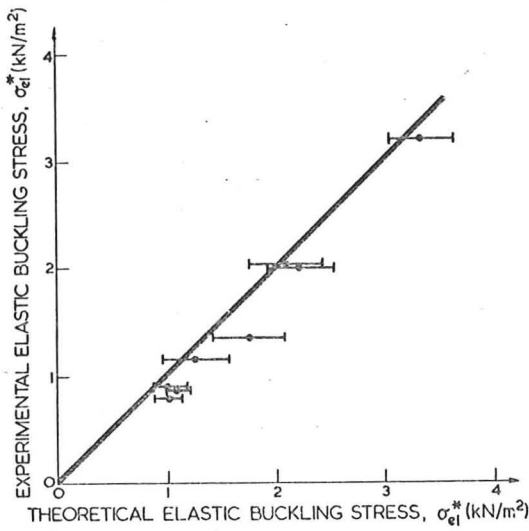
Fig. 4.22 Theoretical and experimental values of σ_{el}^* for rubber models.
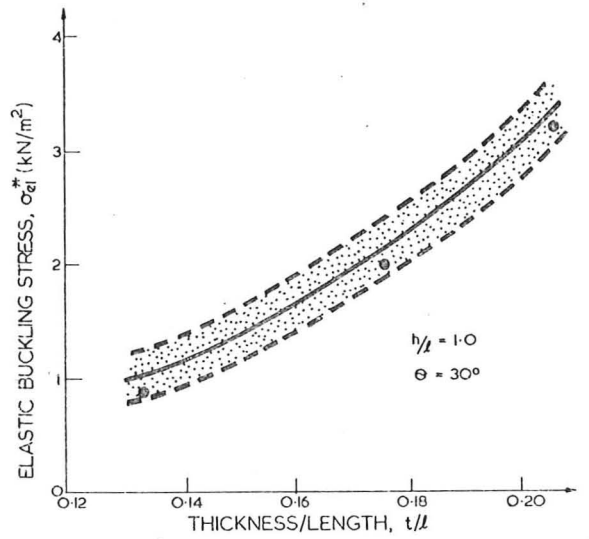
Fig. 4.23 σ_{el}^* as a function of t/ℓ for rubber models.
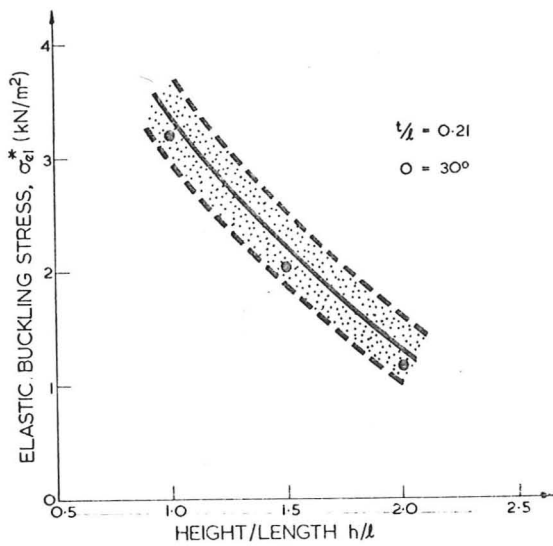
Fig. 4.24 σ_{el}^* as a function of h/ℓ for rubber models.
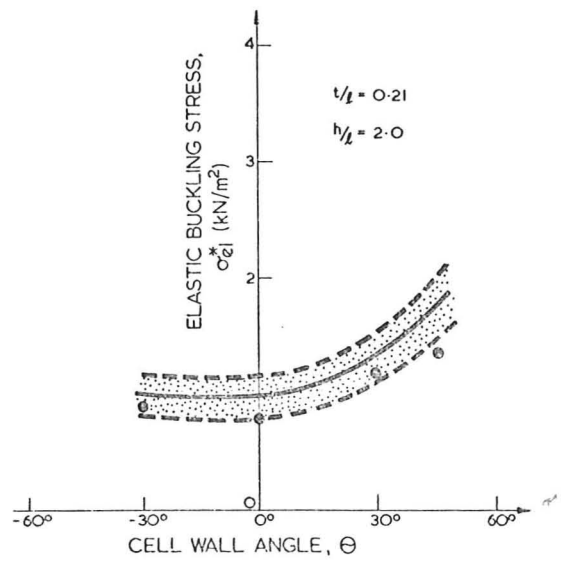
Fig. 4.25 σ_{el}^* as a function of θ for rubber models.

THEORETICAL $\sigma_{el}^* \pm 1\sigma$
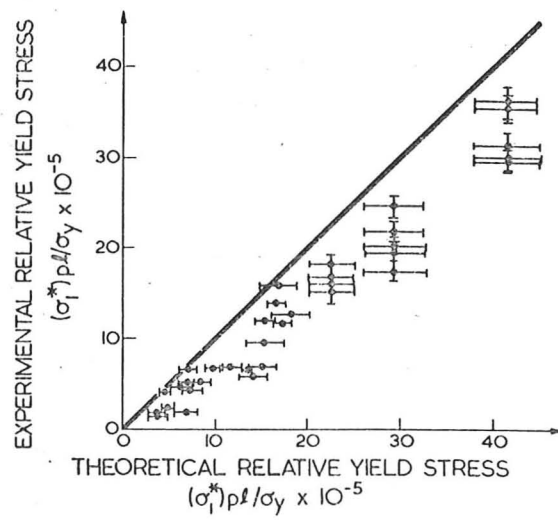
EXPERIMENTAL σ_{el}^*

Fig. 4.26   Theoretical and experimental
              values of $(\sigma_1^*)_{pl}/\sigma_y$.
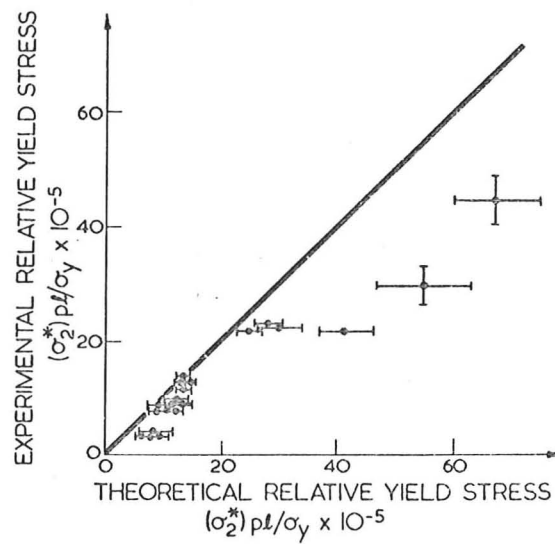
Fig. 4.27   Theoretical and experimental values
              of $(\sigma_2^*)_{pl}/\sigma_y$.
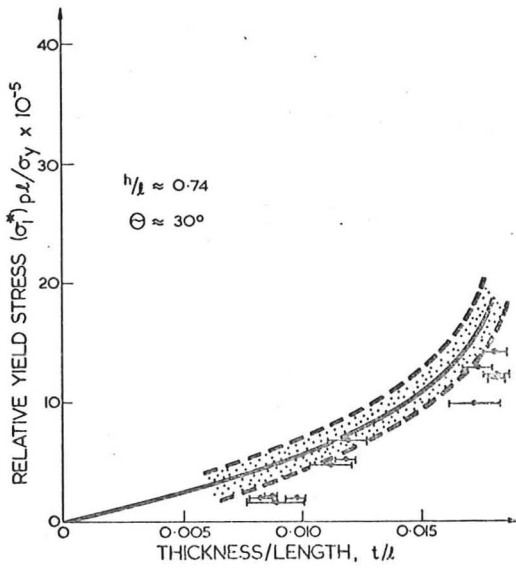
Fig. 4.28 $(\sigma_1^*)_{pl}/\sigma_y$ as a function of t/ℓ.
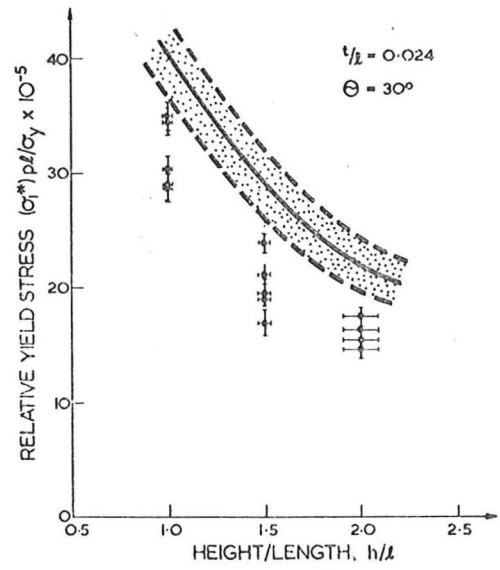
Fig. 4.29 $(\sigma_1^*)_{pl}/\sigma_y$ as a function of h/ℓ.
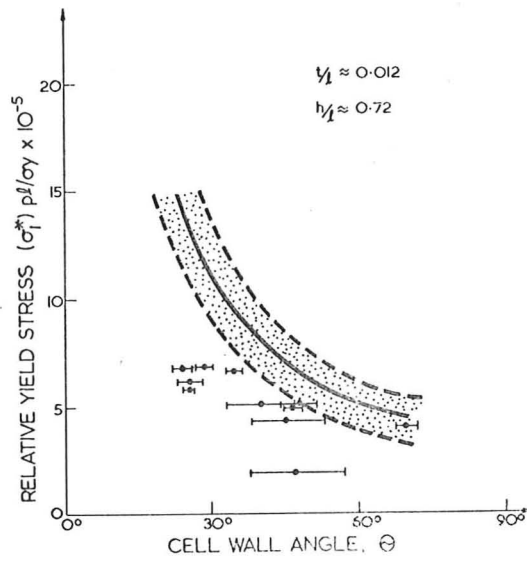
Fig. 4.30 $(\sigma_1^*)_{pl}/\sigma_y$ as a function of θ.
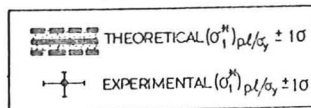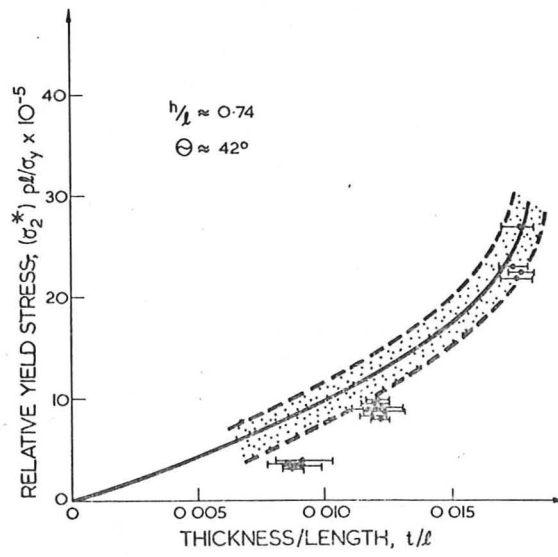
Fig. 4.31 $(\sigma_2^*)_{p1}/\sigma_y$ as a function of t/ℓ.
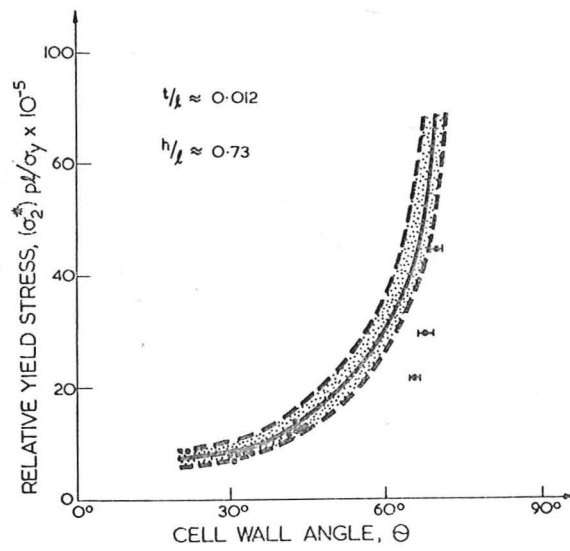
Fig. 4.32 $(\sigma_2^*)_{p1}/\sigma_y$ as a function of θ.
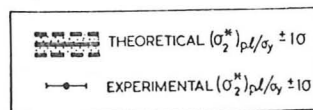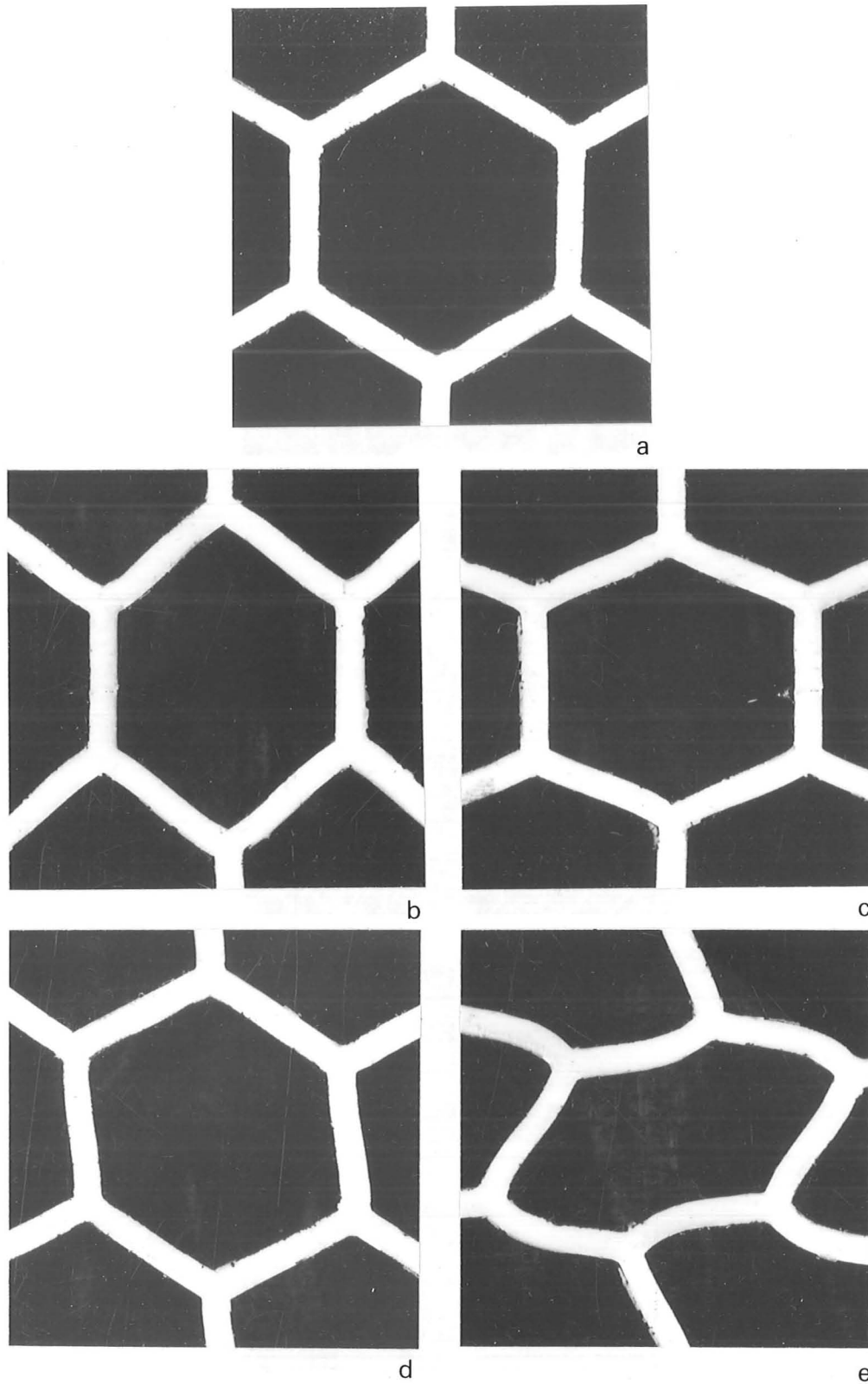
Fig. 4.33   Photographs of a rubber model showing deformation
under various loading conditions: (a) unloaded
(b) compression in the X_1 direction (c) compression
in the X_2 direction (d) shear (e) elastic buckling
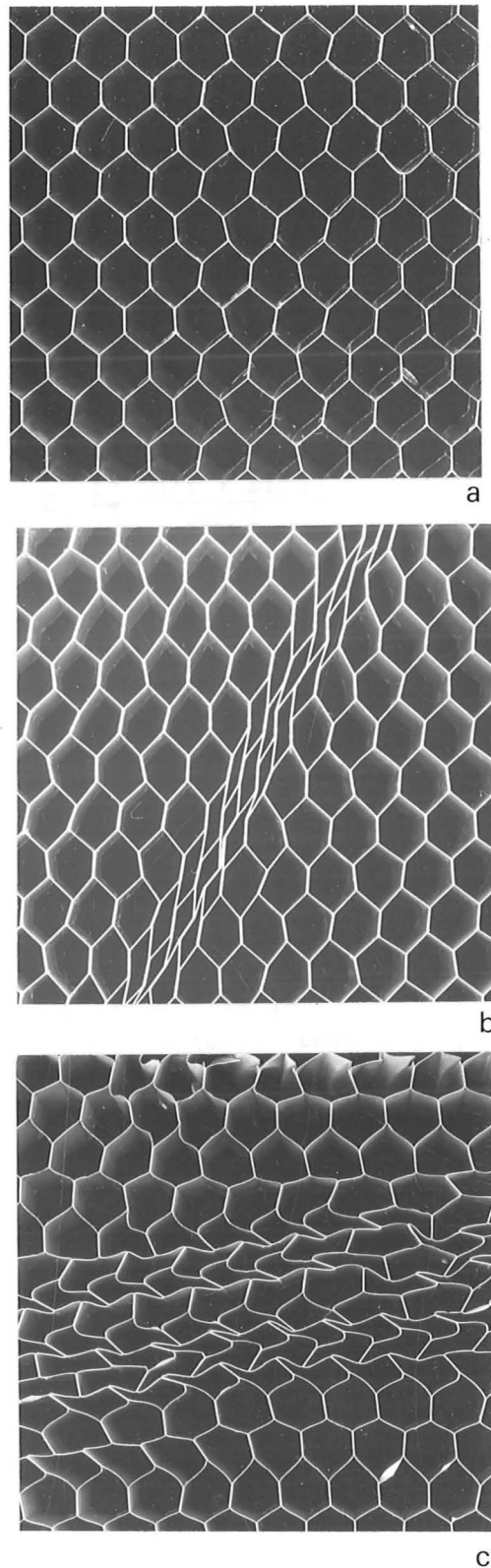
Fig. 4.34   Photographs of aluminium honeycomb specimens
(a) unloaded (b) showing plastic deformation on
loading in the X_1 direction (c) showing plastic
deformation on loading in the X_2 direction

TABLE 4.3:

PROPERTIES OF TWO-DIMENSIONAL CELLULAR STRUCTURES
NEGLECTING AXIAL AND SHEAR DEFORMATIONS

	PROPERTY	GENERAL TWO-DIMENSIONAL HEXAGONAL CELLULAR STRUCTURE	REGULAR HEXAGONAL STRUCTURE
LINEAR ELASTIC PROPERTIES	E_1	$E_s \dfrac{t^3}{\ell^3} \dfrac{\cos\theta}{(h/\ell + \sin\theta)\,\sin^2\theta}$	$\dfrac{4}{\sqrt{3}} E_s \dfrac{t^3}{\ell^3}$
	E_2	$E_s \dfrac{t^3}{\ell^3} \dfrac{(h/\ell + \sin\theta)}{\cos^3\theta}$	
	ν_1	$\dfrac{\cos^2\theta}{(h/\ell + \sin\theta)\,\sin\theta}$	1
	ν_2	$\dfrac{(h/\ell + \sin\theta)\,\sin\theta}{\cos^2\theta}$	
	G	$E_s \dfrac{t^3}{\ell^3} \dfrac{(h/\ell + \sin\theta)}{(h/\ell)^2\,(2h/\ell + 1)\,\cos\theta}$	$\dfrac{1}{\sqrt{3}} E_s \dfrac{t^3}{\ell^3}$
ELASTIC BUCKLING	σ^*_{el}	$E_s \dfrac{t^3}{\ell^3} \dfrac{(\beta^*)^2}{6\,(h/\ell)^2\,\cos\theta}$ See note 2	$0.22\, E_s \dfrac{t^3}{\ell^3};\ \dfrac{E_2}{10}$
PLASTIC COLLAPSE	$(\sigma^*_1)_{pl}$	$\sigma_y \dfrac{t^2}{\ell^2} \dfrac{1}{2\,(h/\ell + \sin\theta)\,\sin\theta}$	$\dfrac{2}{3} \dfrac{t^2}{\ell^2} \sigma_y$
	$(\sigma^*_2)_{pl}$	$\sigma_y \dfrac{t^2}{\ell^2} \dfrac{1}{2\,\cos^2\theta}$	

Notes: 1. $\dfrac{\rho}{\rho_s} = \dfrac{t}{\ell} \dfrac{(h/\ell + 2)}{2\cos\theta\,(h/\ell + \sin\theta)} = \dfrac{2}{\sqrt{3}} \dfrac{t}{\ell}$ for regular hexagons

   2.   Values of β^* are given in Table 3.1.

TABLE 4.4:

PROPERTIES OF TWO-DIMENSIONAL CELLULAR STRUCTURES
IN TERMS OF RELATIVE DENSITY

PROPERTY		GENERAL TWO-DIMENSIONAL HEXAGONAL CELLULAR STRUCTURE	REGULAR HEXAGONAL STRUCTURE
LINEAR ELASTIC PROPERTIES	E_1	$E_s \dfrac{8 \cos^4\theta \ (h/\ell + \sin\theta)^2}{(2 + h/\ell)^3 \sin^2\theta} \left(\dfrac{\rho}{\rho_s}\right)^3$	$\dfrac{3}{2} E_s \left(\dfrac{\rho}{\rho_s}\right)^3$
	E_2	$E_s \dfrac{8 \ (h/\ell + \sin\theta)^4}{(2 + h/\ell)^3} \left(\dfrac{\rho}{\rho_s}\right)^3$	
	ν_1	$\dfrac{\cos^2\theta}{(h/\ell + \sin\theta) \ \sin\theta}$	1
	ν_2	$\dfrac{(h/\ell + \sin\theta) \ \sin\theta}{\cos^2\theta}$	
	G	$E_s \dfrac{8 \cos^2\theta \ (h/\ell + \sin\theta)^4}{(h/\ell)^2 \ (2 \ h/\ell + 1)(2 + h/\ell)^3} \left(\dfrac{\rho}{\rho_s}\right)^3$	$\dfrac{3}{8} E_s \left(\dfrac{\rho}{\rho_s}\right)^3$
ELASTIC BUCKLING	σ^*_{el}	$E_s \dfrac{4 \ (\beta^*)^2 \cos^2\theta \ (h/\ell + \sin\theta)^3}{3 \ (h/\ell)^2 \ (2 + h/\ell)^3} \left(\dfrac{\rho}{\rho_s}\right)^3$	$0.14 \ E_s \left(\dfrac{\rho}{\rho_s}\right)^3$; $\dfrac{E}{10}$
PLASTIC COLLAPSE	$(\sigma^*_1)_{pl}$	$\sigma_y \dfrac{2 \cos^2\theta \ (h/\ell + \sin\theta)}{\sin\theta \ (2 + h/\ell)^2} \left(\dfrac{\rho}{\rho_s}\right)^2$	$\dfrac{1}{2} \sigma_y \left(\dfrac{\rho}{\rho_s}\right)^2$
	$(\sigma^*_2)_{pl}$	$\sigma_y \dfrac{2 \ (h/\ell + \sin\theta)^2}{(2 + h/\ell)^2} \left(\dfrac{\rho}{\rho_s}\right)^2$	

Note: Values of β^* are given in Table 3.1

$$\frac{E_1}{E_s} = C_1 \left(\frac{\rho}{\rho_s}\right)^3$$

$$\frac{E_2}{E_s} = C_2 \left(\frac{\rho}{\rho_s}\right)^3 \qquad \text{with} \quad C_1 \, C_3 = C_2 \, C_4$$
$$\text{(the "reciprocal theorem")}$$

$$\nu_1 = C_3$$

$$\nu_2 = C_4$$

$$\frac{G}{E_s} = C_5 \left(\frac{\rho}{\rho_s}\right)^3$$

$$\frac{\sigma^*_{el}}{E_s} = C_6 \left(\frac{\rho}{\rho_s}\right)^3$$

$$\frac{(\sigma^*_1)_{pl}}{\sigma_y} = C_7 \left(\frac{\rho}{\rho_s}\right)^2$$

$$\frac{(\sigma^*_2)_{pl}}{\sigma_y} = C_8 \left(\frac{\rho}{\rho_s}\right)^2$$

where C_1 to C_8 are constants which depend only on the initial geometry of the cells. The mechanical response is thus determined by three quantities: a cell geometry parameter (C), a property of the solid of which the cells are made (E_s or σ_y) and the relative density (ρ/ρ_s), raised to the power 2 or 3.

Experiments

The experiments were designed to test, as far as possible, all aspects of the equations listed on the tables. All eight of the mechanical properties $(E_1, E_2, \nu_1, \nu_2, G, \sigma^*_{e1}, (\sigma^*_1)_{pl}$ and $(\sigma^*_2)_{pl})$ have been measured and their dependence on cell characteristics investigated. In particular, the density $(t/\ell$ or $\rho/\rho_s)$ has been varied, the cell geometry $(h/\ell$ and $\theta)$ has been systematically varied, and both elastic and plastic cells have been tested, involving different values of material properties (E_s, σ_y).

The results speak for themselves. There can be little question that the theory adequately describes the elastic and plastic properties of two-dimensional cells. The discrepancies are caused by experimental error in measuring cell geometry, (many properties are very sensitive to cell geometry: E_1, for instance varies as t^3), variations in material properties (such as σ_y) or difficulty in defining the "dead", undeformable volume at the nodes.

Applications

This complete analysis of two-dimensional cells and its experimental confirmation is new, and has obvious applications in guiding design with such materials (such as honeycomb sandwich panels, packaging and certain woods).

There is a more important application. By identifying the processes which determine stiffness and strength in foams and the dimensionless groupings of the variables involved, we can now approach the analysis of three-dimensional foams. Their geometry is much more complicated, so much so

that a complete mechanical analysis (like that used here) seems out of the question. But a dimensional analysis appears attractive, and will be pursued in Chapter 5.

CHAPTER 5

THREE-DIMENSIONAL CELLULAR MATERIALS - THEORETICAL ANALYSIS

The behaviour of idealized two-dimensional cellular materials has been presented in Chapters 3 and 4. The results showed that: the elastic moduli are related to the *bending* stiffness of the members; that elastic collapse is caused by *elastic buckling*; and that plastic collapse is initiated by the formation of *plastic hinges* in the members. We now consider how each of these modes of deformation affects the behaviour of three-dimensional cellular materials. This behaviour is examined at two levels: the first analysis, based on dimensional arguments, leads to simple expressions of the form:

$$\frac{\text{Foam property}}{\text{Cell wall property}} = C \ (\text{Relative density})^n$$

for the elastic moduli and the elastic and plastic collapse stresses. This simple analysis, however, is deficient in two ways. The beam bending formulae neglect both shear and axial displacements, and the expression for relative density neglects the contribution of the corners of the cells: both of these effects become significant at high values of t/ℓ. In Section 5.4 we correct for them using a model of pentagonal dodecahedral cells. This leads to a more complete description of behaviour which is remarkably close to the first simple approximation.

5.1 Basic Dimensional Analysis of Mechanical Behaviour

Models for Open and Closed Cell Foams

At the simplest level, an open cell foam can be modelled as a cubic array of members of length, ℓ, and square cross section of

side t (Fig. 5.1). The relative density of the cell, ρ/ρ_s, and the second moment of area of a member, I, are related to the beam dimensions by:

$$\rho/\rho_s \propto (t/\ell)^2 \tag{5.1}$$

and
$$I \propto t^4 \tag{5.2}$$

We note that the adjoining cells are staggered with respect to the first cell so that their members meet the first cell's members at their midpoints. It is this feature of the model which gives rise to bending deformations.

Closed cell foams can be modelled in a similar way, replacing the square struts with square plates of side, ℓ, and thickness, t (Fig. 5.2). Adjoining cells are again staggered. For this model, we find:

$$\rho/\rho_s \propto t/\ell \tag{5.3}$$

and
$$I \propto \ell t^3 \tag{5.4}$$

Linear Elastic Behaviour

Young's modulus is calculated from the linear elastic deflection, δ, of a cantilevered beam of length, ℓ, under an end load, F. This deflection is proportional to $F\ell^3/E_s I$ where E_s is the Young's modulus of the material the beam is made up of (Fig. 5.3). When a uniaxial stress is applied to a cellular material so that each cell wall transmits a force F, its members bend, and the linear elastic deflection is similarly proportional to $F\ell^3/E_s I$. The overall stress and strain in the material are proportional to F/ℓ^2 and δ/ℓ

$$\frac{\rho}{\rho_s} \, \alpha \left(\frac{t}{\ell}\right)^2$$

$$I \, \alpha \, t^4$$
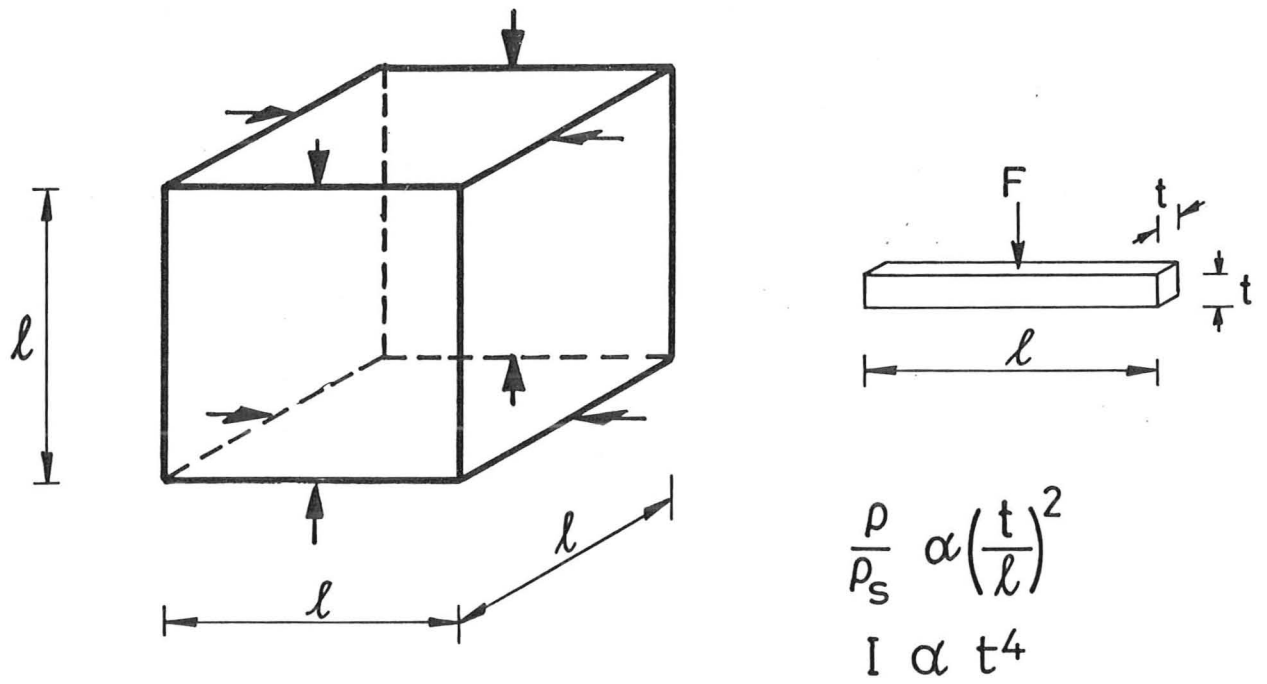
Fig. 5.1   Cubic model of open cell foams

$$F = w\ell$$

$$\frac{\rho}{\rho_s} \, \alpha \, \frac{t}{\ell}$$

$$I \, \alpha \, \ell t^3$$
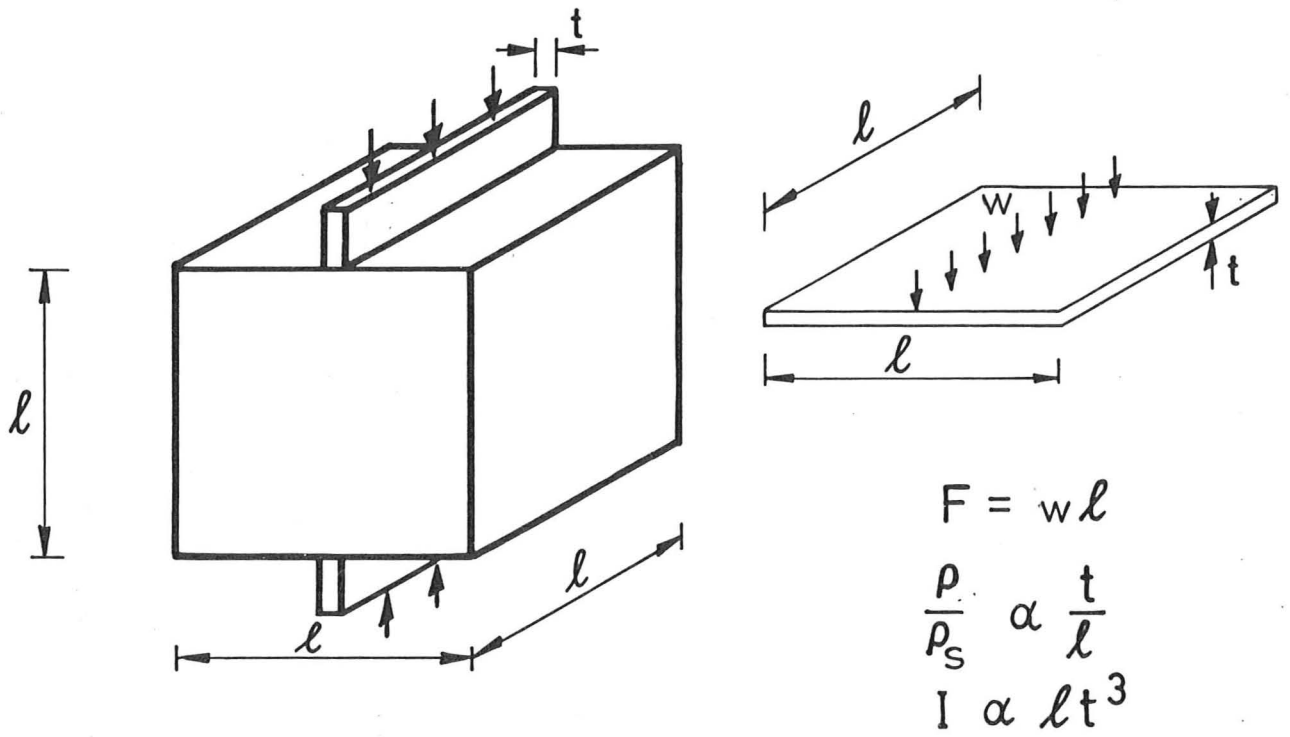
Fig. 5.2   Cubic model of closed cell foams

$$\delta \propto \frac{F\ell^3}{E_s I}$$
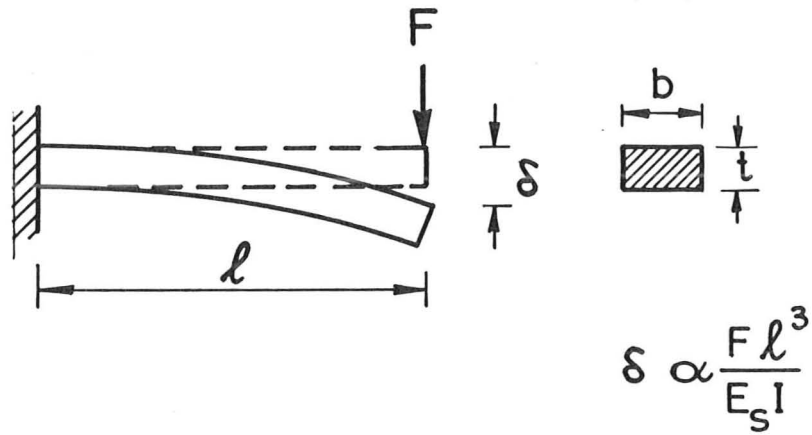
Fig. 5.3 Beam deflection for a cantilever.

$$F_{cr} = \frac{n^2 \pi^2 E_s I}{\ell^2}$$
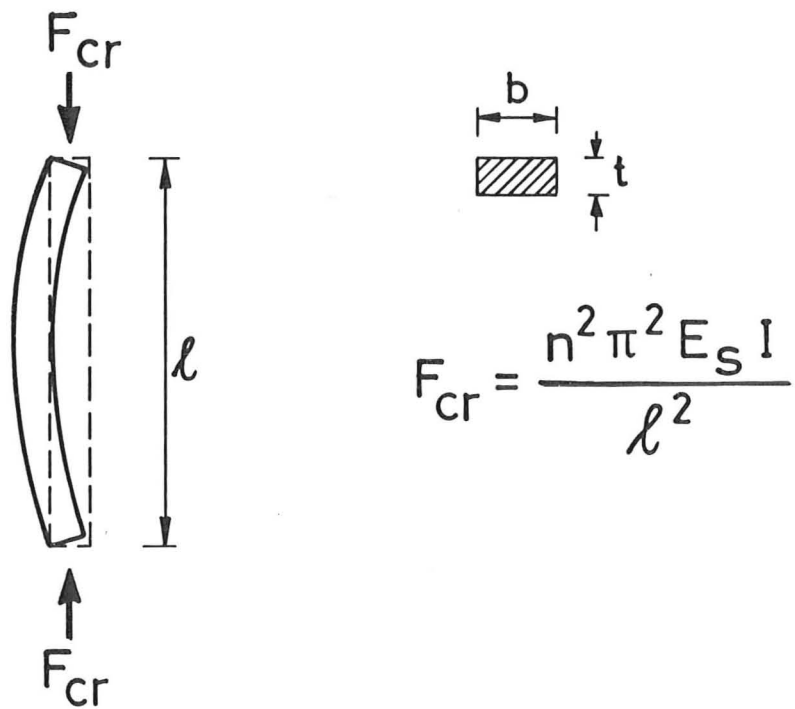
Fig. 5.4 Critical buckling load for a column.

respectively. It follows immediately then, that Young's modulus for the foam is given by:

$$\frac{E}{E_s} = \frac{CI}{\ell^4}$$ (5.5)

and $E/E_s = C (\rho/\rho_s)^2$ for open cell foams while $E/E_s = C (\rho/\rho_s)^3$ for closed cell foams.

Poisson's ratio, ν, is defined as the negative ratio of lateral to applied strain. Since both these deflections are proportional to a bending deflection per cell length, their ratio is a constant. Poisson's ratio is solely a function of cell geometry and is independent of relative density.

The shear modulus is calculated in a similar way to Young's modulus. If a shear stress, τ, is applied to a foam, the cell members again respond by bending. Since the bending deflection, δ, is proportional to $F\ell^3/E_s I$ and the overall stress and strain are proportional to F/ℓ^2 and δ/ℓ respectively,

$$\frac{G}{E_s} = \frac{CI}{\ell^4}$$ (5.6)

It follows that G/E_s is proportional to $(\rho/\rho_s)^2$ for open cell foams and $(\rho/\rho_s)^3$ for closed cell foams.

Non-Linear Elastic Behaviour

Elastic collapse occurs in cellular materials when some members buckle elastically. The critical load at which a column of length, ℓ, Young's modulus, E_s, and second moment of area, I, buckles

is given by Euler's formula, (Fig. 5.4):

$$F_{cr} = \frac{n^2 \pi^2 E_s I}{\ell^2}$$

where the factor n^2 describes the degree of constraint at the ends of the column (see Section 3.2). If this load is reached for an entire layer of cells, they will buckle and so the foam will collapse elastically. The stress at which this occurs, σ^*_{el}, is proportional to F_{cr}/ℓ^2 giving:

$$\frac{\sigma^*_{el}}{E_s} = \frac{CI}{\ell^4} \tag{5.7}$$

or $\sigma^*_{el}/E_s = C(\rho/\rho_s)^2$ and $\sigma^*_{el}/E_s = C (\rho/\rho_s)^3$ for open and closed cells respectively.

Plastic Behaviour

Cellular materials may collapse by a second mechanism if the cell wall material has a plastic yield point: they may collapse plastically. Plastic collapse occurs when every point on a cross-section of a member has reached the plastic yield stress, σ_y, of the cell wall material. For square sections of thickness, t, the fully plastic moment is (Fig. 5.5):

$$M_p = \frac{\sigma_y t^3}{4}$$

If a force F acts in bending on a member of length ℓ in a cellular material, the maximum moment in the member is proportional to $F\ell$. The overall plastic collapse stress for the foam, σ^*_{pl}, is proportional to F/ℓ^2. Combining these expressions gives:
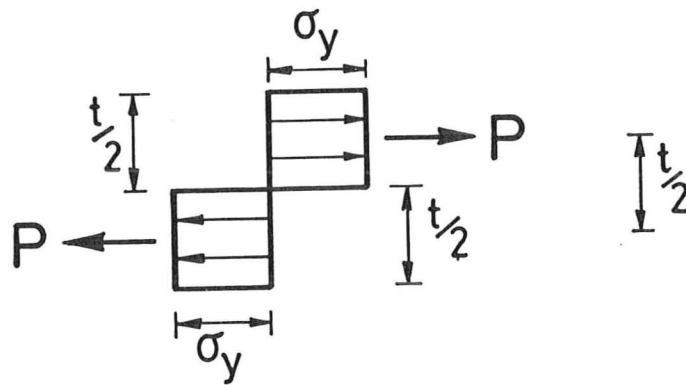
$$M_p = \frac{Pt}{2} = \frac{\sigma_y t^3}{4}$$

Fig. 5.5 Fully plastic moment for a square sectioned beam.

$$\frac{\sigma^*_{p1}}{\sigma_y} = C \left(\frac{t}{\ell}\right)^3 \tag{5.8}$$

For open and closed cells, this becomes, respectively,

$$\sigma^*_{p1}/\sigma_y = C (\rho/\rho_s)^{3/2} \quad \text{and} \quad \sigma^*_{p1}/\sigma_y = C (\rho/\rho_s)^2.$$

The results of Section 5.1 are summarized in Table 5.1.

TABLE 5.1:   Mechanical Properties of Three-Dimensional
Cellular Materials

PROPERTY	OPEN CELLS	CLOSED CELLS
ρ/ρ_s	$C (t/\ell)^2$	$C (t/\ell)$
E/E_s	$C (\rho/\rho_s)^2$	$C (\rho/\rho_s)^3$
ν	C	C
G/E_s	$C (\rho/\rho_s)^2$	$C (\rho/\rho_s)^3$
$\sigma^*_{e\ell}/E_s$	$C (\rho/\rho_s)^2$	$C (\rho/\rho_s)^3$
σ^*_{p1}/σ_y	$C (\rho/\rho_s)^{3/2}$	$C (\rho/\rho_s)^2$

5.2   Anisotropy in Cellular Materials

Two-dimensional cellular materials, as in Fig. 3.1, are iso-
tropic in their plane when $h = \ell$ and $\theta = 30^o$: two independent
elastic constants are required to fully describe the linear elastic
behaviour of such materials.   If h does not equal ℓ, the material
is elastically *anisotropic* and has four independent elastic constants
(see Section 3.1).   We define the shape anisotropy of the cell, A,

as the ratio of h/ℓ, for a constant cell wall angle, θ. Using the equations of Table 4.3 we can calculate how anisotropy affects the material properties; for example, we find:

$$\frac{E_1}{E_2} = \frac{9}{4\ (A + \frac{1}{2})^2}$$

for $\theta = 30^\circ$. We note that E_1/E_2 varies rapidly with A: for instance, it decreases from 1 for isotropic structures (A = 1) to 0.56 for A = 1.5.

Three-dimensional cellular materials are also sometimes aniso-tropic. For example, when polymeric materials are foamed, there is a tendency for the cells to elongate in the direction of the foam rise. Fig. 5.6 shows such an elongated cell: the X_3 axis is the rise direction. This cell is isotropic in the $X_1 X_2$ plane only and has 5 independent elastic constants (see Ch. 3). For loading in a par-ticular direction, the relationships of Section 5.1 are still valid; for example:

$$\frac{E_1}{E_s} = C_1 \left(\frac{\rho}{\rho_s}\right)^2$$

and

$$\frac{E_3}{E_s} = C_3 \left(\frac{\rho}{\rho_s}\right)^2$$

for an open cell foam. But the geometrical constants of proportionality, C_1 and C_3, now depend on the shape anisotropy, A. We now examine this dependence in more detail.
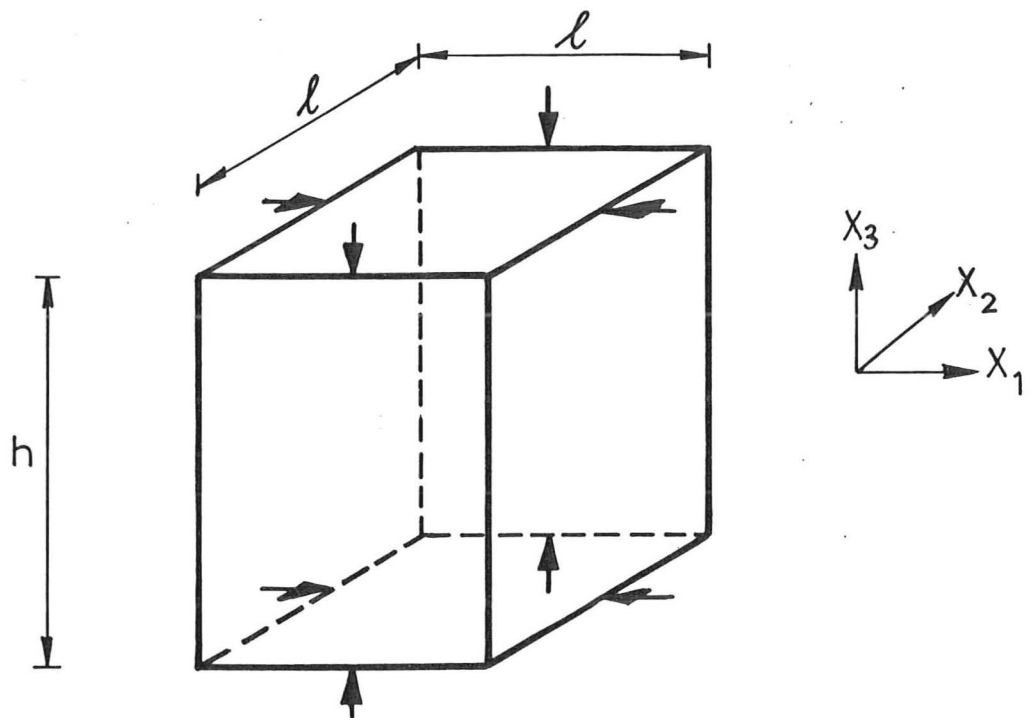
Fig. 5.6 Cell model for an anisotropic material.

The ratio of the Young's moduli in the X_1 and X_3 directions at a given relative density are now given by:

$$\frac{E_1}{E_3} \propto \frac{F\ell}{\delta_1 h \ell} \frac{\delta_3 \ell^2}{Fh} = K_1 A^{-5} \tag{5.9}$$

The ratio of Poisson's ratio for the two load directions is obtained in a similar way:

$$\frac{\nu_1}{\nu_3} \propto \frac{\delta_3 \ell}{\delta_1 h} \frac{\ell}{\delta_1} \frac{\delta_3}{h} = K \left(\frac{\delta_3}{\delta_1}\right)^2 \left(\frac{\ell}{h}\right)^2$$

The ratio of the deflections in the X_1 and X_3 directions depends only on the angles the members of the cell make with the axes, and thus can be incorporated into the constant of proportionality, giving:

$$\frac{\nu_1}{\nu_3} = K_2 A^{-2} \tag{5.10}$$

The ratio of the shear moduli, G_{12}/G_{13}, is:

$$\frac{G_{12}}{G_{13}} = \frac{F\ell}{\ell h \delta_1} \frac{\delta_3 \ell^2}{Fh} = K \frac{h}{\ell} = KA \tag{5.11}$$

The elastic collapse stresses for loading in the X_1 and X_3 directions give:

$$\frac{\sigma^*_{el_1}}{\sigma^*_{el_3}} \propto \frac{h^2}{\ell^2} \frac{\ell^2}{\ell h} = KA \qquad (5.12)$$

while the ratio of the plastic collapse stresses is:

$$\frac{\sigma^*_{pl_1}}{\sigma^*_{pl_3}} \propto \frac{M_p}{h^2 \ell} \frac{\ell^3}{M_p} = KA^{-2} \qquad (5.13)$$

The dependence of each material property on the degree of aniso-tropy is given in Table 5.2. Young's modulus is affected the most by anisotropy: it varies as A^{-5}.

TABLE 5.2: Effect of Anisotropy on Material Properties

$\dfrac{E_1}{E_3}$	$\dfrac{\nu_1}{\nu_3}$	$\dfrac{G_{12}}{G_{13}}$	$\dfrac{\sigma^*_{el_1}}{\sigma^*_{el_3}}$	$\dfrac{\sigma^*_{el_1}}{\sigma^*_{pl_3}}$
A^{-5}	A^{-2}	A	A	A^{-2}

5.3 Contribution of the Faces of Closed Cell Foams to Mechanical Properties

During the foaming process the polymer tends to accumulate in the edges and corners of each cell. In open cell foams, the cell face has become so thin that it has burst and all the polymer is in the cell edges and corners. Even in closed cell foams the faces may be so thin that they contribute very little to the stiffness and strength of the foam.

Previously, we modelled closed cell foams as square plates of side length ℓ and thickness t. In order to examine the contribution of the faces of the cell to stiffness and strength, we now model closed cell foams as square faces of thickness t_f, surrounded by edges of thickness, t_e (Fig. 5.7 a). We also define a new parameter, ϕ, equal to the ratio of the volume of polymer in the face to that in the edge:

$$\phi = \frac{V_{face}}{V_{edge}} = \frac{t_f \, \ell}{t_e^2} \tag{5.14}$$

For an open cell foam ϕ is zero; for a closed cell foam with walls and edges of equal thickness, $\phi = \ell/t$. The relative density of this new cell model is then:

$$\rho/\rho_s \propto (t_e/\ell)^2 \, (1 + \phi) \tag{5.15}$$

We have already seen that the stiffness of a closed cell foam is governed by (Fig. 5.7 b) the beam bending equation:

$$\frac{F}{\delta} \propto \frac{E_s \, I}{\ell^3}$$
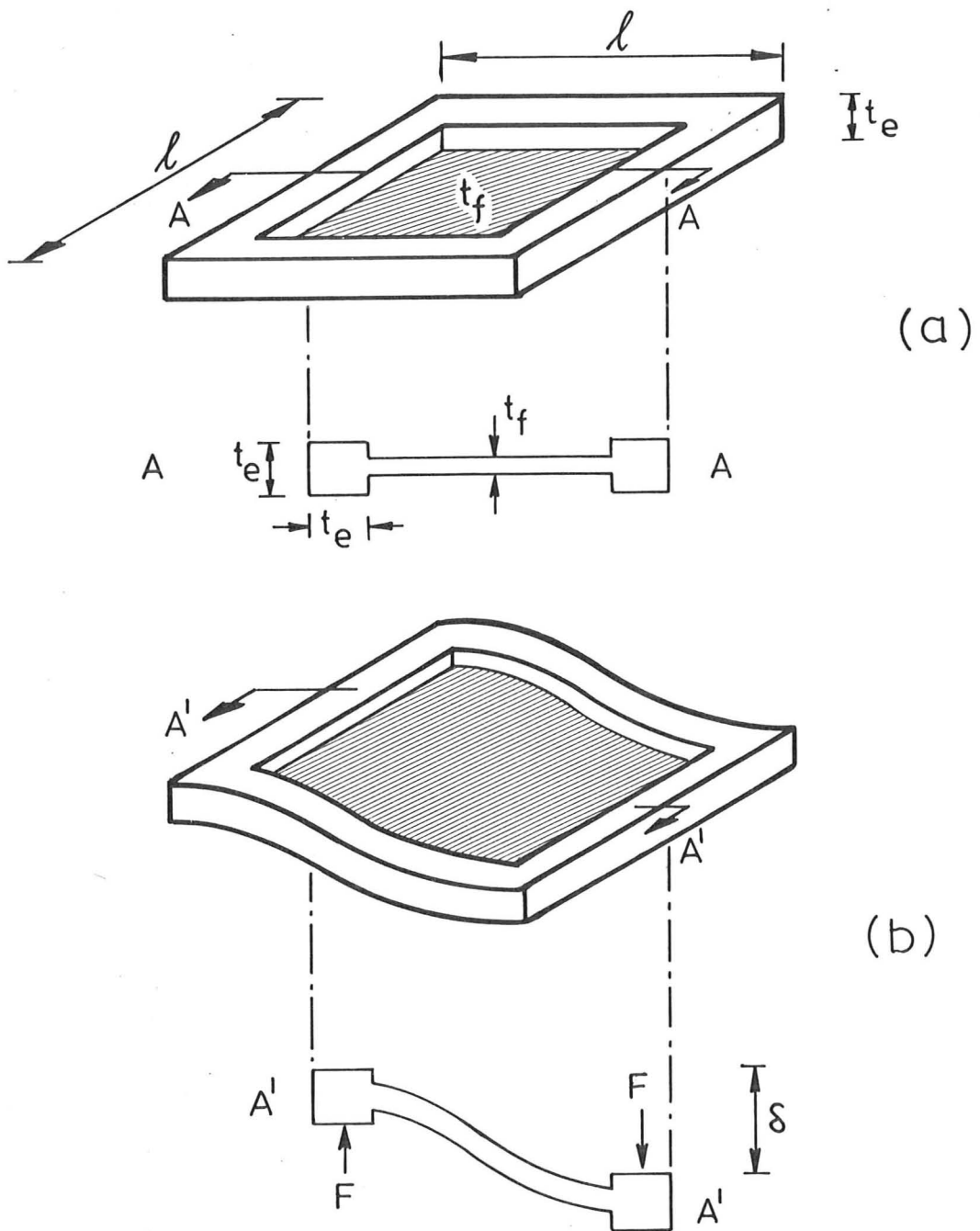
$$\phi = \frac{\text{Vol. face}}{\text{Vol. edge}} = \frac{t_f \ell}{t_e^2}$$

Fig. 5.7 (a) Model for closed cell foams with faces
and edges of different thicknesses.
(b) Bending deflection of model.

The moment of inertia of the cross-section is now:

$$I \propto t_e^4 + t_f^3 \ell$$

This leads to the Young's modulus for the foam:

$$E \propto \frac{F}{\delta \ell} \propto \frac{E_s (t_e^4 + t_f^3 \ell)}{\ell^4}$$

Substituting $t_f = \frac{\phi t_e^2}{\ell}$ gives:

$$\frac{E}{E_s} \propto \left(\frac{t_e}{\ell}\right)^4 \left[1 + \left(\frac{t_e}{\ell}\right)^2 \phi^3\right].$$

Relating t_e/ℓ to ρ/ρ_s (equation 5.15) gives:

$$\frac{E}{E_s} \propto \left(\frac{\rho}{\rho_s}\right)^2 \frac{1}{(1 + \phi)^2} \left[1 + \frac{\rho}{\rho_s} \frac{\phi^3}{1 + \phi}\right] \qquad (5.16)$$

The relative modulus is plotted against the relative density for various values of ϕ in Fig. 5.8. For $\phi = 0$, that is, open cell foams, $E/E_s \propto (\rho/\rho_s)^2$, as before. For large ϕ, equivalent to the square plate model, $E/E_s \propto (\rho/\rho_s)^3$, as before.

Poisson's ratio is independent of relative denisty and therefore, the distribution of the polymer between the edges and faces does not affect it. The shear modulus of a foam is related to bending stiffness in exactly the same way as Young's modulus and thus:

$$\frac{G}{E_s} \propto \left(\frac{\rho}{\rho_s}\right)^2 \frac{1}{(1 + \phi)^2} \left[1 + \frac{\rho}{\rho_s} \frac{\phi^3}{1 + \phi}\right] \qquad (5.17)$$
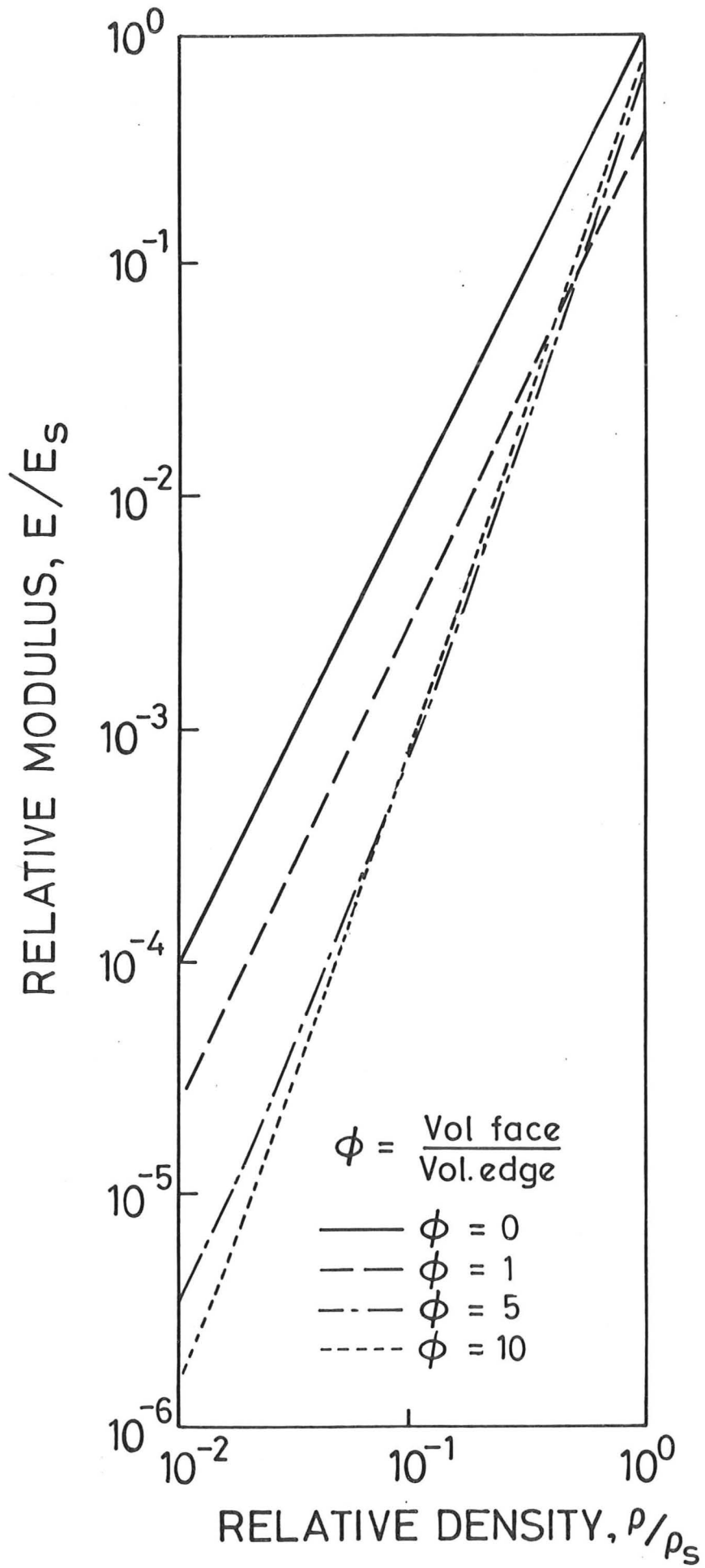
Fig. 5.8 Relative Young's modulus against relative density as a function of φ

The elastic collapse stress is given by:

$$\sigma^*_{el} \propto \frac{E_s I}{\ell^4}$$

Again, this is the same relationship as for Young's modulus and

$$\frac{\sigma^*_{el}}{E_s} \propto \left(\frac{\rho}{\rho_s}\right)^2 \frac{1}{(1 + \phi)} \left[1 + \frac{\rho}{\rho_s} \frac{\phi^3}{1 + \phi}\right] \tag{5.18}$$

Plastic collapse across a section occurs when both the face and edge have yielded completely.

$$\sigma^*_{pl} \propto \frac{F}{\ell^2} \propto \frac{M_{p\ edge} + M_{p\ face}}{\ell^3}$$

From Section 5.1:

$$M_p \propto \sigma_y t^3$$

So:

$$\sigma^*_{pl} \propto \frac{\sigma_y (t_e^3 + t_f^2 \ell)}{\ell^3}$$

Combining with equations (5.14) and (5.15):

$$\frac{\sigma^*_{pl}}{\sigma_y} \propto \left(\frac{\rho/\rho_s}{1 + \phi}\right)^{3/2} \left[1 + \phi^2 \left(\frac{\rho/\rho_s}{1 + \phi}\right)^2\right] \tag{5.19}$$

This is plotted in Fig. 5.9. In the limiting cases of open cell

foams ($\phi = 0$) and closed cell foams of equal face and edge thick-

ness ($\phi = \ell/t_e$), this reduces to the previous relationships:

$$\frac{\sigma^*_{p1}}{\sigma_y} \propto \left(\frac{\rho}{\rho_s}\right)^{3/2} \quad \text{and} \quad \frac{\sigma^*_{p1}}{\sigma_y} \propto \left(\frac{\rho}{\rho_s}\right)^{2} \quad \text{respectively.}$$

Note that open cell foams are stiffer and collapse and yield less

easily than closed cell foams. Many closed cell foams have values

of ϕ which are less than 1 (see Section 6.2) (this occurs, roughly,

when $t_f/\ell = (\rho/\rho_s)^2$). Such foams behave more like open cell foams,

because the bulk of the polymer is concentrated in the cell edges.

5.4 Refinements of the Analysis of Foam Properties

The dimensional analysis of three-dimensional cellular solids

presented in the previous sections is deficient in two ways: the cal-

culation of the relative density is an approximate one, good at low

densities but poor at high; and shear and axial deformations are ig-

nored in the calculation of the beam deflection. Both become increas-

ingly important as the thickness: length ratio of the members, t/ℓ,

becomes larger. In this section, the foam properties are recalculated

to take these deficiencies of the simple dimensional analysis into

account.

We consider only open cell materials in the more detailed analysis;

in Section 5.3 we showed that materials with a low proportion of the

volume of solid polymer in the cell faces also behave as open cell foams.
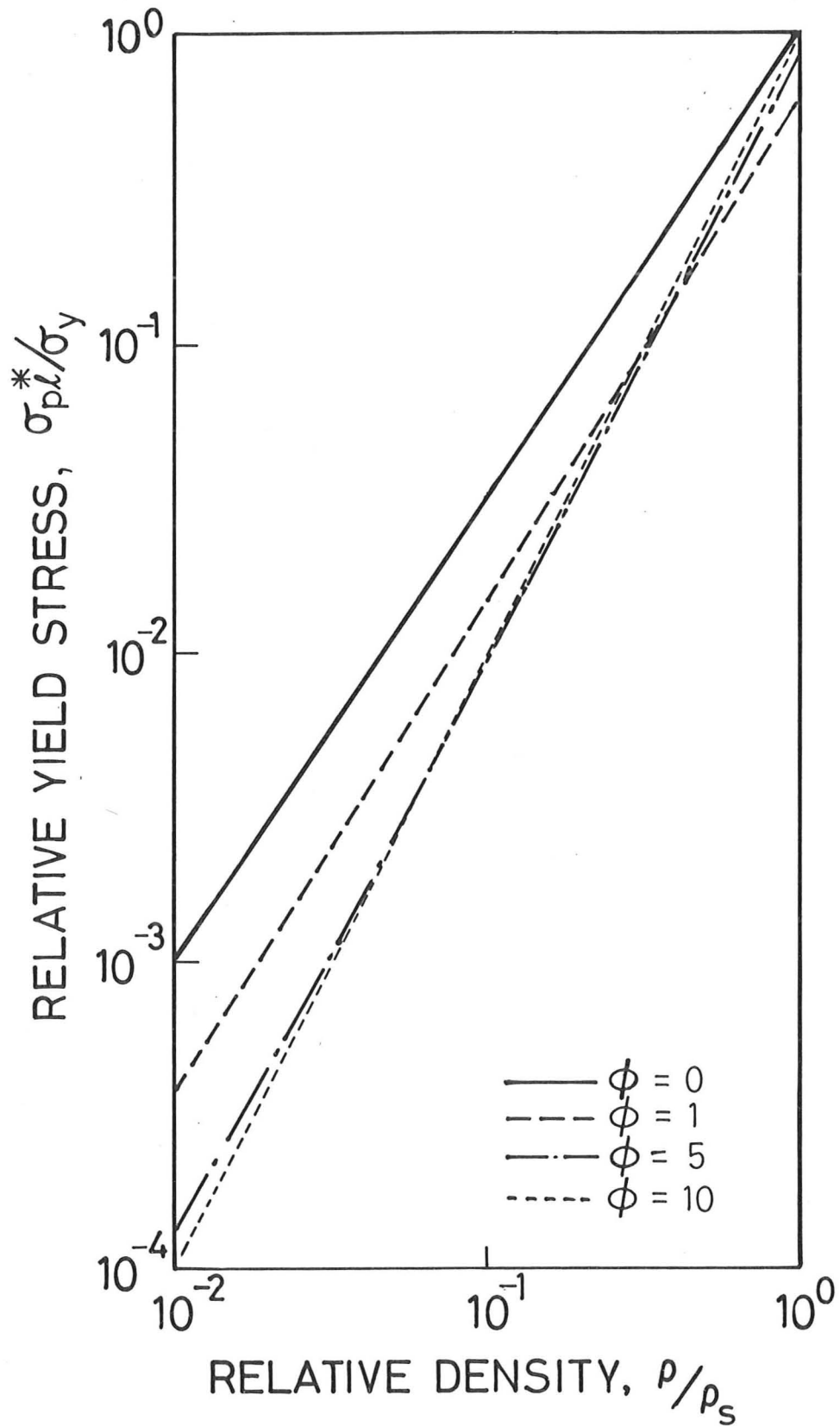
Fig. 5.9 Relative yield stress against relative density
as a function of φ

Relative density

In Section 5.1 we neglected the corners of the cells and found:

$$\frac{\rho}{\rho_s} = C \left(\frac{t}{\ell}\right)^2$$

For cubical cells, the constant of proportionality, C, is equal to three. If the contributions of the corners to the volume of solid material and of the edges to the total volume of the cell are taken into account, the relative density of a cubical cell becomes (Fig. 5.10):

$$\frac{\rho}{\rho_s} = \frac{3t^2 \ell + t^3}{(t + \ell)^3} = \frac{3 (t/\ell)^2 + (t/\ell)^3}{(1 + t/\ell)^3} \qquad (5.20)$$

This expression is exact for cubical cells. But real cells in foams are not cubical; they are (on average) tetrakaidecahedra (Thompson, 1966). Cells in foams pack to fill space and, because of surface tension requirements, try to minimize their surface area for a given volume. As the number of faces on a polyhedron increase and it more closely resembles a sphere, the ratio of surface area to volume decreases (Table 5.3). The cube has a high surface area:volume ratio and is a poor approximation for cell shape.

The pentagonal dodecahedron and the tetrakaidehedron both pack to fill space. The tetrakaidecahedron has a slightly lower surface area to volume ratio, but is not a regular polyhedron. Because it is much
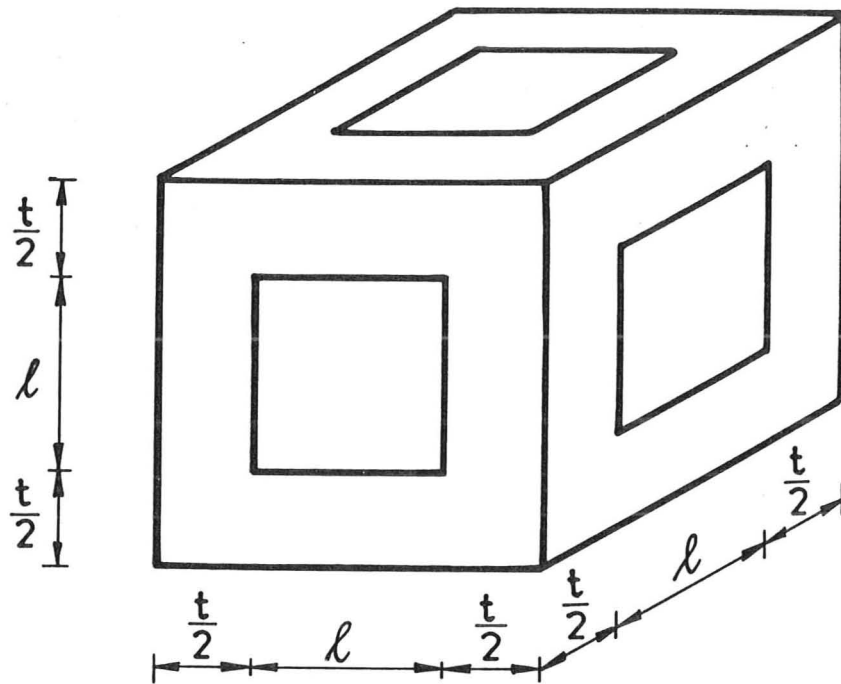
Fig. 5.10   Refined cubic model of an open cell foam.
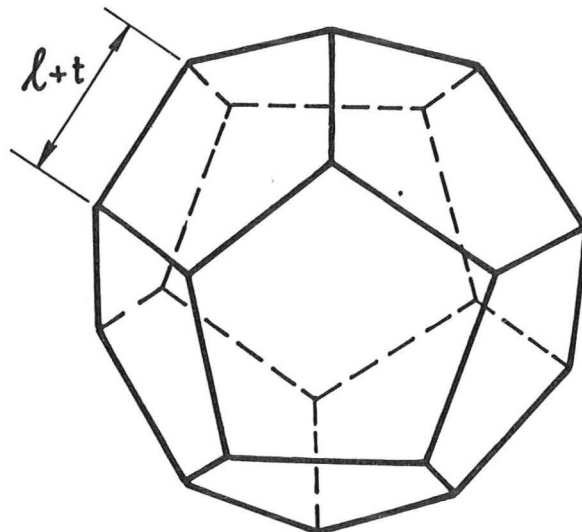
Fig. 5.11   Pentagonal dodecahedral model of an open cell
            foam

TABLE 5.3:   Surface Areas for Some Polyhedra and the
             Sphere of Unit Volume.*

Body	Nature of Surface	Surface Area
Tetrahedron	4 equilateral triangles	7.21
Cube	6 square	6.00
Octahedron	8 equilateral triangles	5.70
Dodecahedron	12 regular pentagons	5.31
Tetrakaidecahedron	6 squares and 8 regular hexagons	5.31
Icosahedron	20 equilateral triangles	5.14
Sphere	∞	4.84

*See Appendix 5A for formulae for surface area and volume.

simpler to do so, we shall take the pentagonal dodecahedron as a satis-
factory approximation of the shape of a unit cell. Assuming a square
cross-section for the members, the relative density of an open cell
structure made up of pentagonal dodecahedra is approximately (Fig. 5.11):

$$\frac{\rho}{\rho_s} = \frac{V_{edges} + V_{corners}}{V_{total}} = \frac{10t\ell^2 + \beta t^3}{7.66 \ (\ell + t)^3} = \frac{(t/\ell)^2 + 0.766 \ (t/\ell)^3}{0.766 \ (1 + t/\ell)^3} \qquad (5.21)$$

The volume of cell is approximately $7.66 \ (\ell + t)^3$. There are 10 edges per
cell, each of volume $t^2\ell$. The volume of the corners is proportional to t^3;
by setting $\beta = 7.66$, the relative density goes to 1 as ℓ approaches
zero.

Although this new equation for ρ/ρ_s is a major improvement on the
simple equation $\rho/\rho_s \propto (t/\ell)^2$, and leads to significant modifications
to the equations for the moduli, non-linear elastic and plastic response
(given below), it is not exact. The chief difficulty in setting up an
exact expression is that of describing the cross-section of the edges
and the corners. Here the problem is partly circumvented by the device
of adjusting the parameter β to make ρ/ρ_s go to 1 when ℓ goes to
zero.

Elastic moduli, with shear and axial deformation included

In Section 5.1 we related the elastic moduli of cellular materials
to the bending stiffness of the beam-like members making up the material.
At low relative densities this is valid since bending is the main deforma-
tion mode in the material. But as the relative density of the material
increases (increasing the thickness:length ratio of the members) shear

and axial deformations become more important. The bending, shearing and axial displacements in the X_2 direction of a beam of rectangular cross-section, bt, inclined by an angle θ from the horizontal, fixed at both ends and with one end displaced in the X_2 direction are (Fig. 5.12):

$$\delta_{bending_2} = \frac{F\ell^3 \cos^2\theta}{E_s \, bt^3}$$

$$\delta_{shear_2} = \frac{3F\ell \cos^2\theta}{E_s \, bt}$$

$$\delta_{axial_2} = \frac{F\ell \sin^2\theta}{E_s \, bt}$$

The shear displacement is based on the analysis of Timoshenko and Goodier (1970) with Poisson's ratio for the beam material equal to 0.4.

In a cellular material, the bending and shearing displacements occur over the unsupported length, ℓ, of the members, while axial displacements occur over the entire length of the member, $\ell + t$ (Fig. 5.11). For a member of square cross-section, t^2, the total deflection is then:

$$\delta_{total} = \frac{F\ell}{E_s \, t^2} \left[\left(\frac{\ell}{t}\right)^2 + 4 + \frac{t}{\ell} \right]$$

if $\cos^2\theta \approx \sin^2\theta$. Using the dimensional argument of Section 5.1 the overall stress is proportional to $F/(\ell + t)^2$ and the strain is proportional to $\delta/(\ell + t)$, which leads to:

$$E \propto \frac{F}{\delta \, (\ell + t)}$$

and

$$\frac{E}{E_s} \propto \frac{(t/\ell)^2}{1 + t/\ell} \left[\frac{1}{(\ell/t)^2 + 4 + t/\ell} \right] \qquad (5.22)$$
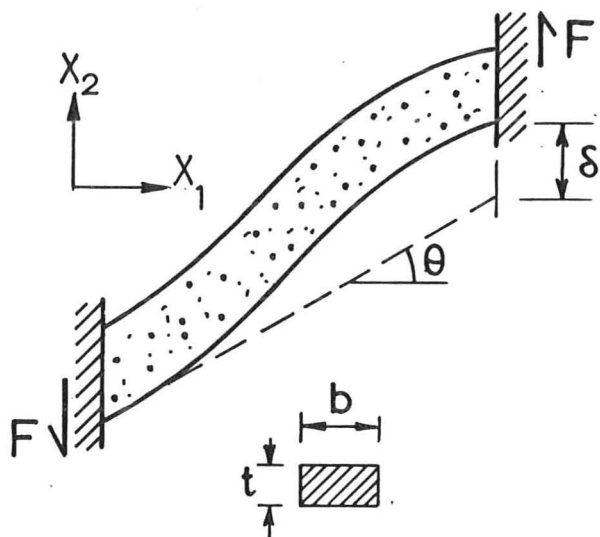
$$\delta \text{ bending 2} = \frac{F\ell^3 \cos^2\theta}{E_s\, b t^3}$$

$$\delta \text{ shear 2} = \frac{3F\ell\cos^2\theta}{E_s\, b t}$$

$$\delta \text{ axial 2} = \frac{F\ell\sin^2\theta}{E_s\, b t}$$

Fig. 5.12 Bending, shear and axial displacements for a beam fixed at both ends and with one end displaced.

Substituting for t/ℓ in equations (5.22) and (5.21) and plotting log E/E_s against log ρ/ρ_s (Fig. 5.13) we find that the relative modulus is nearly proportional to relative density squared over its entire range. But this was the result of the first simple dimensional analysis. Despite its several shortcomings, it appears to give a useful, simple squared rule for relating relative Young's modulus to relative density which has wide generality. The same derivation applies to the shear modulus, giving:

$$\frac{G}{E_s} \propto \frac{(t/\ell)^2}{(1 + t/\ell)} \left[\frac{1}{(\ell/t)^2 + 4 + t/\ell} \right] \tag{5.23}$$

As before, this refined result differs very little from the original, simple, one. Poisson's ratio, as before, is independent of t/ℓ and ρ/ρ_s.

Non-linear elastic behaviour

The edges of the cell were not taken into account in the simple analysis in calculating the total volume of the cell for the relative density or in calculating the area of the cell over which stresses act. We now account for this for the elastic collapse stress of the cell. Using the new definitions of member length, ℓ, and thickness, t, we find the area of a cell is proportional to $(\ell + t)^2$ (Fig. 5.10). The critical buckling load is still:

$$P_{cr} \propto \frac{\pi^2 E_s I}{\ell^2}$$

Giving

$$\frac{\sigma_{el}^*}{E_s} \propto \frac{t^4}{\ell^2 (\ell + t)^2}$$
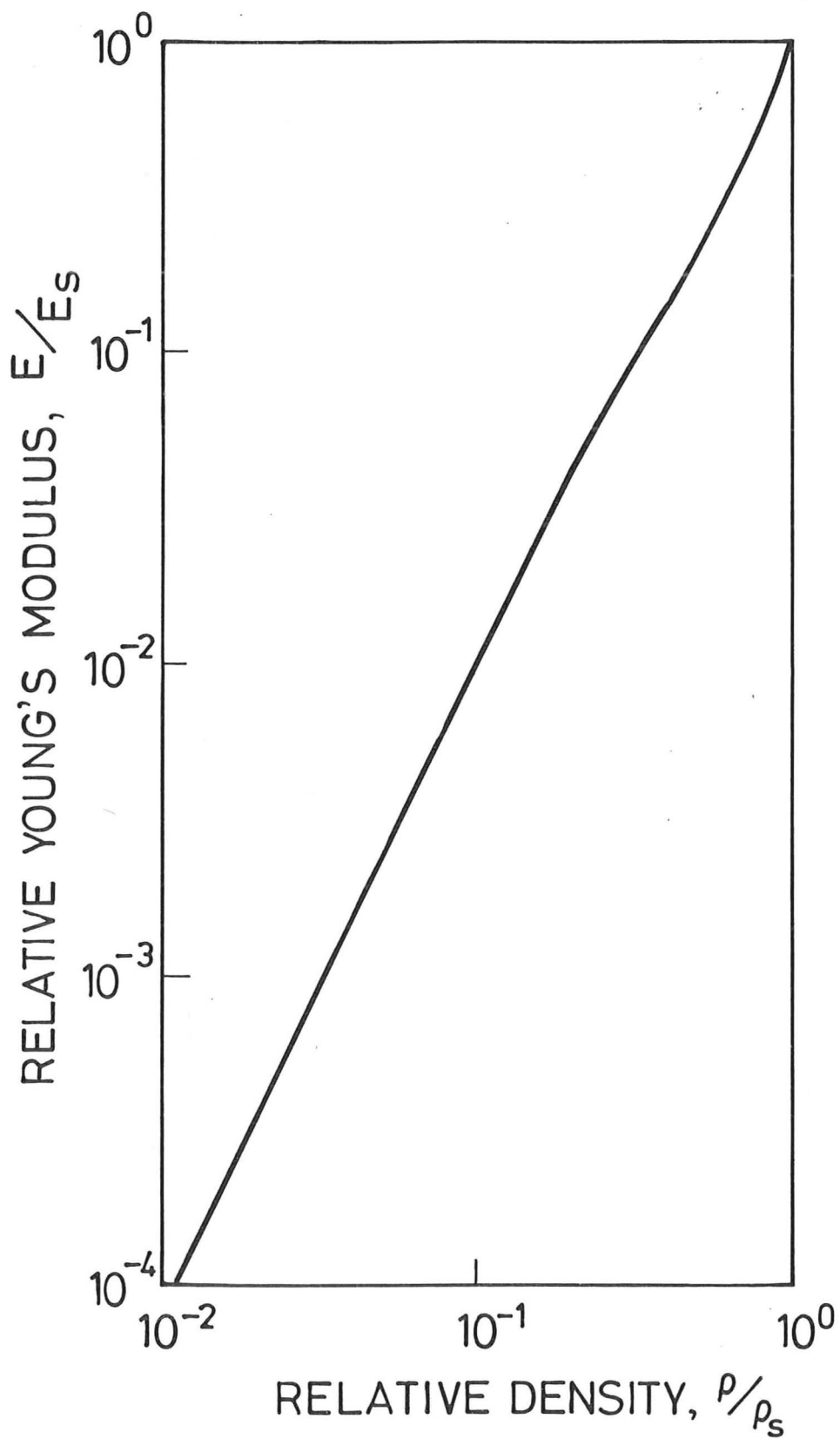
Fig. 5.13 Relative Young's modulus against relative density for the refined model.
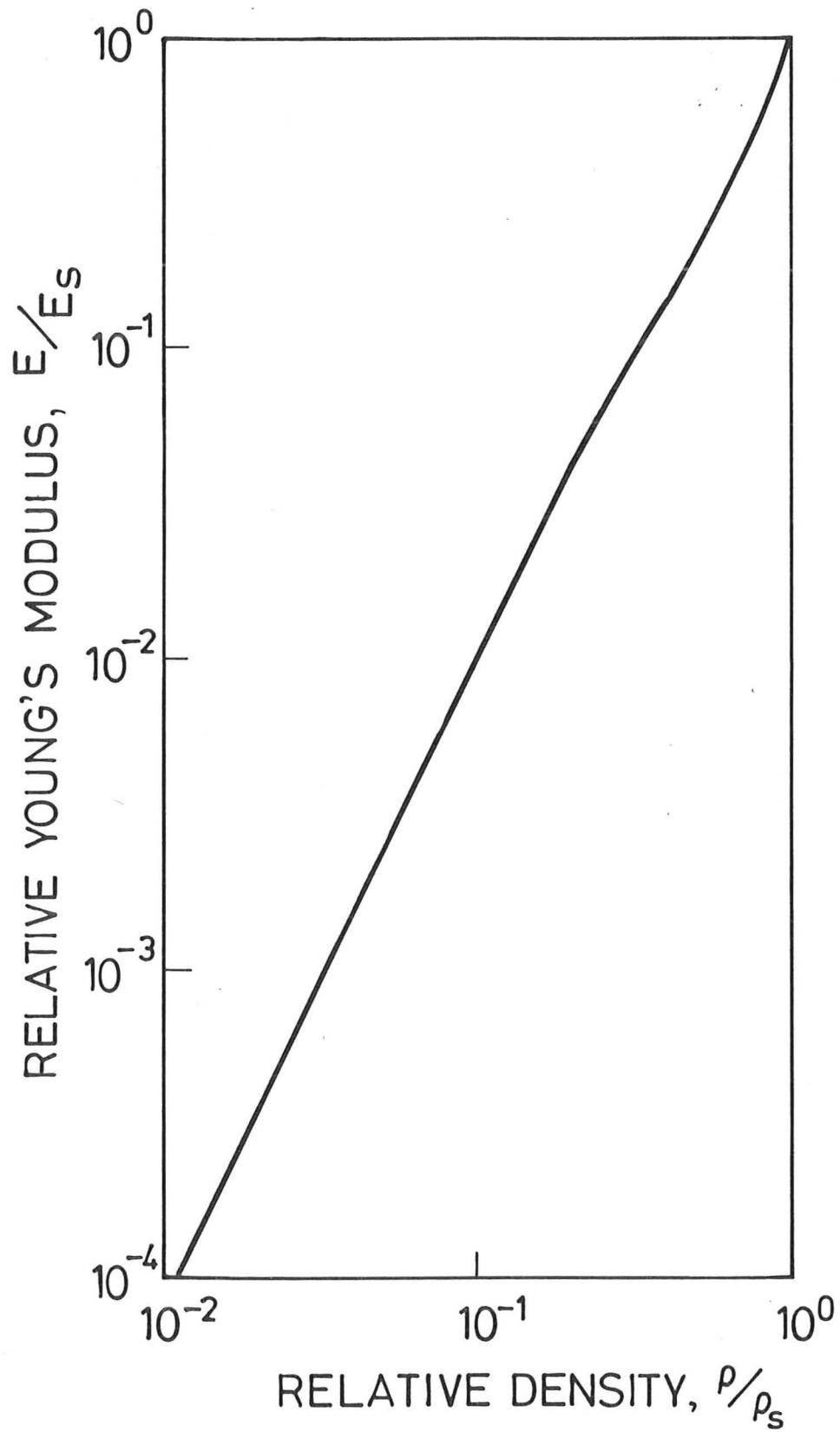
Fig. 5.13 Relative Young's modulus against relative density for the refined model.

or
$$\frac{\sigma^*_{el}}{E_s} \propto \frac{(t/\ell)^4}{(1 + t/\ell)^2} \qquad (5.24)$$

for an open cell foam. The old and new equations for σ^*_{el}/E_s (5.7 and 5.24) are plotted in Fig. 6.9. The simple dimensional analysis gives a constant slope of 2 on a log-log plot. The result of the more refined analysis has a slope of 2 below $\rho/\rho_s \sim 0.02$ (as we would expect since the two analyses converge at low ρ/ρ_s); this slope then increases with relative density.

Plastic collapse

Using the new definition of cell area proportional to $(\ell + t)^2$, the plastic collapse stress becomes:

$$\frac{\sigma^*_{pl}}{\sigma_y} \propto \frac{(t/\ell)^3}{(1 + t/\ell)^2} \qquad (5.25)$$

for an open cell foam. The two results of the simple and the more detailed analyses (equations 5.8 and 5.25) are plotted in Fig. 6.10. Both equations have a slope of $\frac{3}{2}$ (on a log-log plot) at low relative densities. The slope of the result of the simple analysis remains constant at this value while the slope of equation (5.25) increases with relative density.

5.5 Limits of Validity of the Equations

Elastic moduli

The more complete analysis of the elastic moduli of cellular materials just outlined itself breaks down when the material no longer ressembles a

network of beams, but begins to behave like a solid with small holes in it. At a thickness:length ratio of about 1 (or $\rho/\rho_s \approx 0.3$) end effects in the members, which we have up until now ignored, become important. At relative densities greater than 0.3 the analysis of cellular materials becomes very difficult. MacKenzie (1950) has derived expressions for the shear and bulk moduli of solids containing many small holes. These two relationships can be combined with the equations relating the elastic moduli of an isotropic solid to give an expression for the Young's modulus of a solid with holes. This expression is a function of the Poisson's ratio of the solid; we have assumed $\nu_s = 0.3$. Fig. 5.14 and 5.15 show plots of E/E_s and G/G_s against ρ/ρ_s according to MacKenzie's theory. For values of relative density between 0.8 and 1.0, the results lie very close to the lines $E/E_s = (\rho/\rho_s)^2$ and $G/G_s = (\rho/\rho_s)^2$.

In summary, our beam bending models show the Young's and shear moduli are proportional to $(\rho/\rho_s)^2$ for relative densities less than 0.3. Remarkably, models of solids with holes in them also predict E and G equal to $(\rho/\rho_s)^2$ for $0.8 \leq \rho/\rho_s \leq 1.0$. Although we have no theory to predict E and G at relative densities in the difficult range between 0.3 and 0.8, it is unlikely that E and G deviate greatly from a $(\rho/\rho_s)^2$ law. We expect then that a simple square law should predict E and G for all relative densities.

Poisson's ratio is expected to be independent of relative density.

Non-linear elastic behaviour

The elastic buckling stress of a column increases with $(t/\ell)^2$. At large t/ℓ, this stress becomes so large that, in the range of loads and deformations that interest us, some other mechanism is dominant –
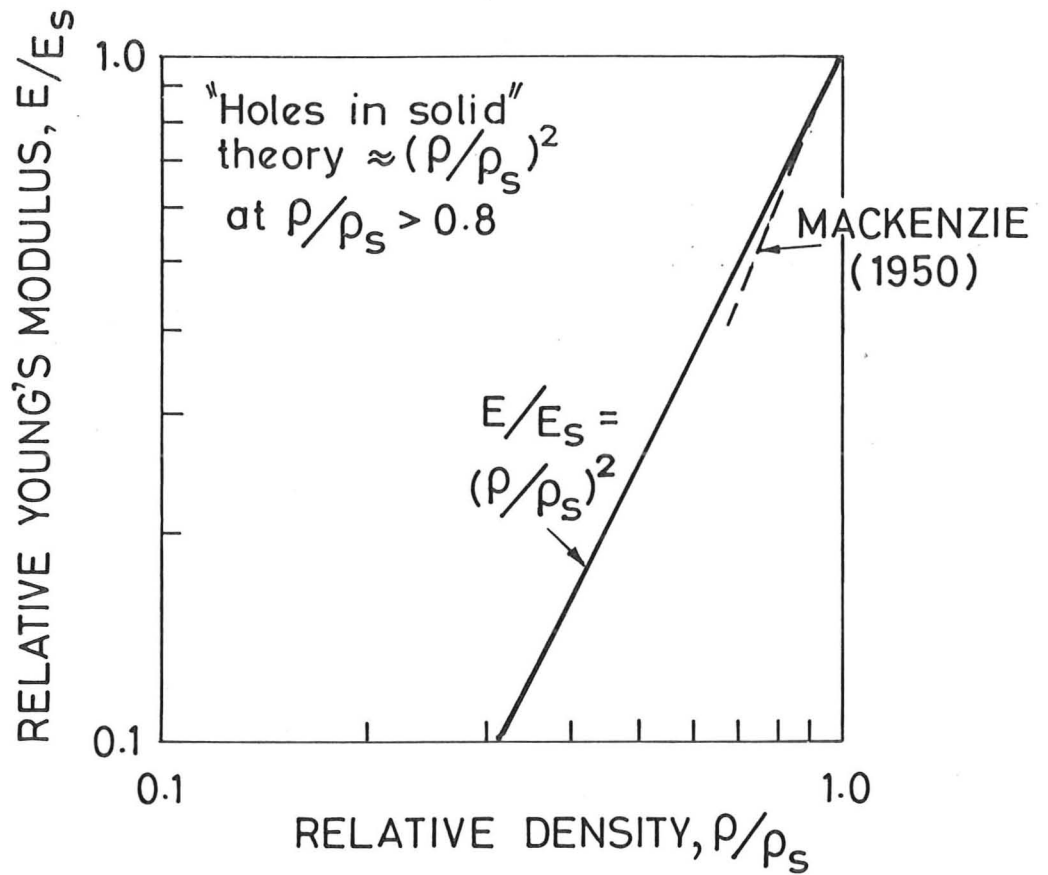
Fig. 5.14 Relative Young's modulus against relative density. MacKenzie's model approximates $E/E_s = (\rho/\rho_s)^2$ for $\rho/\rho_s > 0.8$
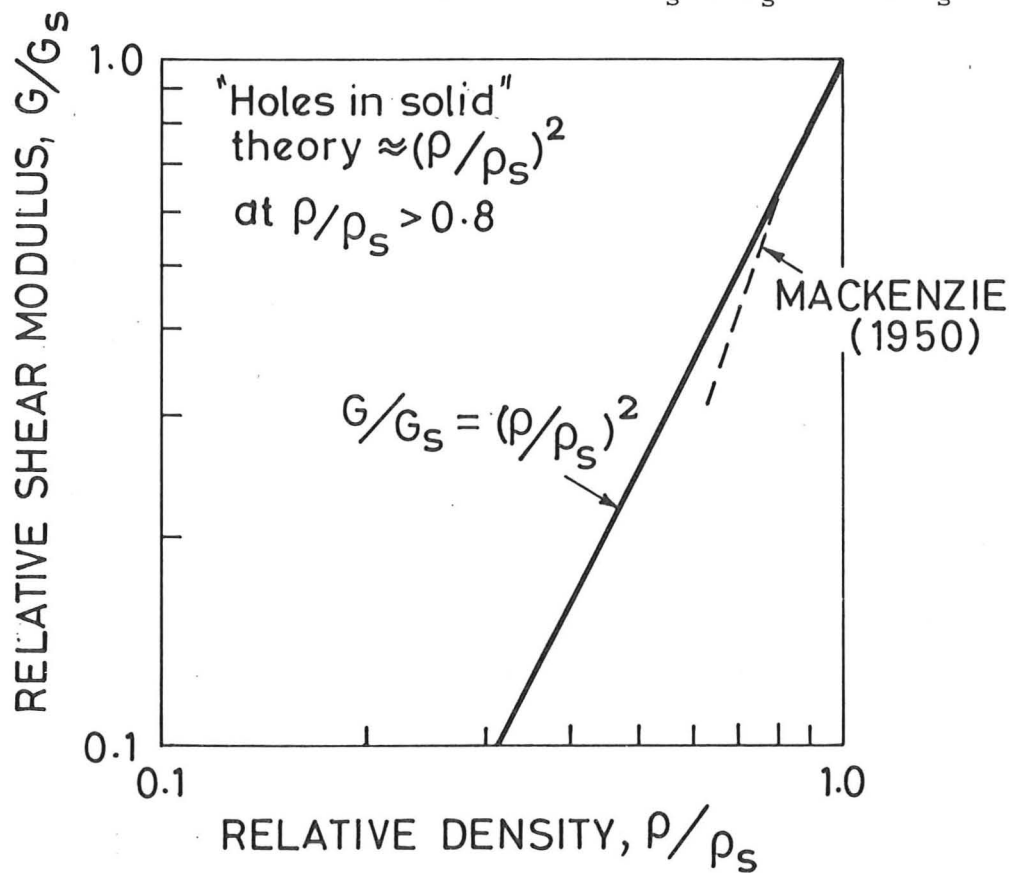
Fig. 5.15 Relative shear modulus against relative density. MacKenzie's model approximates $G/G_s = (\rho/\rho_s)^2$ for $\rho/\rho_s > 0.8$

either because it permits large deformations at loads below the
buckling load, or because it causes plastic or brittle collapse.
When the columns form the members of a cellular solid (as here),
elastic deformations may cause the cell faces to meet, or yielding
and plastic collapse may occur, before the buckling stress is reached.
This becomes increasingly probable as t/ℓ increases. We have as-
sumed that buckling will not appear when $t/\ell \geq 1$. This means that
the equations describing non-linear elastic behaviour are invalid
when $\rho/\rho_s \geq 0.3$.

Plastic collapse behaviour

At low relative densities, the calculation for the plastic collapse
stress is based on the formation of plastic hinges at the ends of the
members of the foam. When the thickness:length ratio, t/ℓ, becomes
large enough the axial stress in a member can exceed the yield stress
of the solid in axial compression before plastic hinges form. The
overall stress required to cause yielding of axially loaded members is:

$$\sigma \approx \sigma_y \frac{t^2}{(\ell + t)^2} \approx \sigma_y \frac{(t/\ell)^2}{(1 + t/\ell)^2}$$

From Section 5.3, the stress required to produce plastic hinges by
bending is:

$$\sigma_{pl}^* = C \, \sigma_y \frac{(t/\ell)^3}{(1 + t/\ell)^2}$$

In Section 6.4 we find that experimentally, $C = 0.30$. These two mechan-
isms occur simultaneously when the thickness:length ratio, t/ℓ, is equal

to 3.3, or the relative density is equal to 0.6. At higher relative densities, plastic collapse occurs by axial compression of the members rather than by the formation of plastic hinges through bending.

5.6 Conclusions

The theory for the mechanics of three-dimensional cellular materials has been developed at two levels, using first a simple, and then a more refined, dimensional analysis. We found that both analyses give the relative Young's modulus, E/E_s, and the relative shear modulus, G/E_s, proportional to $(\rho/\rho_s)^2$ for open cell foams; these equations are valid at relative densities up to 0.3. At relative densities greater than 0.8, MacKenzie's (1950) expressions for E/E_s and G/G_s are also about equal to $(\rho/\rho_s)^2$. No theory has been developed yet for the moduli of materials with relative densities between 0.3 and 0.8; but it is unlikely that these materials behave much differently from the $(\rho/\rho_s)^2$ rule. Remarkably, then, we expect to find E/E_s and G/E_s proportional to $(\rho/\rho_s)^2$ for all relative densities of materials. The dimensional analysis shows that a third elastic constant, Poisson's ratio, is independent of relative density: this result is confirmed by the fact that E and G are both proportional to $(\rho/\rho_s)^2$ and that, at least for isotropic solids, $\nu = -1 + E/2G$. The relative elastic and plastic collapse stresses were found to vary about as $(\rho/\rho_s)^2$ and $(\rho/\rho_s)^{3/2}$ respectively.

Two other aspects of behaviour were also investigated in this chapter. First, in Section 5.2 we examined the effect of shape aniso-tropy on the moduli and collapse stresses. This effect is most pro-nounced for Young's modulus: E_1/E_3 varies as A^{-5}. And in Section 5.3

we studied the contribution of the faces of closed cell foams to stiffness and strength. We found that if the faces are thin compared to the edges, they do not contribute significantly to stiffness or strength and the foam behaves as if it were open-celled.

Appendix 5A: Formulae for Surface Area and Volume of Polyhedra

Polyhedron	Nature of Surface	Surface Area	Volume
Tetrahedron[1]	4 equilateral triangles	$1.73a^2$	$0.118a^3$
Cube[1]	6 squares	$6.00a^2$	$1.000a^3$
Octahedron[1]	8 equilateral triangles	$3.46a^2$	$0.471a^3$
Dodecahedron[1]	12 regular pentagons	$20.65a^2$	$7.663a^3$
Tetrakaidechedron[2]	6 squares and 8 regular hexagons	$26.78a^2$	$11.314a^3$
Icosahedron[1]	20 equilateral triangles	$8.66a^2$	$2.182a^3$

a = edge length

Formulae taken from:

1.   CRC Handbook of Tables for Mathematics (1970) Fourth Ed. Edited by
      R.C. Weast, Chemical Rubber Co., Cleveland, Ohio, p.15.

2.   Underwood, E.E. (1970) "Quantitative Stereology" Addison-Wesley, p.91.

Addendum 5A___Creep Behaviour

If the strain in a foam increases with time under constant stress, it is said to creep. In a cantilever beam undergoing power-law creep, with $\dot{\varepsilon}/\dot{\varepsilon}_o = (\sigma/\sigma_o)^n$, the end load F is related to the rate of change of end deflection, $\dot{\delta}$, by (Fig. 5B.1).

$$F = \frac{2b \ \sigma_o \ n}{2n + 1} \ (\frac{t}{2})^{\frac{2n+1}{n}} \ (\frac{1}{\ell})^{1+\frac{2}{n}} \ \{\frac{(n + 2) \ \dot{\delta}}{\dot{\varepsilon}_o}\}^{\frac{1}{n}} \tag{5B.1}$$

Here n, σ_o and $\dot{\varepsilon}_o$ are creep constants characterizing the material of which the beam is made. If the members of a cellular material creep according to this law and the overall stress and strain-rate are proportional to $F/(\ell + t)^2$ and $\dot{\delta}/(\ell + t)$ respectively, then the material creeps according to:

$$\frac{\dot{\varepsilon}}{\dot{\varepsilon}_o} \propto (\frac{\sigma}{\sigma_o})^n \ \frac{1}{t^{3n+1}} \ (\ell + t)^{2n-1} \ \ell^{n+2} \tag{5B.2}$$

for open cell foams.

The linear elastic result for E/E_s (equation (5.22) ignoring shear and axial deflections) can be obtained from this by letting $n = 1$, $\sigma_o/\varepsilon_o = E_s$ and substituting strain for strain rate. Equation (5B.2) reduces to the plastic collapse result (equation (5.25)) when $n = \infty$ and $\sigma_o = \sigma_y$. We then find:

$$\frac{\dot{\varepsilon}}{\dot{\varepsilon}_o} \propto (\frac{\sigma}{\sigma_y} \ \frac{(\ell + t)^2 \ \ell}{t^3})^n \ \frac{\ell^2}{(\ell + t) \ t} \tag{5B.3}$$
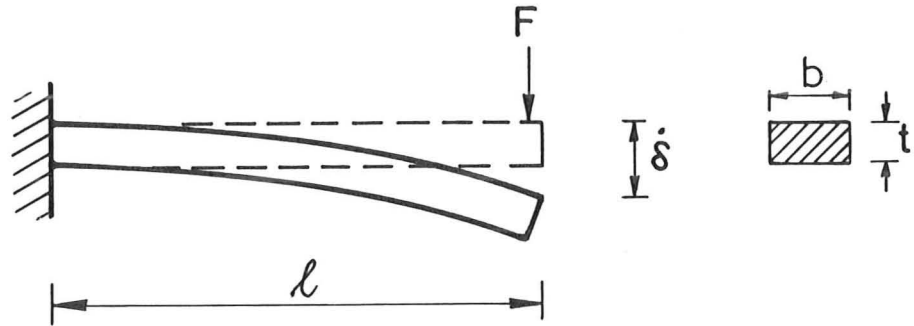
Material obeys $\dfrac{\dot{\epsilon}}{\dot{\epsilon}_o} = \left(\dfrac{\sigma}{\sigma_o}\right)^n$

Fig. 5B.1 Creep deflection of a cantilevered beam.

A number less than one raised to the power infinity equals zero, while a number greater than one goes to infinity. The plastic solution occurs when:

$$\frac{\sigma}{\sigma_y} \frac{(\ell + t)^2 \ell}{t^3} = 1$$

or

$$\frac{\sigma}{\sigma_y} = \frac{(t/\ell)^3}{(1 + t/\ell)^2} \qquad\qquad (5B.4)$$

This is the same as the plastic collapse result obtained in equation (5.25).

Addendum 5B: Brittle Behaviour

A material with cracks of length $2a$ in it will fracture in a brittle manner if the stress level reaches the fracture stress, σ_{fs}, given by:

$$\sigma_{fs} = \sqrt{\frac{E_s \, G_{cs}}{\pi a}}$$

where E_s is the Young's modulus and G_{cs} is the toughness of the material. In a cellular material, the extreme fibre stress in a member in bending is given by:

$$\sigma = \frac{Mt}{2I} \propto \frac{F \ell t}{I}$$

The member will fracture if $\sigma = \sigma_{fs}$ or the force acting on the fibre, F, is:

$$F \propto \sqrt{\frac{E_s \, G_{cs}}{\pi a}} \frac{I}{\ell t}$$

Since the overall stress on the cellular material is proportional to $F/(\ell + t)^2$ the stress at which brittle fracture occurs, σ^*_{bf}, is:

$$\sigma^*_{bf} \propto \sqrt{\frac{E_s \, G_{cs}}{\pi a}} \frac{I}{\ell t \, (\ell + t)^2}$$

or

$$\frac{\sigma^*_{bf}}{\sigma_{fs}} \propto \frac{t^4}{t \ell \, (\ell + t)^2} \propto \frac{(t/\ell)^3}{(1 + t/\ell)^2}$$

for open cell foams with $I \propto t^4$.

CHAPTER 5:   REFERENCES

MacKenzie, J.K. (1950) Proc. Phys. Soc., B63, 2.

Thompson, D.W. (1961) "On Growth and Form", Cambridge University Press, p.119-125.

Timoshenko, S.P. and Goodier, J.N. (1970) "Theory of Elasticity", (3rd ed.) McGraw-Hill, p.121.

CHAPTER 6

THREE-DIMENSIONAL CELLULAR MATERIALS – EXPERIMENTAL METHOD, RESULTS AND DISCUSSION

The model of foam behaviour presented in the last chapter was based on the physical idea that the cell members bend, buckle elastically, or collapse plastically. Evidence for these three modes of deformation are presented in this chapter along with data for the elastic moduli and collapse properties of many types of foams. The mechanical test data are from tests carried out by the author and from results reported in the literature. The data for each property are plotted together over a range of relative densities from 0.01 to 1.00. These results are analyzed in terms of the theoretical calculations given in the previous chapter. The models for the mechanical behaviour of cellular materials are found to give a good description of the large body of experimental data.

6.1 Experimental Method

Three types of foam were tested: an open cell, flexible polyurethane, a closed cell, flexible polyethylene, and a closed cell, rigid polyurethane. (Open cell rigid foams were unobtainable). Some of their properties are listed in Table 6.1. The data for the solid polymer properties have been obtained from reference texts; the variation in these properties between different batches of the same material is large, and they can be changed by the foaming process. This variation is the principal source of error in comparing experiment with theory.

CHAPTER 6

THREE-DIMENSIONAL CELLULAR MATERIALS - EXPERIMENTAL METHOD, RESULTS AND DISCUSSION

TABLE 6.1: Properties of Foams Tested

TYPE OF FOAM	MANUFACTURER	DENSITIES (kg/m^3)	SOLID POLYMER PROPERTIES			Symbol used in Fig. 6.7 - 6.11
			ρ_s (kg/m^3)	E_s (MN/m^2)	σ_y (MN/m^2)	
Open cell flexible polyurethane	Dunlop Ltd. Dunlopillo Division	14.4, 18.5, 24.1, 27.8, 32.4, 51.7	1200[1]	45[2]	-	□
	Harrison and Jones (Holdings) Ltd.	14.2, 17.0, 19.9, 25.3, 29.0	1200[1]	45[2]	-	○
Closed cell flexible cross-linked polyethylene	Frelen Ltd.	29.4, 46.9, 69, 107, 120, 138, 360	910[3]	200[3]	-	◉
Closed cell rigid polyurethane	Bulstrode Plastics & Chemical Co. Ltd.	68, 76, 109, 160	1200[1]	1600[4]	127[4]	■

REFERENCES

1. Roff and Scott (1971) p.453-455.

2. Lazan (1968) p.245.

3. Billmeyer (1971) p.505.

4. Patel and Finnie (1970).

Cubes, approximately five millimeters on a side, of each density of each foam were cut, coated with gold, examined and photographed in the scanning electron microscope. Specimens of each foam were also loaded in tension and compression by means of a small vice within the microscope and photographed as the load was increased.

Young's moduli were measured at room temperature in both tension and compression. Tension tests were performed on specimens approximately 100 mm × 25 mm × 10 mm; compression tests were done on cubes and thin sheets. At least 3 specimens of each density were tested. The elastic and plastic collapse stresses were also measured from compression tests, for the flexible and rigid foams respectively. Young's modulus was not a function of strain rate over the range of rates used in the tests.

Poisson's ratio was calculated from measurements of the incremental displacements of four grids glued onto tensile specimens and checked by measuring the change in dimensions with a vernier gauge. Six pairs of strain measurements were made on each specimen. Linear regression analysis of these measurements was used to calculate mean Poisson's ratios.

Shear moduli were measured using the rig shown in Fig. 6.1. Foam specimens were glued to the plates with cyanoacrylate adhesive and the modulus measured from the load-displacement curve of each specimen. Two specimens of each density were tested. Although this is the loading geometry specified in British Standard 4370 (Part 2, 1973) it is
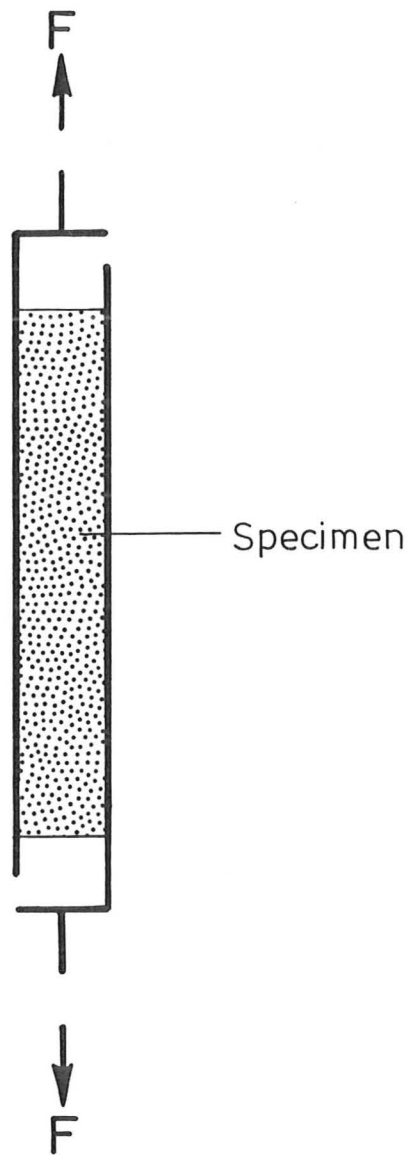
Fig. 6.1   Shear test rig.

not an ideal one because bending moments and tensile forces are super-
imposed on shearing forces. We estimate that errors in measuring
shear moduli in this way do not exceed 20 %.

No measurements were made of the creep behaviour or brittle frac-
ture behaviour of foams.

6.2 Cell Geometry and Deformation

Micrographs of each of the foams tested are shown in Fig. 6.2.
The relative volume of the faces to the edges in the closed cell foams,
ϕ, was measured from many micrographs and found to be 0.1 for the
polyurethane and 4.0 for the polyethylene.

Figs. 6.3 and 6.4 show the progressive compressive loading of two
foams, one flexible, the other rigid. The flexible foam deforms by
bending and buckling and recovers these deformations when unloaded.
Members of the rigid foam bend, and at higher loads, deform plastically
and break. These observations show that the deformation of three-dimen-
sional foams is controlled by the same physical processes as that of the
simpler two-dimensional cells, and led us to the analysis given in
Chapter 5.

6.3 Experimental Results

Typical compression curves for the three foams are shown in
Fig. 6.5. The initial near-linear portion is followed by a plateau,
terminated,at a strain of about 0.6, by a rapid rise in stress. Young's
modulus is taken as the initial slope of the stress-strain curve, the
collapse stress as the intercept of the extrapolations of the initial
slope and the plateau stress.

0.5 mm

a

1 mm

b

0.25mm

c
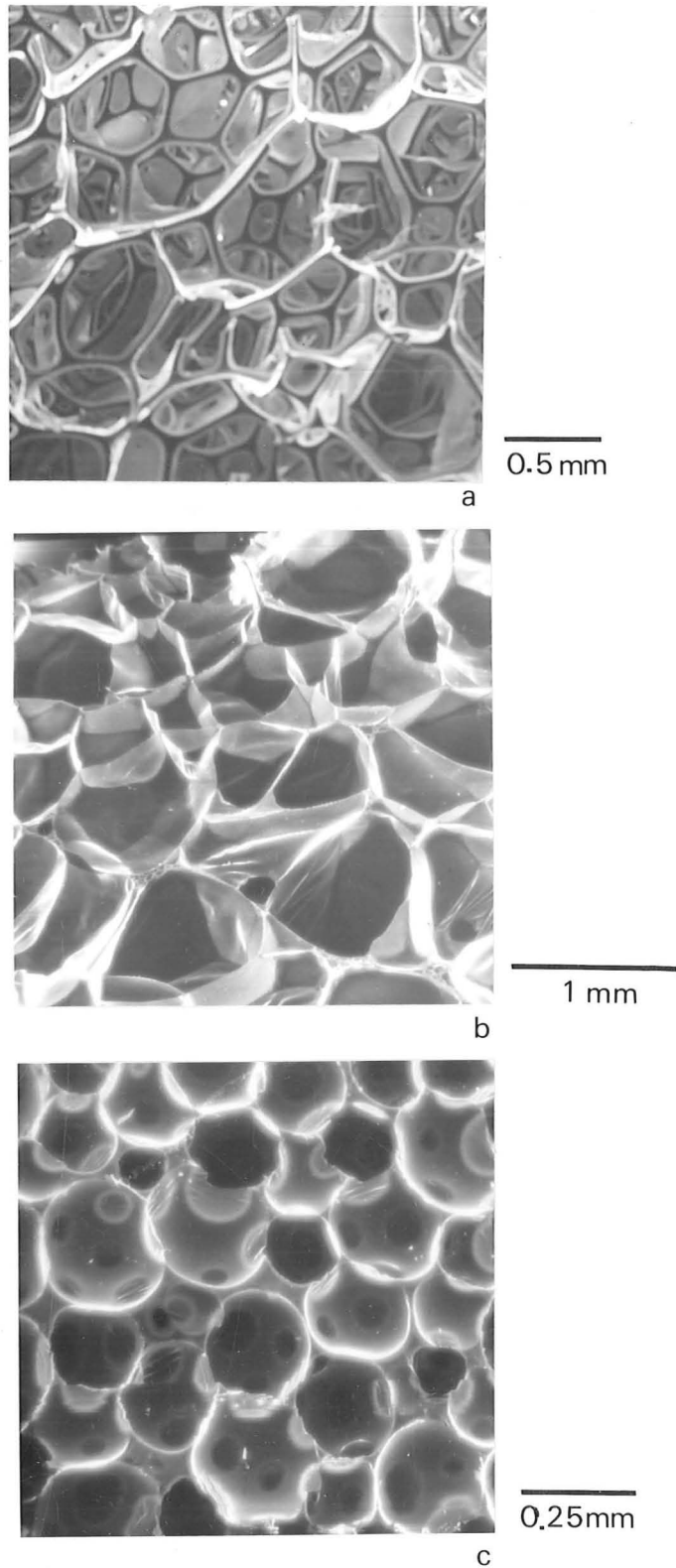
Fig. 6.2 Micrographs of (a) flexible open cell polyure-
thane foam (ρ=14 kg/m^3); (b) flexible closed cell
polyethylene foam (ρ=30 kg/m^3); (c) rigid closed
cell polyurethane foam (ρ=128 kg/m^3).
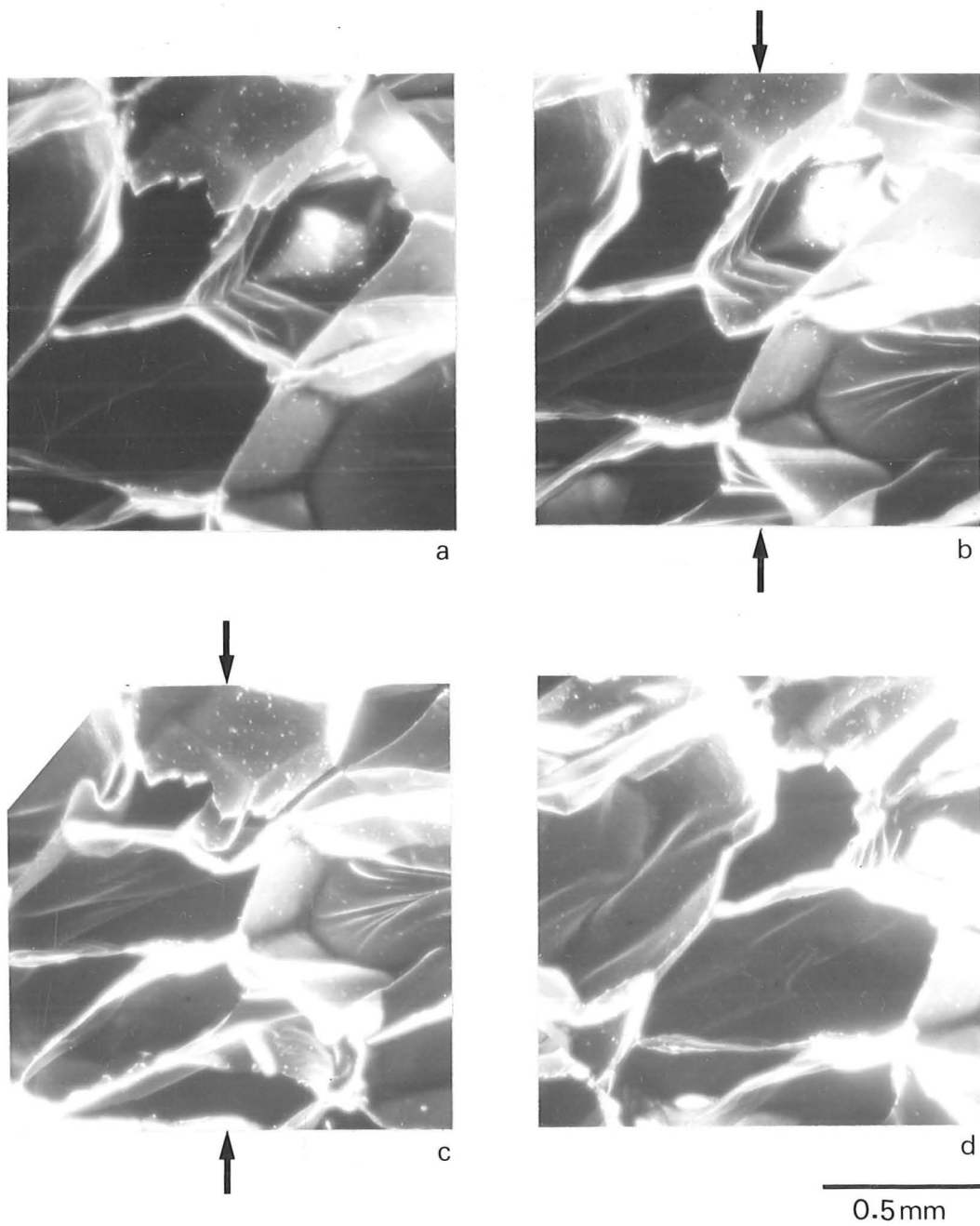
Fig. 6.3 A flexible polyethylene foam (a) unloaded, (b) showing bending deformation under compression, (c) showing elastic buckling under further compressive loading, and (d) unloaded. ($\rho=30$ kg/m^3)
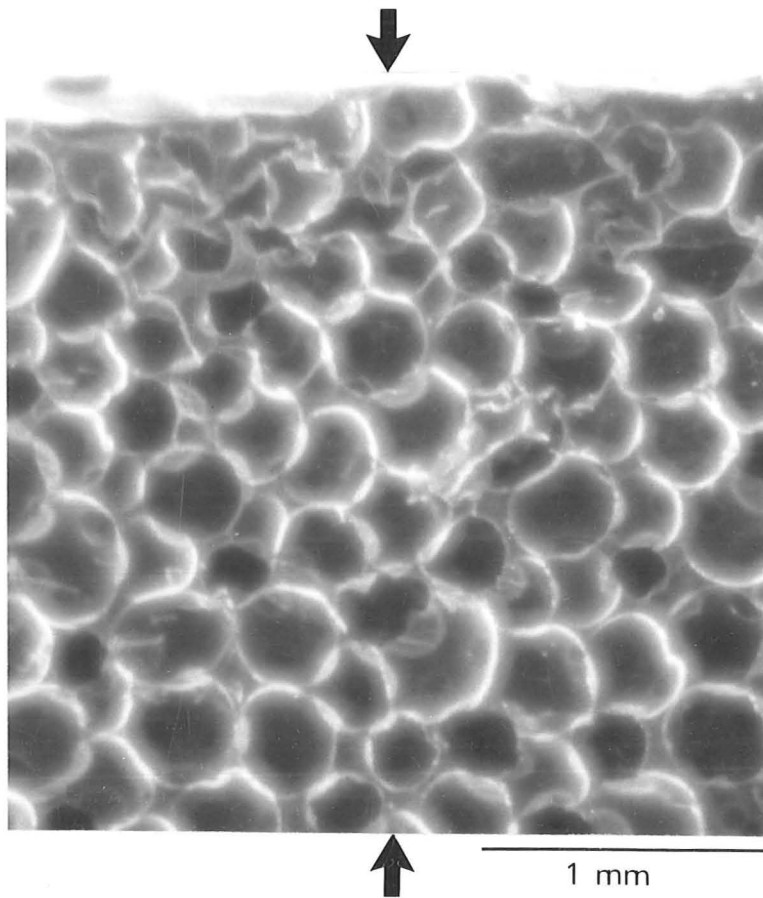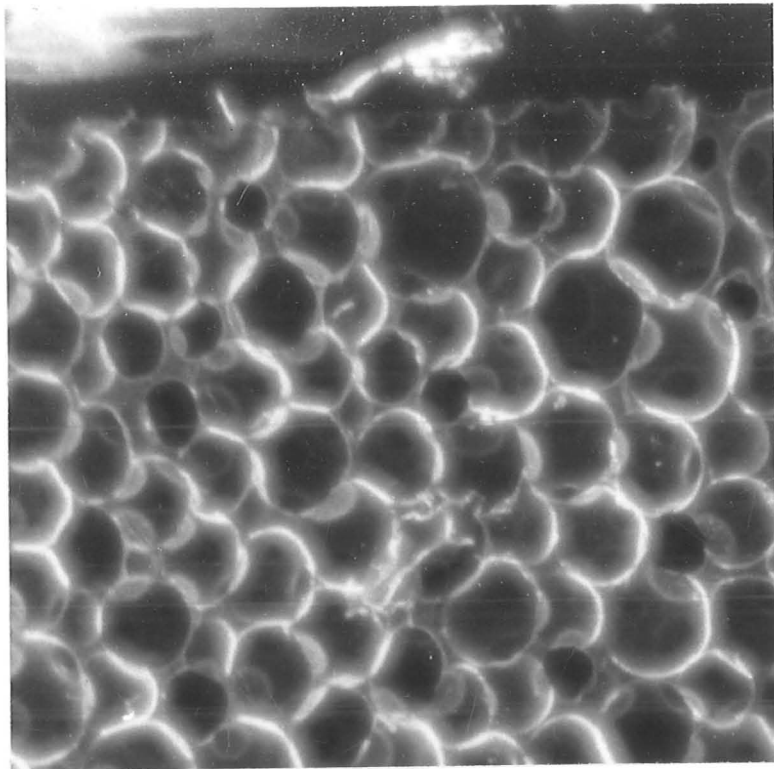
Fig. 6.4   Micrographs showing compressive loading of a rigid
closed cell polyurethane foam.   (ρ=160 kg/m^3)
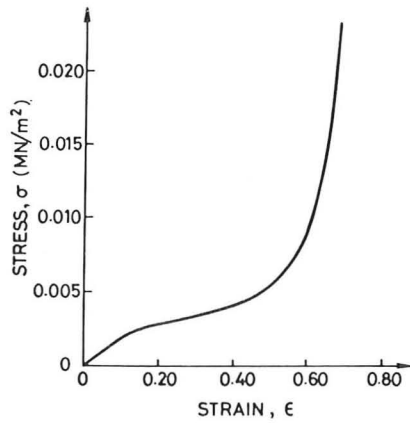
Fig. 6.5 (a)   Stress-strain curve for flexible polyurethane
              foam. (ρ=29 kg/m^3; ρ/ρ_s=0.023; manufactured by
              Harrison and Jones Ltd.)
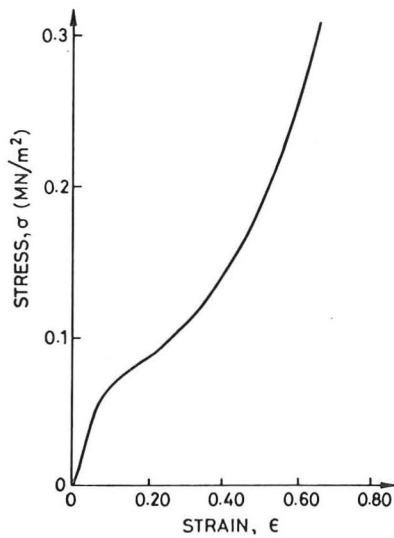
Fig 6.5 (b)   Stress-strain curve for flexible polyethylene
              foam. (ρ=69 kg/m^3; ρ/ρ_s=0.076; manufactured by
              Frelen Ltd.)
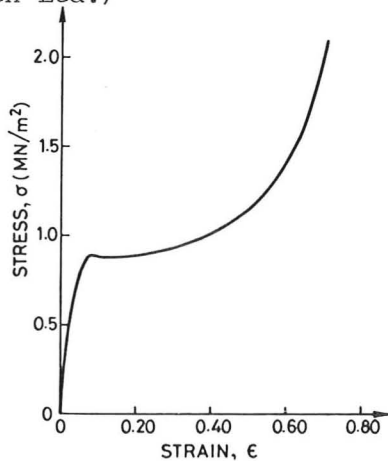
Fig. 6.5 (c)   Stress-strain curve for rigid polyurethane
              foam. (ρ=109 kg/m^3; ρ/ρ_s=0.091; manufactured by
              Bulstrode Plastics and Chemical Co. Ltd.)

The experimental results are assembled in Figs. 6.6 to 6.10.
They show data (from this study and from the literature) for Young's
moduli, Poisson's ratios, the shear moduli and the elastic and plastic
collapse stresses, together with the predictions of the models. Solid
polymer properties for foam data other than our own are quoted in Table 6.2.

Open and closed cell foams are plotted together, for the following
reason. When the cell-edges of a closed cell foam are thickened (because
polymer has accumulated there), the faces carry very little load and the
foam behaves as if it were open-celled. The condition for open cell be-
haviour was discussed in Section 5.3: it was that the quantity, ϕ, which
measures the ratio of the volume of polymer in the cell faces to that in
the edges, be small compared to $1/\rho$. Our closed-celled foams have
$\phi = 0.1$ (rigid polyurethane) and 4.0 (flexible polyethylene): the
first should behave as an open cell foam, and the second should be
intermediate between open-and closed-cell. The data support this view.

6.4 Discussion

Young's modulus

Data for Young's modulus from our study and from the literature,
covering a wide range of relative densities from 0.01 to 1.00, are
plotted in Fig. 6.6. As was discussed in Chapter 5, there are three
regimes of behaviour: at low relative densities (less than 0.3) the
material can be modelled as a network of bending beams while at high
relative densities (greater than 0.8) it behaves like a solid containing
spherical holes. At intermediate densities, modelling the material be-
haviour is difficult: as yet, no theoretical treatment of this regime
exists.

TABLE 6.2:   Solid Polymer Properties of Foams Tested by Other Authors

Author	Foam	ρ_s kg/m^3	E_s MN/m^2	σ_y MN/m^2
Baxter & Jones (1972)	Expanded Polystyrene	1020[1]	2650[1]	−
Brighton & Meazey (1973)	Expanded Polyvinyl Chloride	1400[2]	3000[2]	49[2]
Chan & Nakamura (1969)	Extruded Polystyrene	1050[1]	1400[1]	−
Gent & Thomas (1959)	Rubber Latex Foam	−	2.64[1]	−
Lederman (1971)	Rubber Latex Foam	−	−	−
Matonis (1964)	Rigid Polystyrene	1050[3]	1380[1]	79[1]
Moore et al. (1974)	Polystyrene Acrylonitrile	1065[1]	3670[1]	−
	Polypropylene Copolymer	902[4]	1130[4]	−
Patel & Finnie (1970)	Rigid Polyester Based Polyurethane	1230[1]	1600[1]	127[1]
Phillips & Waterman (1974)	Rigid Polyurethane	1200[5]	1600[6]	−
Traeger (1967)	Rigid PAPI Polyurethane Foam	1200[5]	1600[6]	127[6]
Walsh et al. (1965)	Glass	2511[1]	75000[1]	−

Notes:

1.   Data from work cited.

2.   Roff and Scott (1971) p.112–113 and Harper (1975) p.3–32.

3.   Roff and Scott (1971) p.47.

4.   Bonnin et al. (1969) p.517.

5.   Roff and Scott (1971) p.453.

6.   Patel and Finnie (1970) p.909.
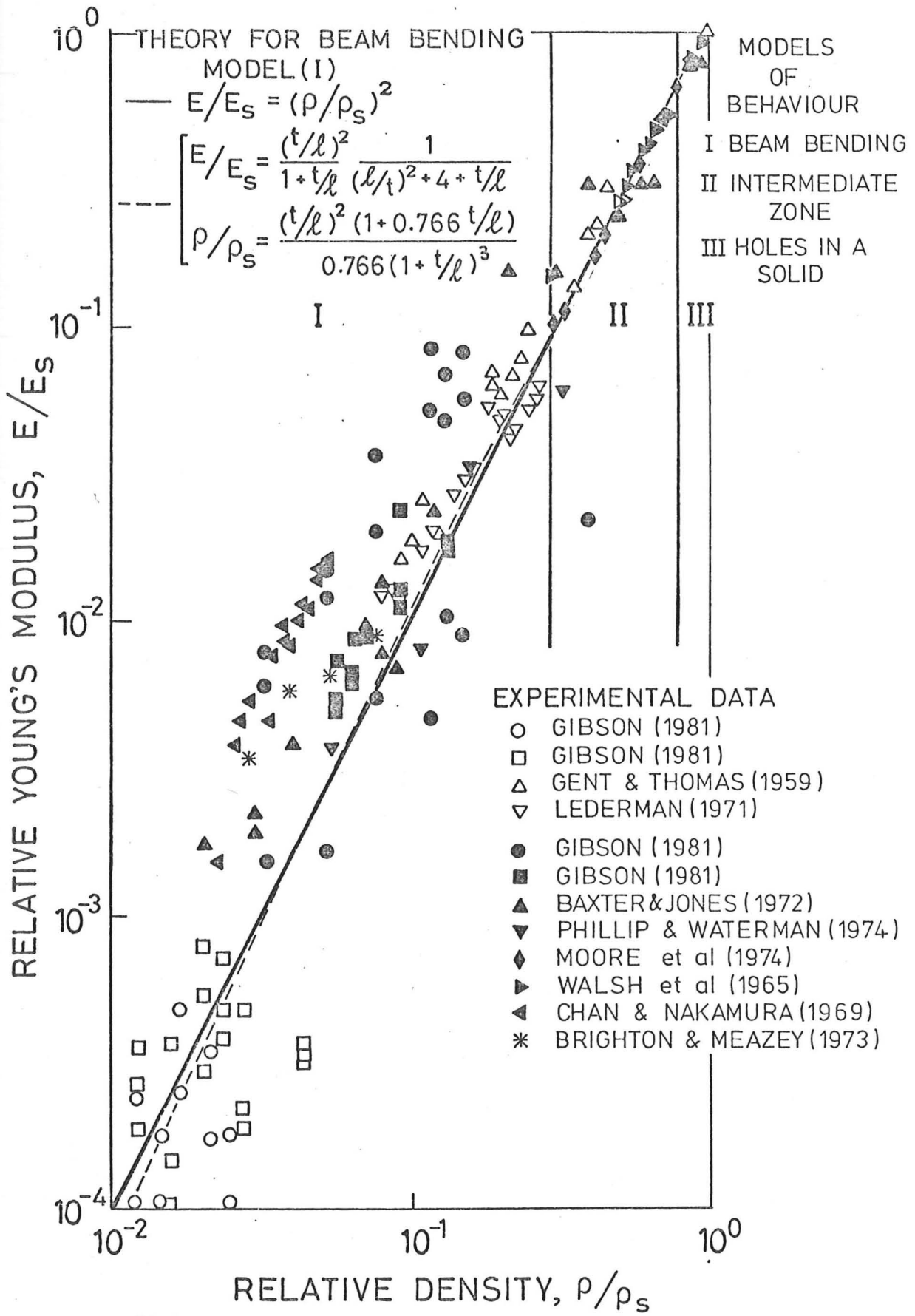
Fig 6.6 Relative Young's modulus, E/E_s, against relative density, ρ/ρ_s. Open symbols represent open cell foams; shaded symbols represent closed cell foams.
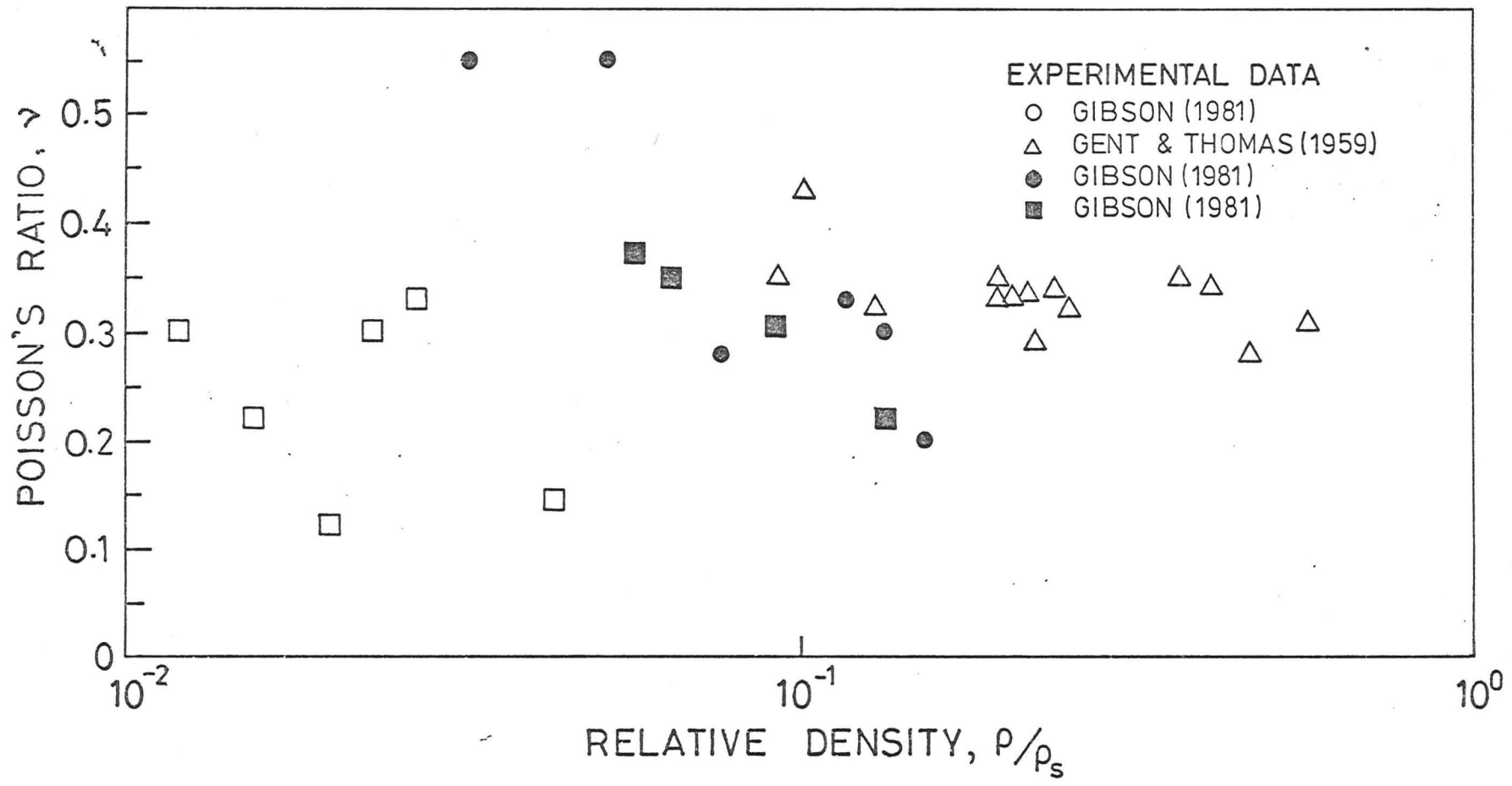
Fig. 6.7 Poisson's ratio, ν, against relative density, ρ/ρ_s. Open symbols represent open cell foams; shaded symbols represent closed cell foams.
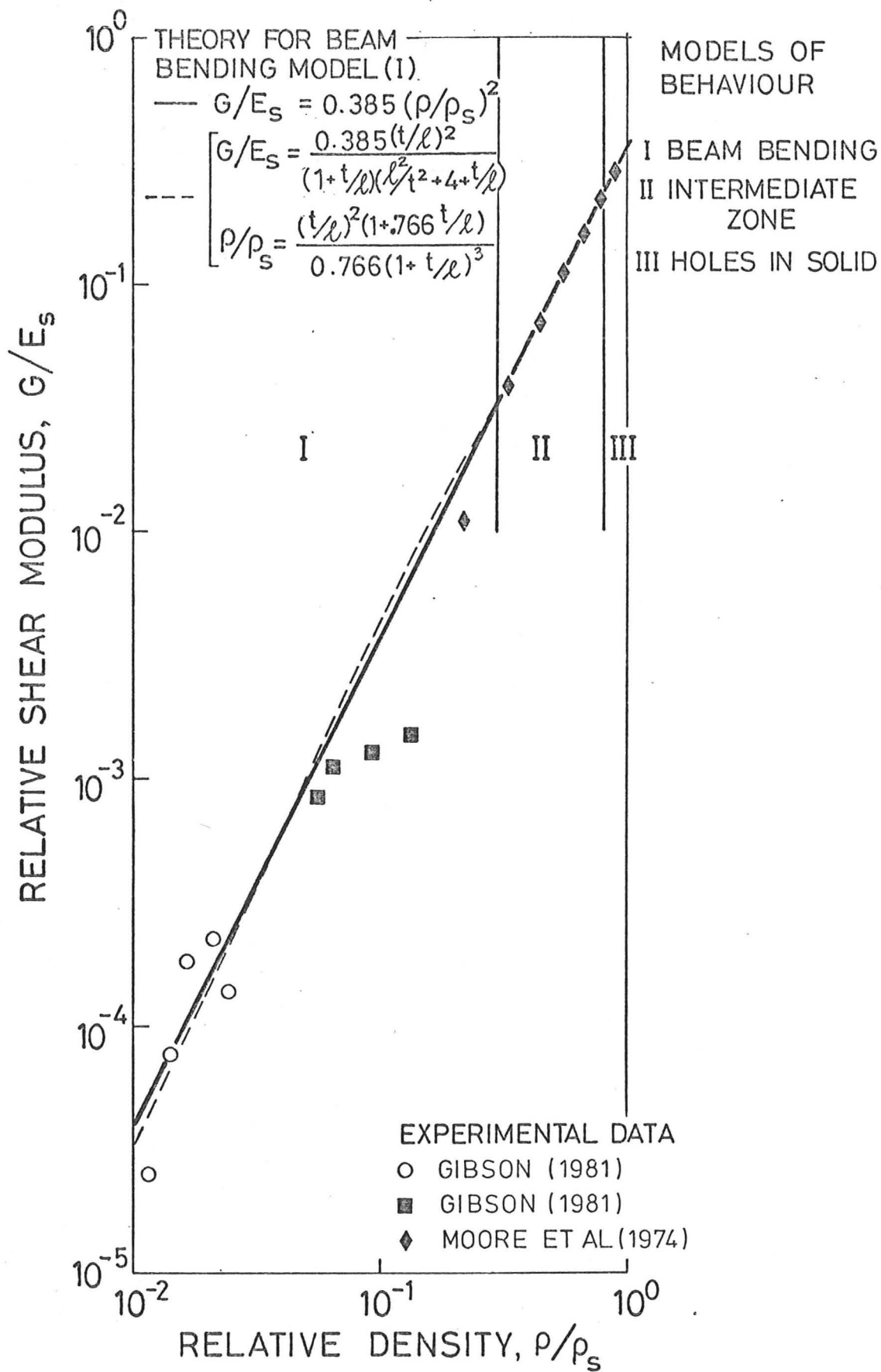
Fig. 6.8 Relative shear modulus, G/G_s, against relative density, ρ/ρ_s. Open symbols represent open cell foams; shaded symbols represent closed cell foams.
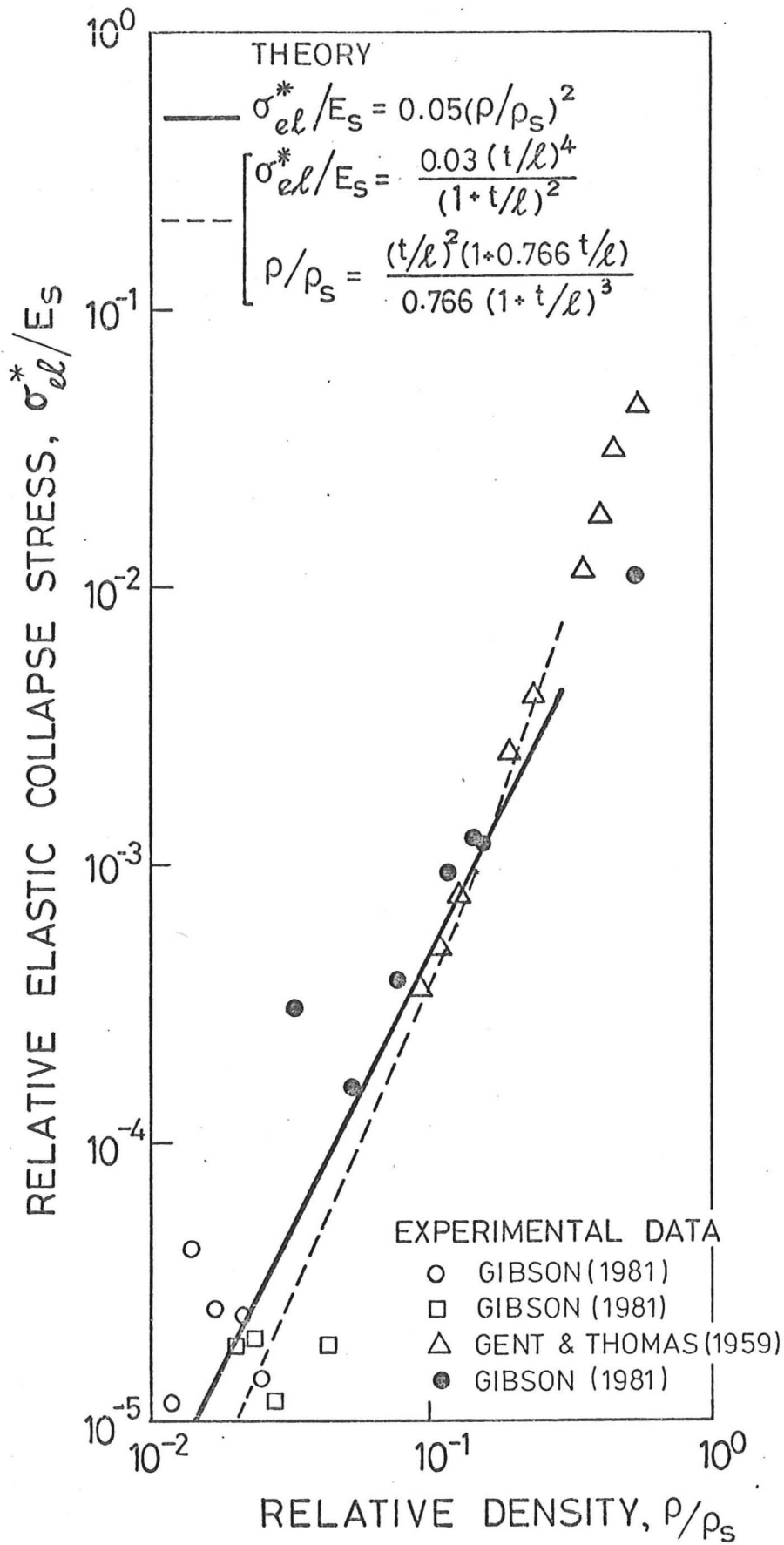
Fig. 6.9 Relative elastic collapse stress, σ^*/E_s, against relative density, ρ/ρ_s. Open symbols represent open cell foams; shaded symbols represent closed cell foams.
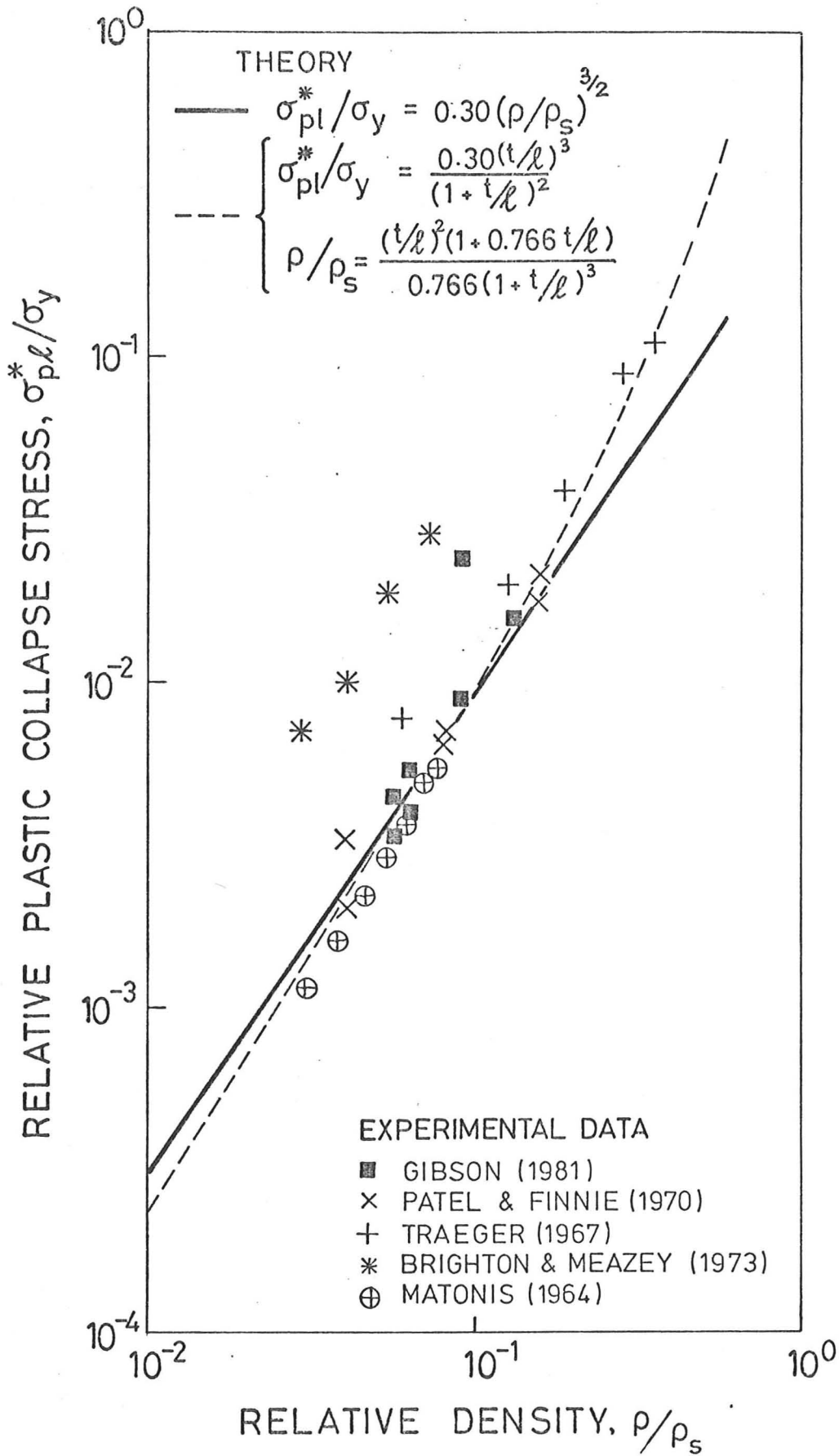
Fig. 6.10 Relative plastic collapse stress, σ^*_{pl}/σ_y, against relative density, ρ/ρ_s. (All data for closed cell foams.)

The two analyses of Young's modulus for low relative densities presented in Chapter 5 both predict $E/E_s = C (\rho/\rho_s)^2$. If groups of data (with $\rho/\rho_s \leq 0.3$) are taken separately, each agrees well with this rule, but there is some variation in the intercept, C, at $\rho/\rho_s = 1$. There are two possible sources for this variation: the geometry of the foams (which determines the constant C) could vary between foams; or, the value we have used for the solid Young's modulus, E_s, could be incorrect. It is likely that the gross foam geometry (and thus C) is about constant for different foams. But, as mentioned earlier, the value of E_s is rarely known with precision – it depends on the degree of polymer chain alignment, on chemical changes brought about by the foaming agent, on the gradual aging and oxidation of the polymer and on other such uncontrolled factors. It seems more likely that it is errors in E_s which cause the apparent variation in C. With the exception of the data of Chan and Nakamura (1969), the best fit line to all the low density data gives C = 1; and this is the value we shall adopt.

This is in remarkable coincidence with the models for high density foams. At relative densities greater than 0.8, the material can be modelled as a solid with widely separated spherical holes in it: MacKenzie (1950) has derived expressions for the shear and bulk moduli of such materials. Assuming Poisson's ratio of the solid to be 0.3, and combining his two expressions, we have found that his model predicts $E/E_s = (\rho/\rho_s)^2$ for ρ/ρ_s greater than 0.8 (see Figs. 5.14 and 5.15). The experimental data again follow this square rule.

This leaves the intermediate régime of relative densities between
0.3 and 0.8. In this régime, the material behaves neither as a net-
work of bending beams, nor as a solid with isolated holes in it. No
model of behaviour is available for this region, but the experimental
data again follow the rule $E/E_s = (\rho/\rho_s)^2$. Thus, over the entire range
of relative densities (from 0.01 to 1.00) the simple $E/E_s = (\rho/\rho_s)^2$
rule applies to both open and closed cell foams, although the model of
foam behaviour changes.

Poisson's ratio

Experimental data for Poisson's ratio for relative densities
between 0.01 and 0.60 are plotted in Fig. 6.7. Poisson's ratio
is independent of relative density: the theory derived in Chapter 5
predicts this result. There is a large amount of variation in the
data (from $\nu = 0.12$ to $\nu = 0.55$) and the average value of Poisson's
ratio is about $\frac{1}{3}$.

Shear modulus

Experimental data have been obtained for the shear modulus of
foams with relative densities between 0.01 and 1.00. The experi-
mental data follows a simple $G/E_s \propto (\rho/\rho_s)^2$ law throughout this range
of relative density. If the constant of proportionality of the relative
Young's modulus law is taken to be 1, and Poisson's ratio for the solid
polymer is assumed to be 0.3, then the constant of proportionality for
shear modulus relationship is $1/|2(1 + \nu)|$ or 0.385, and
$G/E_s = 0.385(\rho/\rho_s)^2$. The experimental data fit this law very well.

Like Young's modulus, there are three zones of behaviour at different relative densities. For $\rho/\rho_s < 0.3$, the material can be modelled as a network of bending struts and the 2 theories of Chapter 5 (which give similar results) apply. At relative densities greater than 0.8 the material can be modelled as a solid with isolated spherical holes in it and MacKenzie's (1950) derivation of shear modulus applies. Finally, at relative densities between 0.3 and 0.8 the material cannot be modelled in either of these ways — this is an intermediate zone for which no theory has been developed. It is likely though, that there is not much deviation from the square relationships of the first and last zones. Again, then, although there are different models of behaviour at different relative densities, the shear modulus can be predicted to be proportional to $(\rho/\rho_s)^2$ at all relative densities. In particular, if $E/E_s = 1 \, (\rho/\rho_s)^2$ and $\nu_s = 0.3$, $G/E_s = 0.385 \, (\rho/\rho_s)^2$. This relationship satisfactorily predicts the experimental results.

Elastic collapse stress

Data for the elastic collapse stress: solid Young's modulus are shown in Fig. 6.9. They closely follow the curve of the second level of theory for σ_{el}^*/E_s (equation (5.24)) with the constant of proportionality equal to 0.03.

We can roughly estimate a theoretical value for this constant as follows. The critical buckling load of a column is (Fig. 5.4):

$$F_{cr} = \frac{n^2 \, \pi^2 \, E_s \, I}{\ell^2}$$

The n^2 factor here relates to the degree of end restraint on the column. For a pinned column, $n = 1$, while $n = \frac{1}{2}$ for a column

Like Young's modulus, there are three zones of behaviour at different relative densities. For $\rho/\rho_s < 0.3$, the material can be modelled as a network of bending struts and the 2 theories of Chapter 5 (which give similar results) apply. At relative densities greater than 0.8 the material can be modelled as a solid with isolated spherical holes in it and MacKenzie's (1950) derivation of shear modulus applies. Finally, at relative densities between 0.3 and 0.8 the material cannot be modelled in either of these ways - this is an intermediate zone for which no theory has been developed. It is likely though, that there is not much deviation from the square relationships of the first and last zones. Again, then, although there are different models of behaviour at different relative densities, the shear modulus can be predicted to be proportional to $(\rho/\rho_s)^2$ at all relative densities. In particular, if $E/E_s = 1\ (\rho/\rho_s)^2$ and $\nu_s = 0.3$, $G/E_s = 0.385\ (\rho/\rho_s)^2$. This relationship satisfactorily predicts the experimental results.

Elastic collapse stress

Data for the elastic collapse stress: solid Young's modulus are shown in Fig. 6.9. They closely follow the curve of the second level of theory for σ_{el}^*/E_s (equation (5.24)) with the constant of proportionality equal to 0.03.

We can roughly estimate a theoretical value for this constant as follows. The critical buckling load of a column is (Fig. 5.4):

$$F_{cr} = \frac{n^2\ \pi^2\ E_s\ I}{\ell^2}$$

The n^2 factor here relates to the degree of end restraint on the column. For a pinned column, $n = 1$, while $n = \frac{1}{2}$ for a column

fixed at one end only. In the analysis of buckling in two-dimensional cellular materials (Chapter 3) we found that members behaved as if they had springs at their ends and one end was free to translate horizontally. The constraint gives n = 0.69 for a regular hexagonal array of members in two-dimensions. Members in three-dimensional cellular materials are constrained in a similar manner. The rotational stiffness of the ends is determined by the bending stiffness of the edges meeting at the ends, and the ends are free to translate with respect to each other. For this end condition n must lie between zero and one. The degree of constraint for a three-dimensional cellular material is higher than for the two-dimensional regular hexagonal cellular material since there are more than two restraining members at each corner so n must be greater than 0.69. It is reasonable, then, to assume that n $\approx$ 0.75 for three-dimensional cellular materials.

The elastic collapse stress is given by:

$$\sigma_{el}^* = \frac{P_{cr}}{\alpha^2 \, (\ell + t)^2}$$

where α^2 is a factor relating the square of the edge length of a cell, $(\ell + t)^2$, to the area over which the stress acts. For a pentagonal dodecahedron, the cross-sectional area of the cell is approximately $7.8 \, (\ell + t)^2$. Combining $\alpha^2 = 7.8$ and n = 0.75 we find:

$$\frac{\sigma_{el}^*}{E_s} = \frac{n^2 \, \pi^2 \, I}{\alpha^2 \, \ell^2 \, (\ell + t)^2}$$

$$\approx \frac{0.06 \, (t/\ell)^4}{(1 + t/\ell)^2}$$

for a square cross-sectioned column of thickness, t. The constant
of proportionality in equation (5.24) is roughly 0.06 from this
calculation. Experimentally we find a slightly lower value, 0.03.

The *strain* at which elastic collapse occurs is simply
$\varepsilon^* = \sigma_{el}^*/E$: this is the strain at which the stress-strain curve
becomes non-linear. We have found that ε^* increases with relative
density from 0.03 to 0.12 for our foams and for those of Gent and
Thomas (1959). Taking the ratio of σ_{el}^*/E_s and E/E_s (equations
5.24 and 5.22), and using the 'best fit' constants of proportionality
for these equations, we find:

$$\varepsilon^* = \frac{\sigma_{el}^*}{E} = \frac{0.03 \ (1 + 4 \ (t/\ell)^2 + (t/\ell)^3)}{1 + t/\ell}$$

This predicted elastic collapse strain rises from 0.03 at low
relative densities to 0.10 for a relative density of 0.30.
(This is the limiting value of relative density for which the elas-
tic collapse stress equation (5.24) is valid.) This agrees well with
our experimental observations.

Plastic collapse

The experimental data shown in Fig. 6.10 follow the curve of the
more refined model very well. Each set of data follows the slope of
the theoretical curve, but with differing constants of proportionality,
C. This is probably due to the difficulty in estimating the yield stresses
of the solid polymers the foams are made up of, σ_y. We have taken C = 0.30.
The value of the proportionality constant can be estimated by noting that
for a square cross-section, t^2, the fully plastic moment is equal to
$\sigma_y \ t^3/4$, that the cross-sectional area of a pentagonal dodecahedron is
about $(2.8 \ (\ell + t))^2$, and that there are 5 vertices per cell.

$$\sigma^*_{p1} = \frac{5M_p}{\alpha^2 \ell (\ell + t)^2}$$

$$= 0.15 \ \sigma_y \frac{(t/\ell)^3}{(1 + t/\ell)^2}$$

This approximate analysis shows that the constant of proportionality should be about 0.15. The measured value of 0.30 is not unreasonable, then.

6.5 Conclusions

The theoretical predictions all give good agreement with experiments over a large range of relative density. Open and closed cells can be treated identically if the volume ratio of polymer in the faces to edges is small for closed cell foams. A square law relationship holds for both the Young's and the shear moduli of foams with respect to relative density over the entire range of relative densities from 0.01 to 1.00, although two distinct mechanisms of deformation occur at low and high relative densities.

Experimentally determined values of the constant of proportionality for each mechanical property are listed in Table 6.3 along with the rule for mechanical behaviour using these constants. Not all of the data shown in Figs. 6.6 to 6.10 yield these constants. This is probably due to the difficulty in estimating the solid polymer properties. For design purposes with a particular type of foam, it may be more suitable to write the theoretical equations for a property, Q in the form:

$$Q = C \ Q_s \ (\rho/\rho_s)^n$$

TABLE 6.3:   Summary of Mechanical Behaviour of Three-Dimensional Cellular Materials

MECHANICAL PROPERTY	C	FINAL THEORETICAL LAW	SIMPLE LAW	ρ/ρ_s LAW VALID FOR
RELATIVE DENSITY, ρ/ρ_s	–	$\dfrac{(t/\ell)^2(1 + 0.766\ t/\ell)}{0.766\ (1 + t/\ell)^3}$	$(t/\ell)^2$	All
RELATIVE YOUNG'S MODULUS, E/E_s	1	$\dfrac{(t/\ell)^2}{1 + t/\ell}\ \dfrac{1}{(\ell/t)^2 + 4 + t/\ell}$	$(\rho/\rho_s)^2$	All
POISSON'S RATIO, ν	0.33	independent of t/ℓ	independent of ρ/ρ_s	All
RELATIVE SHEAR MODULUS, G/E_s	0.385	$\dfrac{0.385\ (t/\ell)^2}{1 + t/\ell}\ \dfrac{1}{(\ell/t)^2 + 4 + t/\ell}$	$0.385\ (\rho/\rho_s)^2$	All
RELATIVE ELASTIC COLLAPSE STRESS, σ^*_{el}/E_s	0.03	$\dfrac{0.03\ (t/\ell)^4}{(1 + t/\ell)^2}$	$0.05\ (\rho/\rho_s)^2$	$\rho/\rho_s < 0.30$
RELATIVE PLASTIC YIELD STRESS, σ^*_{pl}/σ_y	0.30	$\dfrac{0.30\ (t/\ell)^3}{(1 + t/\ell)^2}$	$0.30\ (\rho/\rho_s)^{3/2}$	$\rho/\rho_s < 0.63$

and do an experiment to determine the products of $C \, Q_s$. The theory developed should enable designers to predict foam behaviour using a simple power-law relationship between the foam property and relative density.

REFERENCES - CHAPTER 6

Baxter, S. and Jones, T.T. (1972) Plastics and Polymers 40, 69.

Billmeyer, F.W. (1971) "Textbook of Polymer Science", Second Edition. Wiley Interscience.

Bonnin, M.J., Dunn, C.M.R. and Turner, S. (1969) Plastics and Polymers 37, 517.

Brighton, C.A. and Meazey, A.E. (1973) "Expanded Polyvinyl Chloride" in Expanded Plastics - Trends in Performance Requirements - A Micro Symposium Organized by Q.M.C. Industrial Research Ltd. Sept. 25, 1973, London.

British Standards Institution (1973) BS 4370 Methods of Test for Rigid Cellular Materials - part 2, method 6.

Chan, R. and Nakamura, M. (1969) J. of Cellular Plastics 5, 112.

Gent, A.N. and Thomas, A.G. (1959) J. of Applied Polymer Science 1, 107.

Harper, C.A. (1975) "Handbook of Plastics and Elastomers" McGraw-Hill.

Lazan, B.J. (1968) "Damping of Materials and Members in Structural Mechanics", Pergamon.

Lederman, J.M. (1971) J. of Applied Polymer Science 15, 693.

MacKenzie, J.K. (1950) Proc. Phys. Soc. B63, 2.

Matonis, V.A. (1964) SPE Journal Sept., 1024.

Moore, D.R., Couzens, K.H. and Iremonger, M.J. (1974) J. of Cellular Plastics 10, 135.

Patel, M.R. and Finnie, I. (1970) J. of Materials 5, 909.

Phillips, P.J. and Waterman, N.R. (1974) Polymer Engineering and Science 4, 67.

Roff, W.J. and Scott, J.R. (1971) "Fibres, Films, Plastics and Rubbers - a Handbook of Common Polymers", Butterworths.

Traeger, R.K. (1967) J. of Cellular Plastics 3, 405.

Walsh, J.B., Brace, W.F. and England, A.W. (1965) J. American Ceramic Society 48, 605.

CHAPTER 7

CASE STUDY: THE STRUCTURE AND MECHANICS OF CORK

7.1 Introduction

Cork has a remarkable combination of properties. It is
light yet resilient; it is an outstanding insulator for heat and
sound; it has a high coefficient of friction; and it is impervious
to liquids, chemically stable and fire-resistant. Such is the de-
mand that production now exceeds half a million tonnes a year (and
one tonne of cork has the volume of 56 tonnes of steel).

In pre-Christian times cork was used (as we still use it today)
for fishing floats and soles of shoes. When Rome was beseiged by
the Gauls in 400 B.C., messengers crossing the Tiber clung to cork
for buoyancy (Plutarch, 100). Pepys' Diary (1666) records its use
as a possible new material in the construction of barricados. And
ever since man has cared about wine, he has cared about cork to keep
it sealed in flasks and bottles. *"Corticum abstrictum pice demovebit
amphorae** ..."* sang Horace (27 B.C.), to celebrate the anniversary
of his miraculous escape from death from a falling tree. But it was
the Benedictine Abbey at Hautvillers where, in the 17th century, the
technology of stopping wine bottles with clean, unsealed cork was
perfected. Its elasticity and chemical stability mean that it seals
the bottle without contaminating the wine, even when it must mature
for many years. No better material is known, even today.

---

*"pull the cork, set in pitch, from the bottle ..."

Commercial cork is the bark of an oak (*Quercus suber*) which grows in Portugal, Spain, Algeria and California. Pliny (who met an untimely end in the great eruption of Vesuvius in 79 A.D.) describes it thus:

> "The Cork-Oak is a small tree, and its acorns are bad in quality and few in number; its only useful product is its bark which is extremely thick and which, when cut, grows again". (Pliny, 77).

Modern botanists add that the cork cells (*phellem*) grow from the equiaxed cortex cells via an intermediate structure knows as cork cambium (*phellogen*). Their walls are covered with thin layers of unsaturated fatty acid (*suberin*) and waxes which make them impervious to air and water, and resistant to attack my many acids (Esau, 1965; Zimmerman and Brown, 1971; Eames and MacDaniels, 1951). All trees have a thin layer of cork in their bark. Quercus suber is unique in that, at maturity, the cork forms a layer several centimeters thick around the trunk of the tree.

Its function in nature is to insulate the tree from heat and loss of moisture, and perhaps to protect it from mechanical damage by animals (suberin tastes unpleasant). We use it today for thermal insulation in refrigerators and rocket boosters, acoustic insulation in submarines and recording studios, as a seal between mating surfaces in woodwind instruments and internal combustion engines, as an energy-absorbing medium in flooring, shoes and packaging, and as a damped elastic solid in cricket balls and shuttlecocks. Its use has widened further since 1892, when a Mr. John Smith of New York patented a

process for making cork aggregate by the simple hot-pressing of
cork particles: the suberin provides the necessary bonding.

Cork occupies a special place in the history of microscopy and of
plant anatomy. When Robert Hooke perfected his microscope, around
1660, one of the first materials he examined was cork. What he
saw led him to identify the basic unit of plant and biological
structure, which he termed "the cell". His book "Micrographia"
(Hooke, 1664) records it thus:

> *"I no fooner defcern'd thefe (which were indeed the*
>
> *firft microfcopical pores I ever faw, and perhaps,*
>
> *that were ever feen, for I had not met with any*
>
> *Writer or Perfon that had made any mention of them*
>
> *before this) but me thought I had with the difcovery*
>
> *of them, prefently hinted to me the true and intelli-*
>
> *gible reafon of all the Phenomena of Cork".*

Hooke's careful drawings of cork cells show their roughly hexagonal
shape in one section, and their box-like shape in the other (Fig. 7.1).
Hooke noted that the cells were stacked in long rows, with very thin
walls *"as thofe thin films of Wax in a Honey-comb"*.

Subsequent descriptions of cork-cell geometry add very little to
this. Esau (1965), for example, describes cork as "approximately pris-
matic in shape - often somewhat elongated parallel to the long axis
of the stem". Lewis (1928) concluded that their shape lay "somewhere
between orthic and prismatic tetrakaidecahedrons". Eames and MacDaniels
(1951) simply described them as "polygonal", but their drawing, like
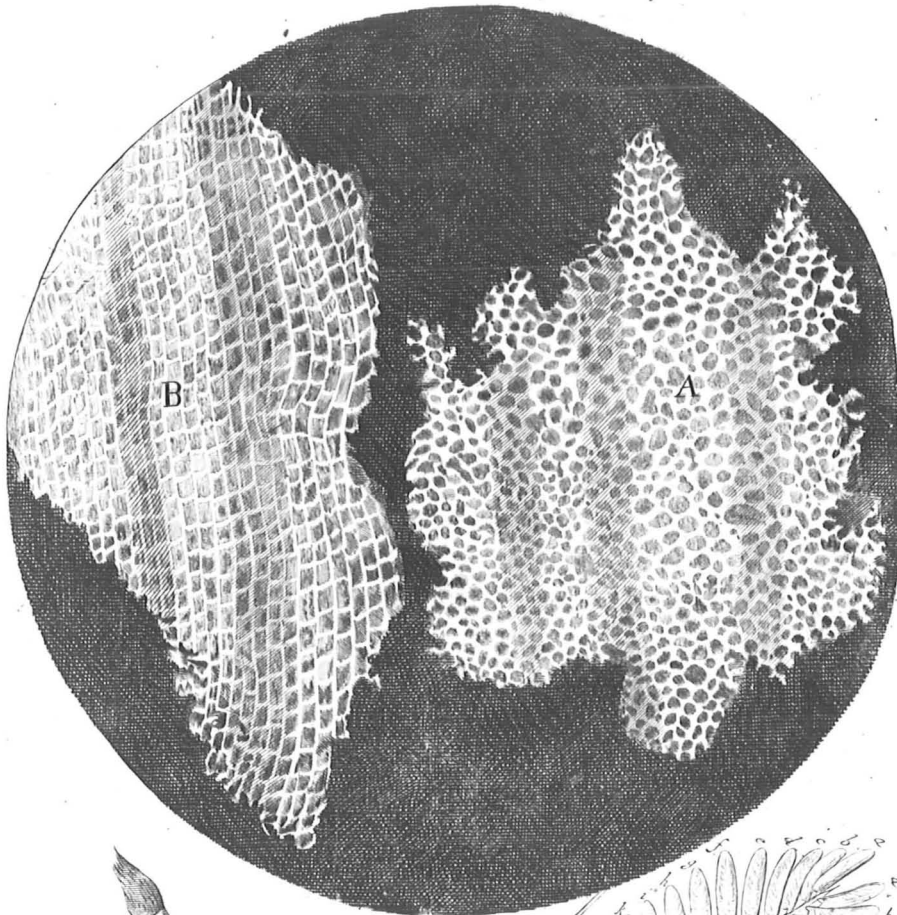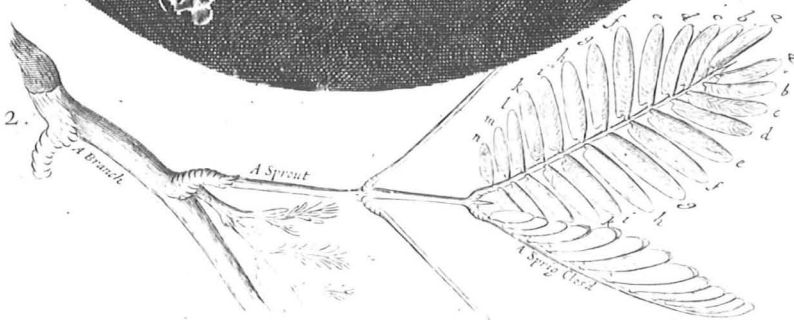
Fig. 7.1 Radial (A) and tangential (B) sections of cork, as seen by Robert Hooke through his microscope in 1664.

Hooke's, shows the approximate hexagonal shape in one section and their box-like shape in the other two.

These descriptions conflict, and none are quite correct. Our aim has been to characterise the cellular structure of commercial cork and to relate it to its mechanical properties.

7.2 Experimental Method

We cut cubes of cork for microscopy (making each cut with a new razor blade) such that the cut faces lay normal to the axis (X_2), a radius (X_1), and a tangent (X_3) of the trunk of the tree. Each cube was cut oversize and then trimmed to the final size (roughly 5 mm on a side) by taking thin silvers from each face: this gives a cleaner cut, with less cell distortion. The cubes were lightly coated with gold and examined by scanning electron microscopy.

Some of the cubes were mounted in a deformation stage (like a small machine vice) and deformed and photographed progressively in compression and tension along the normals to the faces. For tensile tests, two faces of the cube were glued to the platens of the vice.

Larger cubes (15 mm on a side), cut in the same way, were tested in tension and compression so that the stress-strain curves and Poisson's ratios could be recorded. Similar cubes, cut after a rotation of 45° about one of the 3 axes, were used to measure shear moduli. Other larger cubes were cyclically loaded to progressively higher stresses, recording the stress-strain curve on each cycle.

Friction on wet and dry cork was examined by sliding a steel slider down an inclined cork plane, measuring the angle of inclination at which motion started.

7.3　The Geometry of Cork Cells

Fig. 7.2 shows the three faces of a cube of cork. In one section, the cells are roughly hexagonal; in the other two, they are shaped like little bricks, stacked as one would stack them in building a wall. The similarity with Hooke's drawing (Fig. 7.1) is obvious.

From micrographs such as these, the cell shape can be deduced. At their simplest, the cells are closed hexagonal prisms (Fig. 7.3) stacked in rows so that the hexagonal faces register and are shared by two cells; but the rows are staggered so that the membranes forming the hexagonal faces are not continuous across rows. Fig. 7.4 shows how the cells lie with respect to the trunk of the tree. The axes of the hexagons lie parallel to the radial (X_1) direction. Then a cut normal to the radial direction shows the hexagonal cross-sections of the prismatic cells; any cut containing the radial direction shows the rectangular section of the prisms, stacked like bricks in a wall because of the staggering of the rows.

At higher magnifications, the scanning microscope reveals details which Hooke could not see, because their scale is comparable with the wavelength of light. Six out of the eight walls of each cell are corrugated (Fig. 7.5). Each cell has 2 or 3 complete corrugations, so that it is shaped like a little concertina, or bellows.

Fig. 7.6 and Table 7.1 summarise the observations and catalog the dimensions of the cork cells. The cell walls have a uniform thickness of about 1 μm. The aspect ratio of the cells, z/ℓ, is about 2; this is rather larger than the value (1.7) which minimises the surface area of a close-packed array of hexagons. The
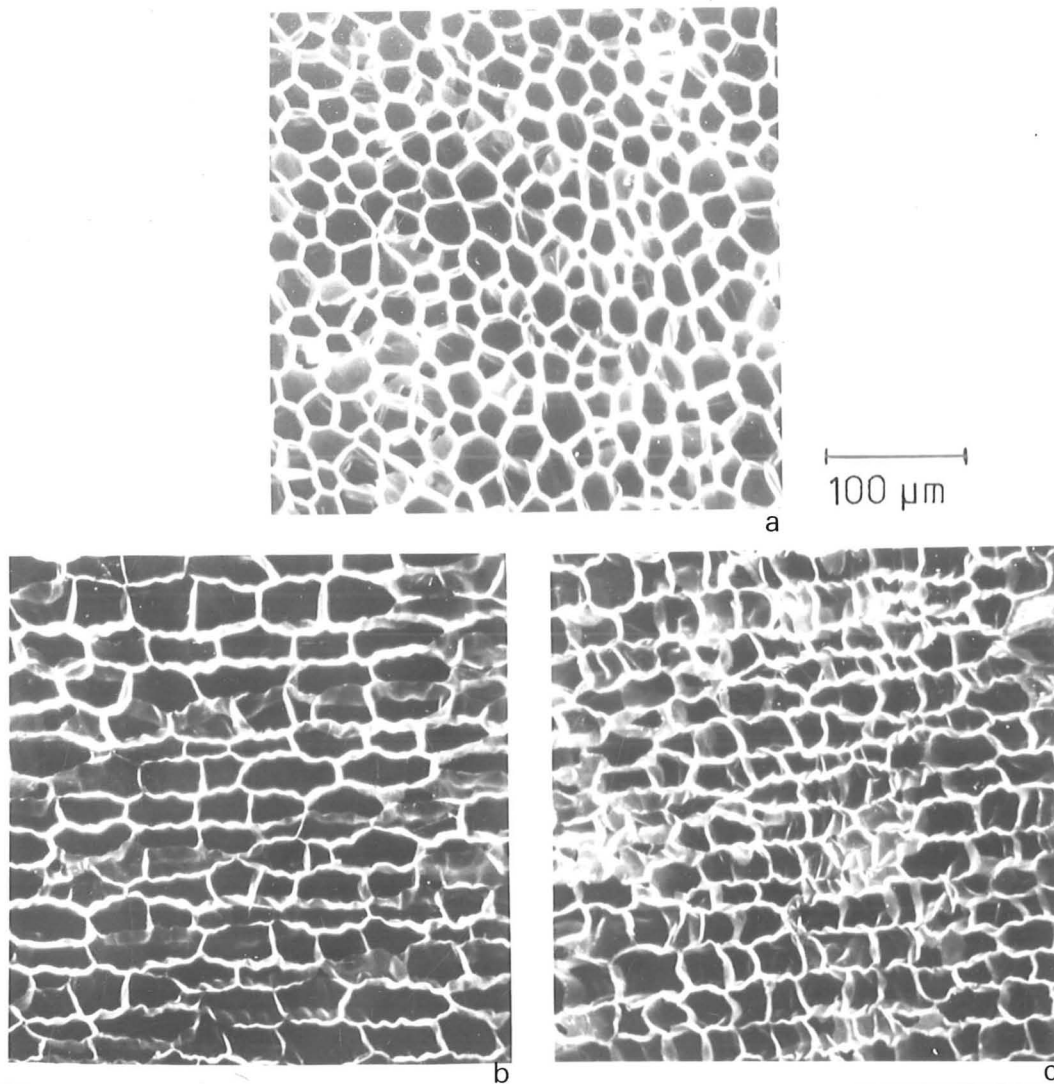
Fig. 7.2 Scanning electron micrographs of (a) radial, (b) axial, and
(c) tangential sections of cork.
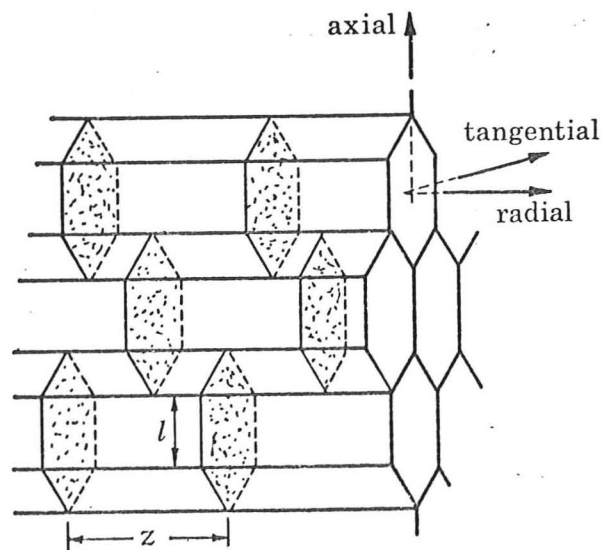
Fig. 7.3 The shape of cork cells, deduced from the micrographs
shown in Figure 7.2. There are, of course, imperfections
in the structure, and the cell walls are not straight
(as here) but corrugated.
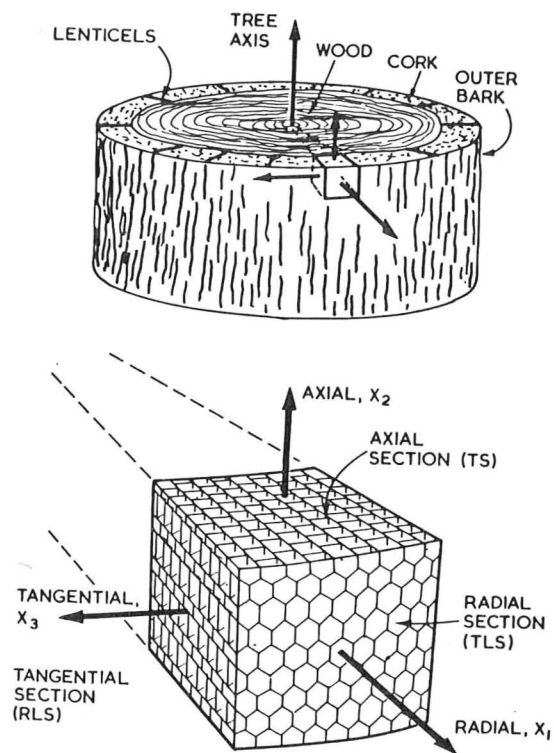
Fig. 7.4   Diagram of cork tree and cork, showing axis system and cells.

50 µm

(a)
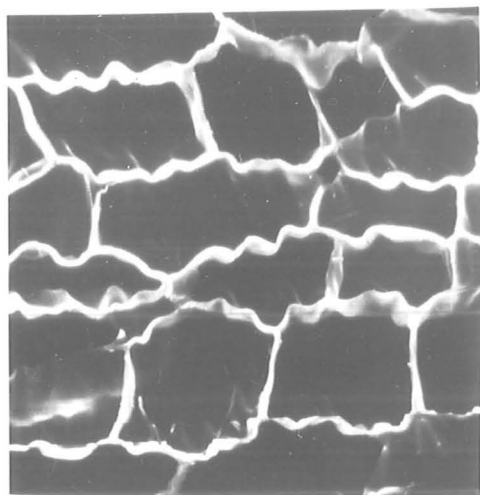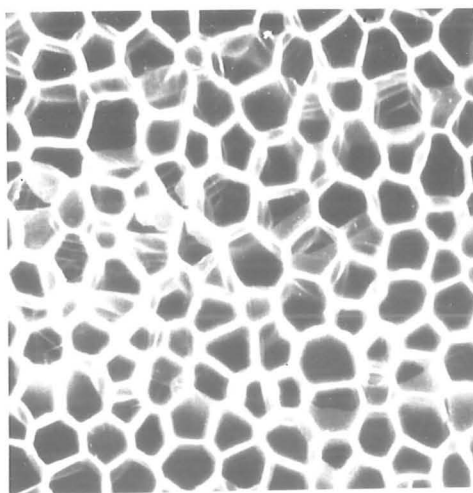
100 µm

(b)

Fig. 7.5 Scanning electron micrographs of cork cells, showing corrugations. (a) Tangential and (b) radial sections.

$z \approx 40\,\mu m$

$t \approx 1\,\mu m$

$l \approx 20\,\mu m$

l

$2a \approx 5.6\,\mu m$

$\lambda \approx 15\,\mu m$
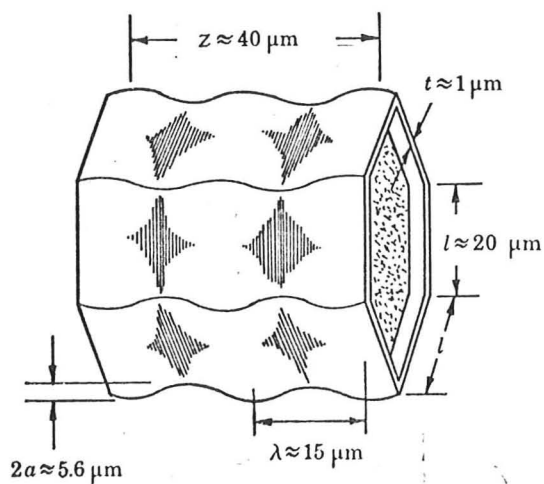
Fig. 7.6 A corrugated cell, showing dimensions.

radial section of the structure does not always show hexagonal sections: 5, 6, 7 and 8-sided figures are all observed. But the average number of sides per cell in the radial section is very close to 6; Lewis (1928) finds 5.978. This, of course, is an example of the operation of Euler's law (Euler, 1752), which asserts (when applied to a 3-connected net) that the average number of sides per cell is 6. The cells themselves are very small: there are about 20,000 of them in a cubic millimeter. They are much smaller than those in any commercial foamed plastic.

If the cell walls have a uniform thickness t, and the prisms have length z and hexagonal face edge ℓ, then the density ρ of the cork is related to that of the cell wall material ρ_s by:

$$\frac{\rho}{\rho_s} = \frac{t}{\ell}\left[\frac{\ell}{z} + \frac{2}{\sqrt{3}}\right] \qquad (7.1)$$

The density of the cell wall material is close to 1150 kg/m^3 (Appendix 7A). The mean density of the corks we studied was 170 kg/m^3, so the relative density is $\rho/\rho_s \approx 0.15$. That calculated from equation (7.1) using the average values in Table 7.1, is .078. This discrepancy is in part due to the corrugations in the cell walls, which (when included) increase the calculated density to 0.1; and in part due to narrow bands of high density associated with growth rings.

TABLE 7.1: CELL DIMENSIONS IN COMMERCIAL CORK

Dimension		
Cell wall thickness	t (μm)	1 ± 0.5
Prism height	z (μm)	43 ± 4
Prism edge-length	ℓ (μm)	21 ± 4
Cell volume $\frac{3\sqrt{3}\ell^2 h}{2}$	V (μm)^3	5×10^4
*Number of cells/mm^3	N (mm^{-3})	2×10^4
Corrugation wave length	λ (μm)	15 ± 2.3
Corrugation amplitude	a (μm)	2.8 ± 1
Measured density	ρ (kg/m^3)	170

*Hooke (1664) measured 7.7×10^4/mm^3; Cooke (1948)
gives 1.2×10^4/mm^3.

7.4 Elastic Deformation of Cork

Mechanical Tests

We recorded the stress-strain curves of cork cubes, in compression and tension, loaded along the radial, axial and tangential directions. Fig. 7.7 is a complete compressive stress-strain curve. The material is linear-elastic up to about 7 % strain*, when elastic collapse gives an almost horizontal plateau. This extends to about 70 % strain when complete collapse of the cells causes the curve to rise steeply. Fig. 7.8 shows the linear elastic part of the loading curve for compression along the three orthogonal directions.

---

*This strain, ε, is defined by:

$$\varepsilon = \ell_o/\ell - 1$$

where ℓ_o is the height of the undeformed cork cube and ℓ its length after deformation.
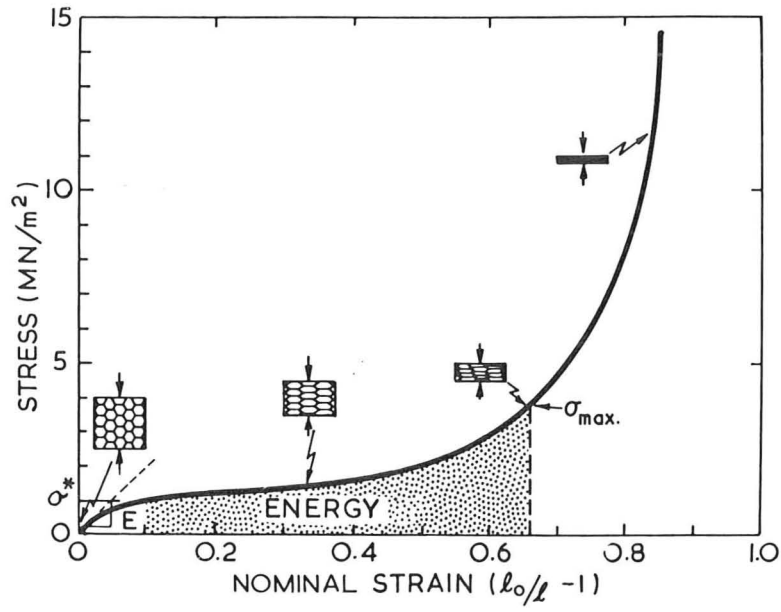
Fig. 7.7   Stress-strain curve for cork.
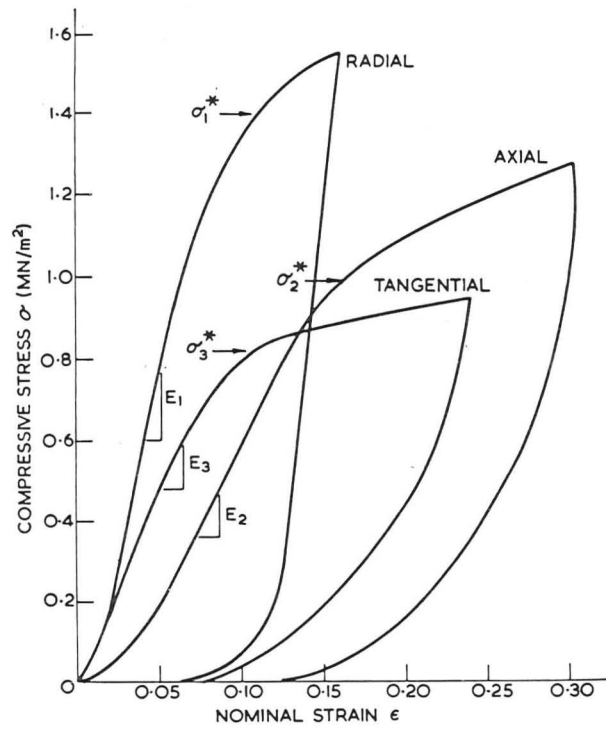
Fig. 7.8   Stress-strain curves for cork, compressed along its three axes.
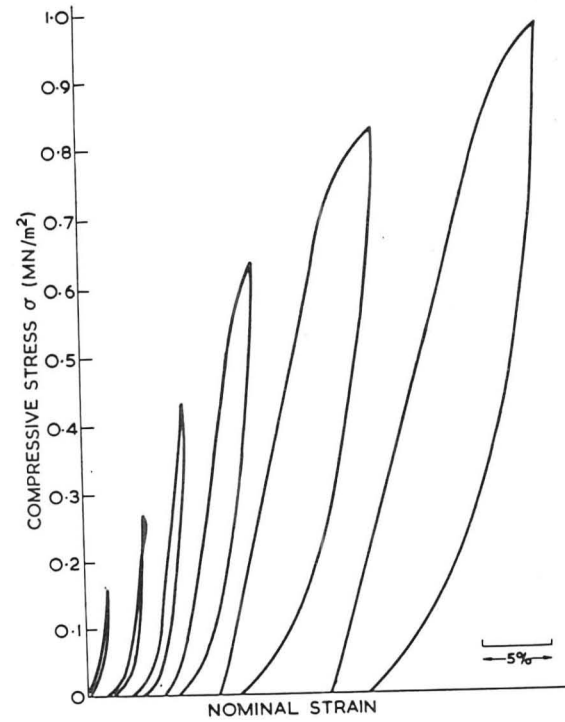
Fig 7.9   Stress-strain loops for cork loaded to progressively higher strains. Each loop has a large area, indicating a large energy dissipation.

Young's moduli, the shear moduli and Poisson's ratios are re-corded in Table 7.2. (Each number is a mean of several measurements. When the moduli in two directions differed by no more than the experimental error, the two have been bracketted and a single value given). The modulus along the prism axis is roughly twice that along the other two directions. The moduli (and the other properties) have circular symmetry about the prism axis. In the plane normal to this axis, cork is roughly isotropic, as might be expected from its structure.

The table lists the stress (σ^*) and the strain at the start of the plateau in compression, and the fracture stress (σ_f) and strain in tension. In compression, elastic collapse occurs at about 7 % strain. Tensile fracture along the prism axis occurs at 5 % strain, but in the other two directions the strain is larger: about 8 %.

Finally, the table lists the loss coefficient:

$$\eta = \frac{D}{2\pi U}$$

where D is the energy dissipated in a complete tension-compression cycle and U is the maximum energy stored during the cycle. Half-cycle loops are shown in Fig. 7.9, at a frequency of about 10^{-2} hertz; a loss coefficient of similar magnitude is found up to 4 khertz, with a peak of 2 khertz (Fernandez, 1978). The loss coefficient rises from 0.1 at low strain amplitudes to 0.3 at high. This is a high loss and gives cork good damping and sound-absorbing properties, and a high coefficient of friction (Section 7.6).

TABLE 7.2: MECHANICAL PROPERTIES OF CORK

YOUNG'S MODULUS

Radial, $\quad E_1 \quad = \quad 20 \pm 7$ MN/m^2

Axial, $\qquad E_2$
Tangential, E_2 $\Big]$ $= 13 \pm 5$ MN/m^2

**SHEAR MODULUS*

In 1-2 plane G_{12}
In 1-3 plane G_{13} $\Big]$ $= 2.5 \pm 1.0$ MN/m^2

In 2-3 plane G_{23} $= 4.3 \pm 1.5$ MN/m^2

POISSON'S RATIO†

$\nu_{12} = \nu_{21} = \nu_{13} = \nu_{31} = 0 \quad \pm \quad 0.05$

$\nu_{23} = \nu_{32} \qquad\qquad = 0.5 \pm 0.05$

COLLAPSE STRESS AND STRAIN IN COMPRESSION

Radial, $\qquad \sigma_1^* = 0.8 \pm 0.2$ MN/m^2, 4 % strain

Axial, $\qquad \sigma_2^*$
Tangential, σ_3^* $\Big]$ $= 0.7 \pm 0.2$ MN/m^2, 6 % strain

FRACTURE STRESS AND STRAIN IN TENSION

Radial, $\qquad \sigma_{f1} = 1.0 \pm 0.2$ MN/m^2, 5 % strain

Axial, $\qquad \sigma_{f2}$
Tangential, σ_{f3} $\Big]$ $= 1.1 \pm 0.2$ MN/m^2, 9 % strain

LOSS COEFFICIENT

Radial, $\qquad \eta_1 \quad = \quad 0.1 \quad$ at $\quad$ 1 % strain

Axial, $\qquad \eta_2$
Tangential, η_3 $\Big]$ $= \quad 0.3 \quad$ at 20 % strain

---

* The method of obtaining G_{12} $\quad G_{13}$ $\quad$ and $\quad G_{23}$ is given in Appendix 7C.

† The quantity ν_{12} is defined by $\nu_{12} = -\dfrac{\varepsilon_{22}}{\varepsilon_{11}}$ and so forth.

Microscopy

When cork deforms, the cell walls bend and buckle. We found that the behaviour when the axis of deformation lay along the prism axis differed from that when the axis of deformation lay across the prisms.

Deformation across the prism axis bends the cell walls, and later, in compression, causes them to buckle (Fig. 7.10) giving very large recoverable strains (of order 1).

Tensile deformation along the prism axis unfolds the corrugations (Fig. 7.11), straightening the prism walls. About 5 % extension is possible in this way; by then the walls have become straight, and further tension at first stretches and then breaks them, causing the cork to fail. Compressive deformation, on the other hand, folds the corrugations. The folding is unstable; once it reaches about 10 %, a layer of cells collapses completely, suffering a large compressive strain (Fig. 7.12). Further compression makes the boundary of this layer propagate; cells collapse at the boundary, which moves through the cork like a Luders band through steel, or a drawing band through polyethylene. We did not observe this instability when compressing across the axis.

7.5 Comparison of Measurements with Theory

Theory of Deformation in the Plane Normal to the Prism Axis

The in-plane deformation of a two-dimensional array of hexagonal cells (like cork when viewed down the prism axis) has been analysed
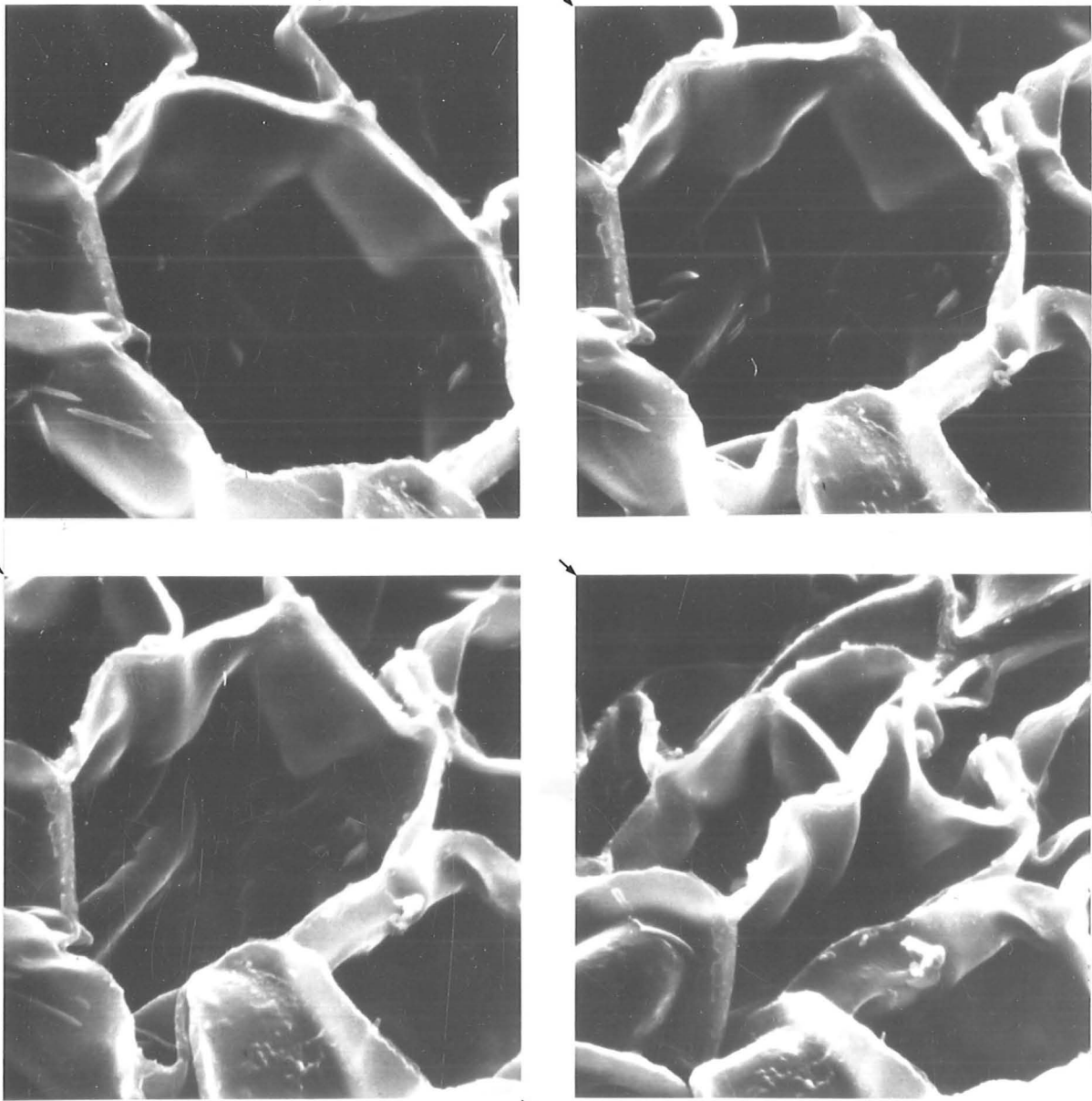
Fig. 7.10 Micrographs showing the bending and buckling of cell walls as cork is compressed across the prism axis.

50 µm
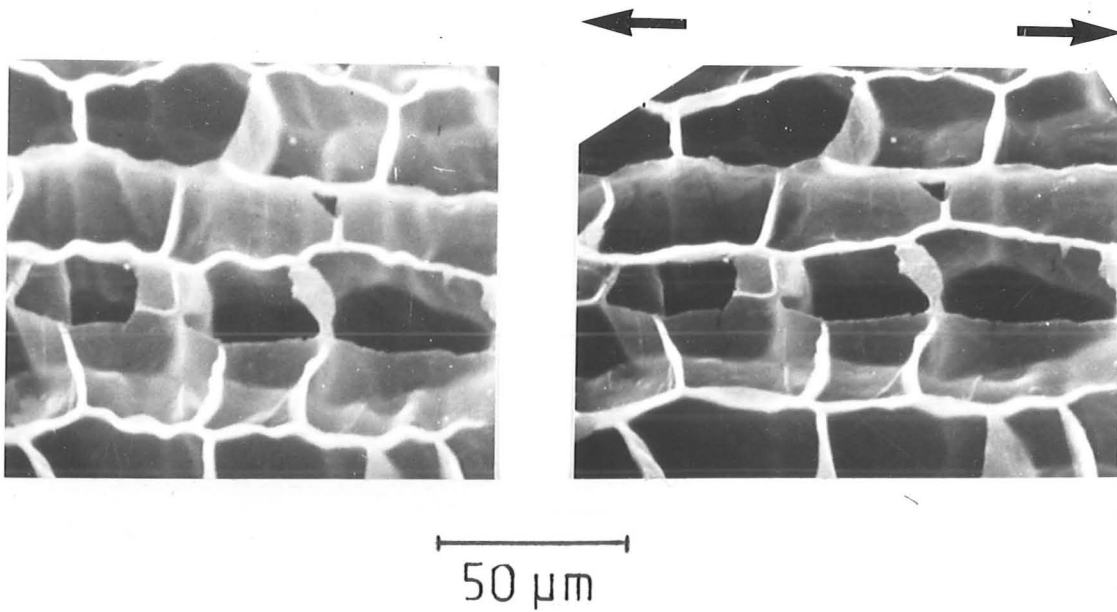
Fig. 7.11   Micrographs showing the progressive straightening of cell walls as cork is pulled in the radial direction.

100 µm
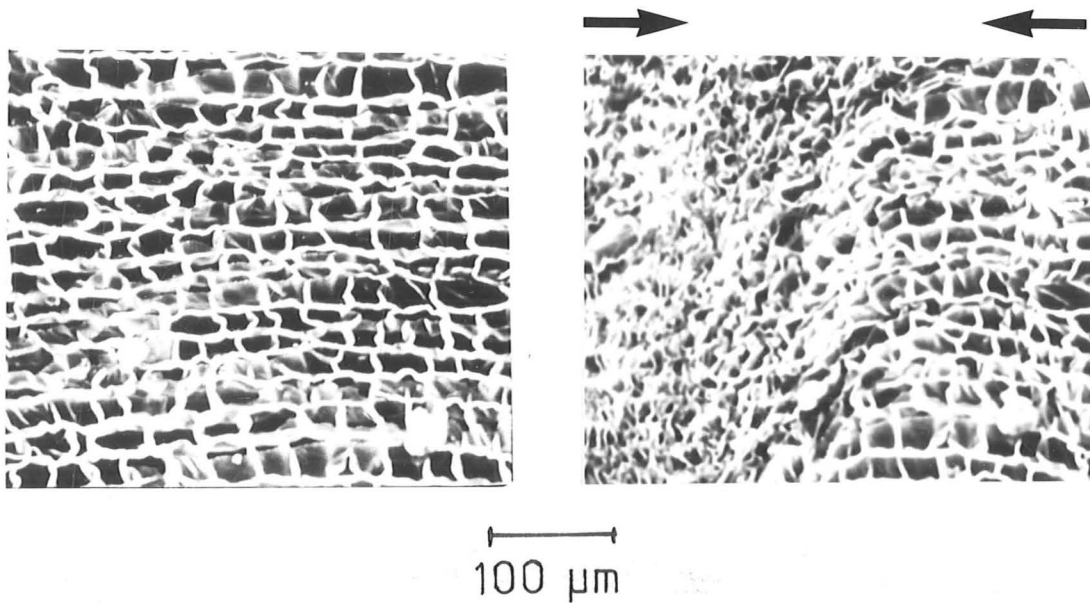
Fig. 7.12   The catastrophic collapse of cork cells compressed in the radial direction (along the prism axis).

completely in Chapter 3. Using the expressions given in Table 4.3
for the elastic properties of regular two-dimensional hexagonal
cells, along with equation (7.1) and Table 7.1, we find:

$$E_2 = E_3 = 0.5 \ E_s \left(\frac{\rho}{\rho_s}\right)^3 \qquad (7.2)$$

$$G_{23} = G_{32} = 0.13 \ E_s \left(\frac{\rho}{\rho_s}\right)^3 \qquad (7.3)$$

$$\nu_{23} = \nu_{32} = 1.0 \qquad (7.4)$$

$$\sigma_2^* = \sigma_3^* = 0.05 \ E_s \left(\frac{\rho}{\rho_s}\right)^3 \qquad (7.5)$$

Here E_s and ρ_s are the modulus and density of the solid of which
the cell walls are made, and ρ is the overall density of the cellular
material (the cork).

The form of the equations can be understood by noting that both
the bending stiffness and the buckling load of a beam vary as the cube
of the thickness t of the beam. For a given cell size, the density
ρ increases linearly with t, so the moduli and collapse stresses of
the structure vary as ρ^3. The collapse strain is given by $\varepsilon^* = \sigma_2^*/E_2 = 0.1$.
Below this strain the structure is linear-elastic. Above, it is non-linear
but still elastic. Buckling allows deformation to continue until the cell
walls touch (at a nominal strain of $(1 - \rho/\rho_s)$), allowing a large strain
at almost constant stress.

Theory of Deformation Parallel to the Prism Axis

If a honeycomb of regular prismatic cells like that of Fig. 7.3 is compressed parallel to the prism axis, the modulus is determined by the axial compression of the material in the cell walls. This leads to the obvious result

$$E_1 = 0.70 \ E_s \ (\frac{\rho}{\rho_s}) \qquad (7.6)$$

This equation predicts a modulus which is far larger (by a factor of 50 or more) than that given by our experiments.

We think the discrepancy arises because, in deriving eqn. (7.6) we have neglected the corrugations in the cell walls. Our micrographs (Fig. 7.11) show that the corrugations fold or unfold like the bellows of a concertina, when the cork is compressed or pulled. The axial stiffness of a corrugated cell with wall thickness t and corrugation-amplitude a is derived in Appendix 7B. It is:

$$E_1 = 0.7 \ E_s \ (\frac{\rho}{\rho_s}) \ \{\frac{1}{1 + 6 \ (\frac{a}{t})^2}\} \qquad (7.7)$$

with $a \approx 3t$ (as in cork), the corrugations reduce the modulus by a factor of 50.

This deformation has another interesting feature. Axial compression produces no lateral expansion, because the cells simply fold up. We therefore expect:

$$\nu_{12} = \nu_{21} = \nu_{13} = \nu_{31} = 0 \qquad (7.8)$$

Elastic collapse in the X_1 direction seems to occur when the load is sufficient to cause buckling with a wavelength equal to twice the cell height, z. We think this is because the cooperative buckling of neighbouring cells, or of larger groups of cells, can then take place. It can easily be shown that an unsupported cell wall buckles with this wavelength when:

$$\sigma_1^* = \frac{\pi^2 z}{6\sqrt{3}\ \ell\ (1 + 2z/3\ell)^3}\ E_s\ \left(\frac{\rho}{\rho_s}\right)^3 \qquad (7.9)$$

$$\approx 0.05\ E_s\ \left(\frac{\rho}{\rho_s}\right)^3$$

Comparison of Experiment with Theory

The properties of ρ_s and E_s of the cell walls of cork are discussed in Appendix 7A. Our best estimates are:

$$\rho_s = 1150\ \text{kg/m}^3$$

$$E_s = 9\ \text{GN/m}^2$$

Using this information, and the dimensional data given in Table 7.1, we calculate the moduli for cork given in Table 7.3.

<u>TABLE 7.3: MODULI AND COLLAPSE STRESSES</u>

MODULI			CALCULATED	MEASURED
E_1	(MN/m^2)	(Eqn. 7.7)	20	20 ± 7
E_2, E_3	(MN/m^2)	(Eqn. 7.2)	15	13 ± 5
G_{12}, G_{21}, G_{13}, G_{31}	(MN/m^2)	($-$)	($\sim$)	2.5 ± 1
G_{23}, G_{32}	(MN/m^2)	(Eqn. 7.3)	4	4.3 ± 1.5
ν_{12}, ν_{13}, ν_{21}, ν_{31}		(Eqn. 7.8)	0	0 ± 0.05
$\nu_{23} = \nu_{32}$		(Eqn. 7.4)	1.0	0.5 ± 0.05
COMPRESSIVE COLLAPSE STRESS				
σ_1^*	(MN/m^2)	(Eqn. 7.9)	0.75	0.8 ± 0.2
σ_2^*, σ_3^*	(MN/m^2)	(Eqn. 7.5)	1.5	0.7 ± 0.2

Agreement is remarkably good. In particular, our understanding of the cork structure allows us to explain the isotropy in the plane normal to the radial direction; the factor of two difference between Young's modulus in the radial direction and in the other two; the striking difference in the values of Poisson's ratio; and the elastic collapse load. The biggest discrepancy is in the value of Poisson's ratios ν_{23} and ν_{32}, and is probably due to a variation in cell shape and orientation.

We may now formulate a complete constitutive law for the linear elastic behaviour of cork (see also Appendix 7C). It is described by:

$$\varepsilon_{11} = \frac{1}{E_1} \sigma_{11}$$

$$\varepsilon_{22} = \frac{1}{E_2} \sigma_{22} - \frac{\nu_{23}}{E_2} \sigma_{33}$$

$$\varepsilon_{33} = -\frac{\nu_{23}}{E_2} \sigma_{22} + \frac{1}{E_2} \sigma_{33}$$

$$\gamma_{23} = \frac{1}{G_{23}} \sigma_{23}$$

$$\gamma_{31} = \frac{1}{G_{12}} \sigma_{31}$$

$$\gamma_{12} = \frac{1}{G_{12}} \sigma_{12}$$

Here σ_{11}, ε_{11} etc. are the normal stresses and strains and σ_{23}, γ_{23} etc. are the shear stresses and engineering shear strains. The moduli themselves are given in the last column of Table 7.3.

7.6 Applications

For at least 2000 years, cork has been used (among other things) for "floats for fishing nets, and bungs for bottles, and also to make the soles for womens' winter shoes" (Pliny, 77). Few materials have such a long history or have survived so well the competition from man-made substitutes. We now examine briefly how the special structure of cork has suited it so well to its uses.

Bungs for Bottles and Gaskets for Woodwind Instruments

Connoisseurs of wine agree that there is no substitute for corks made of cork. Plastic corks are hard to insert and remove; they do

not always give a very good seal; and they may contaminate the wine. Cork corks are inert, easy to insert and remove and seal well over a large surface area for as long as the wine need be kept. The excellence of the seal is a result of the elastic properties of the cork. It has a low Young's modulus (E); but, much more important, it has a low bulk modulus (K) also. Solid rubber and solid polymers above their glass transition temperature have a low E but a large K, and it is this that makes them hard to force into a bottle, and which gives a poor seal when they are inserted.

One might expect that the best seal would be obtained by cutting the axis of the cork parallel to the prism axis of the cork cells: then the circular symmetry of the cork and of its properties are matched. And this idea is correct: the best seal is obtained by cork cut in this way. But natural cork contains *lenticels:* tubular channels that connect the outer surface of the bark to the inner surface, allowing oxygen into, and CO_2 out from the new cells that grow there. A glance at Fig. 7.4 shows that the lenticels lie parallel to the prism axis, and that a cork cut parallel to this axis will therefore leak. This is why almost all commercial corks are cut with the prism axis (and the lenticels) at right angles to the axis of the bung.

A way out of this problem is shown in Fig. 7.13. The base of the cork, where sealing is most critical, is made of two discs cut with the prism axis (and lenticels) parallel to the axis of the bung itself. The leakage-problem is overcome by gluing the two discs together so that the lenticels do not connect. Then the cork, when forced into the bottle, is compressed (radially) in the plane in which it is isotropic, and it therefore exerts a uniform pressure on the inside of the neck of the bottle.

Fig. 7.13 A section through a champagne cork, and through a normal cork.

Cork makes good gaskets for the same reason that it makes good bungs: it accommodates large elastic distortion and volume change, and its closed cells are impervious to water and oil. Thin sheets of cork are used, for instance, for the joints of woodwind and brass instruments. The sheet is always cut with the prism axis (and lenticels) normal to its plane. The sheet is then isotropic in its plane, and this may be the reason for so cutting it. But it seems more likely that it is cut like this because Poisson's ratio for compression down the prism axis is zero. Then, when the joints of the instrument are mated, there is no tendency for the sheet to spread in its plane and wrinkle.

Friction for Shoes and Floor Covering

Manufacturers who sell cork flooring sometimes make the remarkable claim that it retains its friction, even when polished or covered with soap. Fig. 7.14 shows our measurements of the coefficient of friction of a rough slider on a cork surface, before and after applying a generous coating of soapy water. The figure shows two novel features: the coefficient of friction increases with the load, violating Amontons' Law (Amontons, 1699); and it is changed only very little by the soap.

Friction between a shoe and a cork floor has two origins (Fig. 7.15). One is *adhesion*: atomic bonds form between the two contacting surfaces, and work must be done to break and reform them if the shoe slides. Between a hard slider and a tiled or stone floor, this is the only source of friction; and since it is a surface effect, it is completely destroyed by a film of polish or soap. The other source of friction is due to *anelastic loss*. When a rough slider moves on a cork floor, the bumps on the slider deform the cork. If cork were perfectly elastic, no net work would be done: the work done in deforming the cork would be recovered as the slider moves on. But if the cork has a high loss coefficient (as it
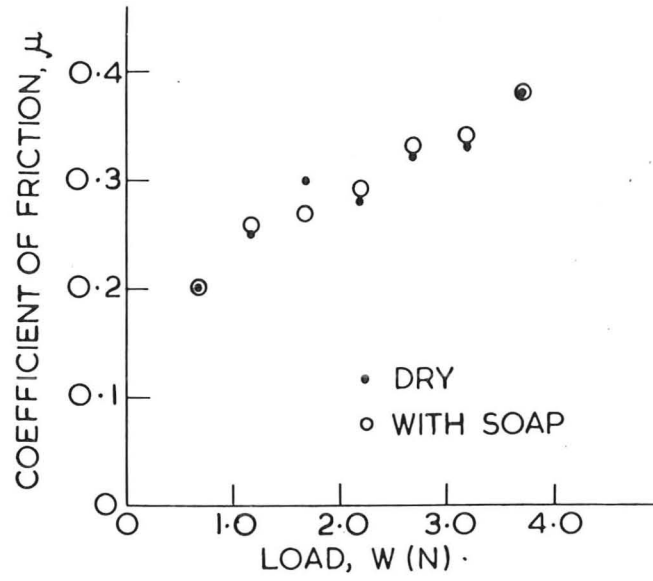
Fig. 7.14 The coefficient of friction of a rough slider on cork, dry and with soap solution.
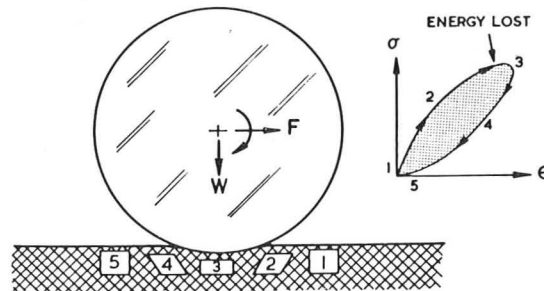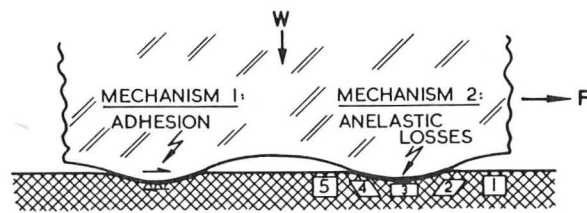
Fig. 7.15 Adhesive and anelastic mechanisms of friction.

does) then it is like riding a bicycle through sand: the work done in deforming the material ahead of the slider is not recovered as the slider passes on, and a large coefficient of friction appears. This anelastic loss is the main source of friction when rough surfaces slide on cork; and since it depends on processes taking place below the surface, not on it, it is not affected by films of polish or soap. Exactly the same thing happens when a cylinder or sphere rolls on cork (Fig. 7.15), which therefore shows a high coefficient of rolling friction.

Energy Absorption and Packaging

Many of the uses of cork depend on its capacity to absorb energy. Cork is attractive for the soles of shoes and flooring because, as well as having good frictional properties, it is resilient under foot, absorbing the shocks of walking. It makes good packaging because it compresses on impact, limiting the stresses to which the contents of the package are exposed. It is used as handles of tools to insulate the hand from the impact loads applied to the tool. In each of these applications it is essential that the stresses generated by the impact are kept low, but that considerable energy is absorbed.

Cellular materials are particularly good at this. The stress-strain curve for cork (Fig. 7.7) shows that the collapse stress of the cells (eqn. 7.5 and Table 7.2) is low, so that the peak stress during impact is limited. And large compressive strains are possible, absorbing a great deal of energy as the cells progressively collapse. In this regard, its structure and properties resemble polystyrene foam, which has replaced cork (because it is cheap) in many packaging applications.

Insulation

The cork tree is thought to surround itself with cork to prevent loss of water in hotter climes. The two properties involved - low thermal conductivity and low permeability to water - make it an excellent material for the insulation of cold, damp, habitations. Caves fall into this category: the hermit caves of Southern Portugal, for example, are liberally lined with cork. For the same reasons, crates and boxes are sometimes lined with cork. And the cork tip of a cigarette must appeal to the smoker because it insulates (a little) and prevents the tobacco getting moist.

Not a great deal is known about heat flow through cellular materials. Flow by conduction depends only on the amount of solid in the foam (ρ/ρ_s) and so it does not depend on the cell size (Traeger, 1967). Flow by convection does depend on the cell size (Fig. 7.16), because convection currents start easily in large cells, carrying heat from one side of the cell to the other. But when cells are less than about 1 mm in size, convection does not contribute significantly (Baxter and Thomas, 1972). Flow by radiation, too, depends on cell size: the smaller the cells, the more times the heat has to be absorbed and reradiated, and the lower is the rate of flow (Baer, 1964).

So the small cells are an important feature of cork. They are very much smaller than those in any foamed plastic (Table 7.1), and give exceptional insulating properties to the material.

Indentation and Bulletin Boards

Cellular materials densify when they are indented; the requirement that volume is conserved, so important in solving indentation
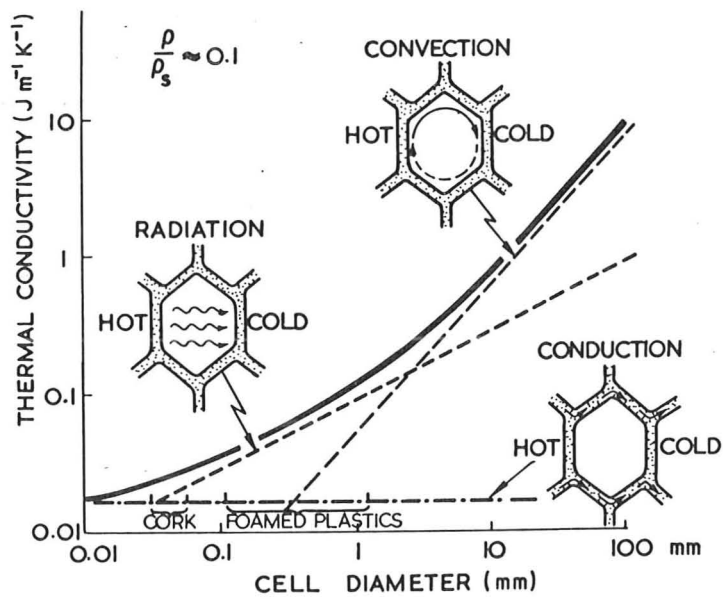
Fig. 7.16   Heat transmission through cellular solids.   Cork has cells
which are smaller than those in commercial foamed plastics.
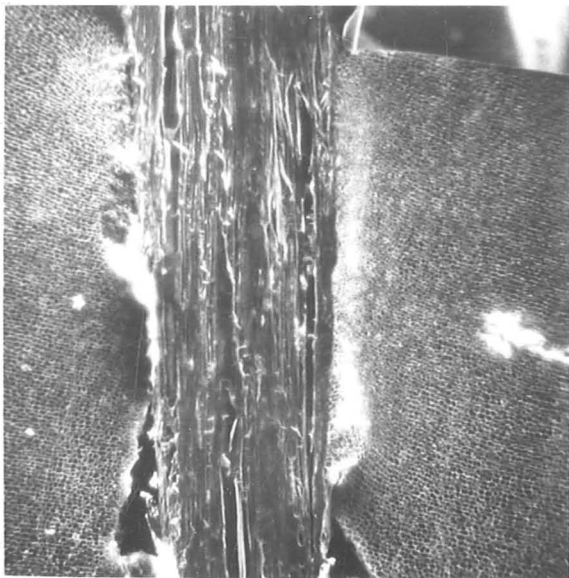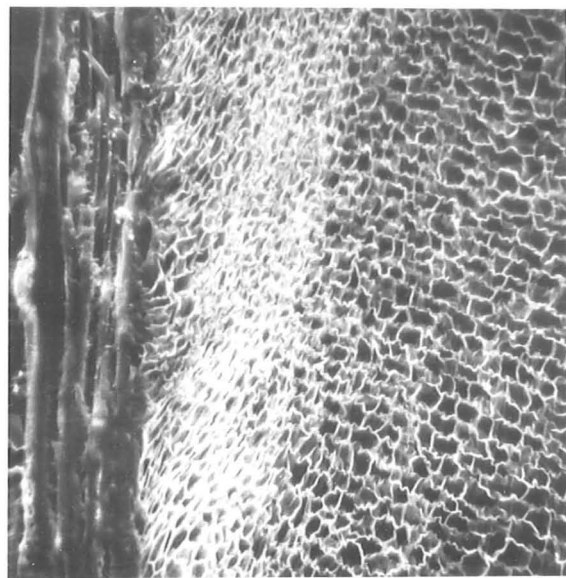
Fig. 7.17   An indenter, forced into cork.   The cells have collapsed in a
thin layer surrounding the indenter; elsewhere they are undeformed.

problems for fully dense solids, no longer applies. So when a sharp object, like a drawing pin, is stuck into cork, the deformation is very localised (Fig. 7.17). A layer of cork cells, occupying a thickness of only about one quarter of the diameter of the indenter, collapses, suffering a large strain. The volume of the indenter is taken up by the collapse of the cells so that no long range deformation is necessary. For this reason the force needed to push the indenter in is small. And, since the deformation is (non-linear) elastic, the hole closes up when the pin is removed.

7.7 Conclusions

We have found that the cells in cork can be described as roughly hexagonal prisms. The elastic behaviour of cork in the plane normal to the prism axis can be described quite well using the theory developed in Chapter 3 for the mechanics of regular, two-dimensional cellular materials. The behaviour of cork in the plane parallel to the prism axis has been calculated using techniques similar to those of Chapter 3; there is also good agreement between these calculations and the observed behaviour. Because of this understanding of the structure and mechanics of cork, based on the mechanics of idealized two-dimensional cellular materials, we can now explain why cork is such a suitable material for many of its applications.

APPENDIX 7A: THE PROPERTIES OF THE CELL WALL OF CORK

Values for the density and Young's modulus of the cork cell wall, ρ_s and E_s respectively, have been estimated by taking the weighted mean of the densities and Young's moduli of its components. The results are:

$$\rho_s = 1150 \text{ kg/m}^3$$

and

$$E_s = 8.9 \text{ GN/m}^2$$

Our estimate of ρ_s is consistent with the observation of Kelvin (1890) who observed that a cork cube immersed in water sank when a pressure of 20 atmospheres was applied to the water.

TABLE 7A.1: PROPERTIES OF CORK CELL WALL

CONSTITUENT	% of cork cell wall	s.g.	E (GN/m^2)	m.p. ($^\circ$C)
Suberin	40	.90[2]	9.0[3]	102[4]
Cerin, friedelin and wax	5	.85–1.00[5]	9.0[3]	60–95[5]
Lignin	27	1.4[6]	2.0[6]	–
Cellulose	12	1.5[6]	25.0[6]	–
Tannin	6	1.00[7]	5.0[7]	–
Glycerine	6	1.26[8]	4.7[3]	18[8]
Ash (Na, K, Mg)	4	.12[8]	18[9]	–

Notes

1. Guillemonat, A. (1960) Ann. Fac. Sci. Marseille 30, 43; Martin, J.T. and Juniper, B.E. (1970), "The Cuticles of Plants", Arnold, London, p.151.

2. Fatty acids generally have a specific gravity of approximately 0.92.

3. E for suberin, cerin wax and glycerine were calculated from a melting point correlation.

4. Dibrucine salt of suberic acid has a melting point of 102 $^{\circ}$C. From: Dictionary of Organic Compounds v.4 (1965) Eyre and Spottiswade, London.

5. Eshbach, O. (1952) Handbook of Engineering Fundamentals, Wiley, N.Y., 2nd ed., p.13-85.

6. Mark, R.E. (1967) "Cell Wall Mechanics of Tracheids", Yale University Press. New Haven, Conn.

7. Values for specific gravity and Young's modulus for tannin were unobtainable. We estimate these values to be similar to those for suberin and cerin.

8. Clark, J.B. (1957) Physical and Mathematical Tables, Oliver and Boyd, Edinburgh.

9. Kaye, G.W.C. and Laby, T.H. (1973) Tables of Physical and Chemical Constants, 14th ed., Longman, London.

APPENDIX 7B: THE AXIAL STIFFNESS OF A CORRUGATED TUBE

Fig. 7B.1 shows a section of a tube with hexagonal section and height λ. If the tube is straight, an axial load produces an axial shortening δ_a due to straightforward compression. Considering one wall of the tube, of section $t\ell$, carrying an end-load P, we have:

$$\frac{P}{t\ell} = E_s \frac{\delta_a}{\lambda}$$

from which

$$\delta_a = \frac{\lambda P}{t\ell\, E_s} \qquad (7B.1)$$

Consider now the corrugated wall. For a load P so small that the laterial deflection does not increase significantly (so that the constraints exerted by one wall on its neighbours can be neglected), the moment M at the point X is:

$$M = Pa \, \sin \frac{2\pi X}{\lambda}$$

The strain energy of bending in the wall is:

$$U_M = \int_0^\lambda \frac{M^2}{2EI} \, dx \qquad (7B.2)$$

$$= \frac{3P^2 \, a^2 \, \lambda}{E_s \, \ell t^3}$$
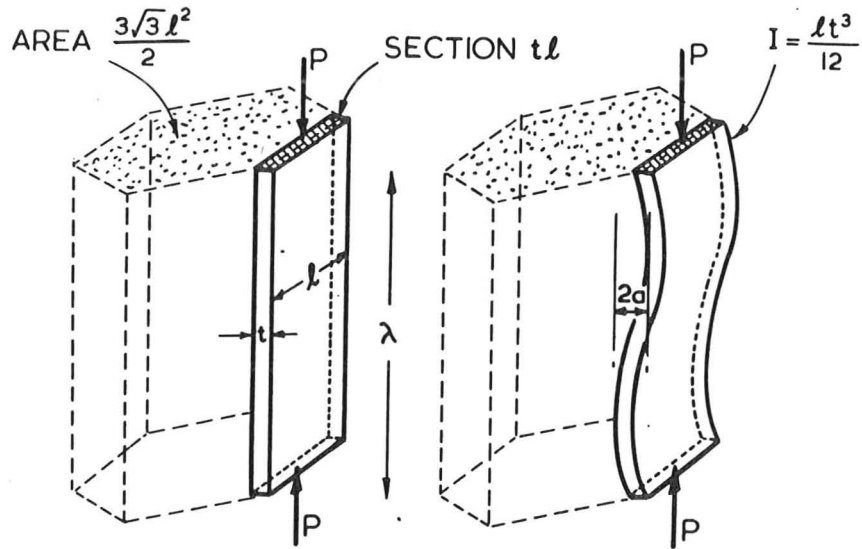
Fig. 7B.1   Young's modulus for a corrugated hexagonal prism, loaded down the prism axis.

This is equal to the work $\frac{1}{2} P\delta_b$ done by P in producing an axial displacement δ_b, caused by bending. The total deflection of the wall is then:

$$\delta^{TOT} = \delta_a + \delta_b = \frac{P\lambda}{t\ell\, E_s} \left(1 + 6 \frac{a^2}{t^2}\right) \qquad (7B.3)$$

Now a uniform stress σ applied to the end face of the hexagon gives a load P per wall of:

$$P = \frac{\sqrt{3}\, \ell^2\, \sigma}{2}$$

and a deflection δ^{TOT} over a length λ corresponds to a strain

$$\varepsilon = \frac{\delta^{TOT}}{\lambda}$$

from which the modulus of the corrugated hexagons is:

$$E_1 = \frac{2t\, E_s}{\sqrt{3\ell}\, \left(1 + 6 \frac{a^2}{t^2}\right)} \qquad (7B.4)$$

Finally, using $\rho/\rho_s = t/\ell\, (\ell/2 + 2/\sqrt{3})$ we obtain:

$$E_1 = 0.7 \frac{E_s}{\left(1 + 6 \frac{a^2}{t^2}\right)} \left(\frac{\rho}{\rho_s}\right) \qquad (7B.5)$$

APPENDIX 7C: THE MODULI OF CORK

The observations reported in Sections 7.3 and 7.4 show that both the structure and properties of cork are approximately axisymmetric. The linear-elastic behaviour is described by:

$$\varepsilon_{k\ell} = S_{ijk\ell} \, \sigma_{ij} \qquad (7C.1)$$

where $\varepsilon_{k\ell}$ and σ_{ij} are the strain and stress tensors. Axisymmetry reduces the number of independent compliances S to five.

$$
\begin{aligned}
\varepsilon_{11} &= S_{1111} \, \sigma_{11} + S_{1122} \, \sigma_{22} + S_{1122} \, \sigma_{33} \\[2mm]
\varepsilon_{22} &= S_{1122} \, \sigma_{11} + S_{2222} \, \sigma_{22} + S_{2233} \, \sigma_{33} \\[2mm]
\varepsilon_{33} &= S_{1122} \, \sigma_{11} + S_{2233} \, \sigma_{22} + S_{2222} \, \sigma_{33} \\[2mm]
\varepsilon_{23} &= 2 \, (S_{2222} - S_{2233}) \, \sigma_{23} \\[2mm]
\varepsilon_{31} &= 2 \, S_{1212} \, \sigma_{31} \\[2mm]
\varepsilon_{12} &= 2 \, S_{1212} \, \sigma_{12}
\end{aligned}
\qquad (7C.2)
$$

(The equation for ε_{23} is obtained by rotating $S_{ijk\ell}$ through 45° about the X_1 axis and equating S'_{2222}, in the new axis set, to S_{2222}.)

The measurement of four of these compliances is straightforward: cubes are cut with faces normal to the axial, radial and tangential directions (Fig. 7.4), and Young's modulus and Poisson's ratio measured

by conducting simple tensile or compression tests parallel to each
axis in turn. Form these tests we obtain:

$$\frac{1}{E_1} = S_{1111}$$

$$\frac{1}{E_2} = \frac{1}{E_3} = S_{2222}$$

$$\frac{\nu_{12}}{E_1} = \frac{\nu_{13}}{E_1} = \frac{\nu_{21}}{E_2} = \frac{\nu_{31}}{E_2} = -S_{1122}$$

$$\frac{\nu_{23}}{E_2} = \frac{\nu_{32}}{E_2} = -S_{2233}$$

(7C.3)

The modulus G_{23} in the $X_2 X_3$ plane is obtained from these
measurements:

$$\frac{1}{G_{23}} = \frac{2(1 + \nu_{23})}{E_2} = 2(S_{2222} - S_{2233}) \qquad (7C.4)$$

To determine the other shear modulus, G_{12}, we rotate the cork through
45° about the X_3 axis, to cut a cube with one face normal to X_3,
and the other two at 45° to X_1 and X_2. A simple compression test
in the new X_1 direction then gives a new Young's modulus, E'. By
rotating $S_{ijk\ell}$ through 45° about X_3, we find:

$$S'_{1111} = \tfrac{1}{4} S_{1111} + \tfrac{1}{4} S_{2222} + \tfrac{1}{2} S_{1122} + \tfrac{1}{2} S_{1212} \qquad (7C.5)$$

But this is simply $1/E'$. Substituting for this and the other

compliances and noting that:

$$G_{12} = G_{21} = G_{13} = G_{31} = \frac{1}{2\ S_{1212}} \qquad (7C.6)$$

we obtain $$\frac{1}{G_{12}} = \frac{4}{E'} - \frac{(1 - 2\ \nu_{12})}{E_1} - \frac{1}{E_2} \qquad (7C.7)$$

which correctly reduces to $G = E/2\ (1 + \nu)$ for the isotropic case.

For cork the equation is further simplified because $\nu_{12} = 0$. This

is the equation we have used to obtain G_{12} from experimental mea-

surements of E', E_1 and E_2.

CHAPTER 7 - REFERENCES

Amontons (1969) Histoire de l'Académie Royale des Sciences avec les Mémoires de Mathématique et de Physique, p.206.

Baer, E. (1964) "Engineering Design in Plastic", Van Nostrand Reinhold, New York, Ch. 15, p.1027.

Baxter, S. and Jones, T.T. (1972) Plastics and Polymers, 40, 69.

Cooke, G.B. (1948) Econ. Bot. 2, 393.

Eames, A.J. and MacDaniels, L.H. (1951) "An Introduction to Plant Anatomy", McGraw-Hill, London.

Esau, K.E. (1965) "Plant Anatomy", Wiley, p.340.

Euler (1752) Novi Commentarii Academiae Scientiarum Petropolitanae 4, 109. (Opera (1), 26, 71, 1758).

Fernandez, L.V. (1978) Inst. Nac. Invest. Agrar. Madrid, Spain, No. 6, p.7.

Hooke, R. (1664) "Micrographia", The Royal Society, p.112.

Horace, Q. (27 B.C.) Odes Book III, Ode 8, line 10.

Kelvin, Lord (1890) Mathematical and Physical Papers, Vol. III, Cambridge University Press, p.19.

Lewis, F.T. (1928) Science 68, 635.

Pepys, S. (1666) The Diary of Samuel Pepys (July 14, 1666), ed. by Henry B. Wheatley, G. Bell and Sons Ltd., London, 1952, Vol. V, p.342.

Pliny (77) Natural History, 16.34.

Plutarch (100) Parallel Lives, II, XXV, 154, Life of Camillus.

Traeger, R.K. (1967) Jnl. of Cellular Plastics, 3, 405.

Zimmerman, M.H. and Brown, C.L. (1971) "Trees Structure and Function", Springer, p.88.

CHAPTER 8

ON MATERIAL SELECTION IN PACKAGING

8.1 Introduction

Packaging surrounds most things we buy or do. Food is packaged,
parcels through the post are packaged, and within a car or aeroplane,
we ourselves are carefully packaged. It is hard to say exactly how
much is spent on it (estimates suggest that up to 20 % of retail
costs are those of the packaging). The sums involved are certainly
considerable (Morton, 1978) and the potential return on any improve-
ment is large.

Despite this, scientists have paid little attention to packaging,
except perhaps where human safety is concerned (Pinkel, 1960). Although
most large firms have a packaging department, it is more concerned with
wrapping things up than in optimising the package. The type and amount
of packaging material is often traditional, chosen with little regard
for the mechanics of the problem. Eggs, for instance, are sometimes
marketed in clear plastic egg boxes of roughly the same shape as the
more familiar cardboard ones. Handlers suggest that eggs, so packaged,
break more often. This may just be prejudice against a new technology,
but if it is not, then one material has been substituted for another
with no regard for material properties, in an application which calls
for properly chosen protection. Such a lack of analysis is typical
of much packaging.

Why, then, does the packaging industry neglect the mechanics of
the problem it faces? The answer may lie in the complexity of the
packaging process. The package must protect against drop, impact,
puncture, crushing when stacked and contamination by air, water or
other chemicals. And it must attract potential buyers by its aesthetic
appeal. Consider, for instance, the job of protecting a given component

CHAPTER 8

ON MATERIAL SELECTION IN PACKAGING

8.1 Introduction

against being dropped. To design against damage, three things must be known: (a) the height and frequency of drops, (b) the maximum deceleration the component can survive, and (c) the properties of the material to be used for the package.

Limited data for the first of these are available (B.S. 1133, Allen, 1972) from instrumented packages dispatched by post and by other transport systems. When the drop height is well specified (as in Army supply drops) the package can be chosen for minimum weight and cost with success, but for the most part, such information is not available.

The maximum tolerable deceleration is rarely known. For most objects it is high: even a very fragile thing can sustain 10 g, provided the package spreads the force evenly over its surface.

The third area, that of material response to load, is studied experimentally, but usually in a way which ignores the mechanics of the package.

There is, of course, a further consideration: cost. A package so perfect that no component ever breaks is, almost always, too expensive. Some loss must be lived with, and its cost in financial terms and in terms of customer frustration must be balanced against the cost of the package itself.

8.2 Simple Theory

The material property currently used in package design is the *cushion factor* ϕ (Gordon, 1974). It is a dimensionless quantity, defined, at a given stress, as the stress divided by the energy

absorbed per unit volume in reaching that stress (i.e. the area under the stress-strain curve up to the stress in question). Fig. 8.1 shows the cushion factor for 3 materials, plotted against stress. If C were constant (which, as Fig. 8.1 shows, it is not) and independent of strain and strain-rate, then it is easily shown that the maximum deceleration, $\ddot{y}_{max}$, when a component, packaged in a thickness S of packaging, falls from height h, is:

$$\ddot{y}_{max} = \frac{\phi h}{S} g \qquad (8.1)$$

where g is the acceleration due to gravity and dots mean differentiation with respect to time.

Eqn. (8,1), the basis of much package design, suggests that a single material parameter, ϕ, contains all the material properties of importance in selecting materials for a package. But in deriving it, the damping capacity and rate-dependence of the material have been ignored. Worse, the cushion factor varies with stress and there is no way of knowing from eqn. (8.1) what stress (and thus what cushion factor) is appropriate.

To improve on it, the package must be modelled as a mass-spring-dashpot system (Fig. 8.2). Its equation of motion is:

$$M\ddot{y} + C\dot{y} + f(y) = 0 \qquad (8.2)$$

where y is measured as shown in Fig. 8.2, M, is the mass of the component (neglecting the self-mass of the packaging material), C is the damping coefficient and f(y) is the restoring force due to the spring.
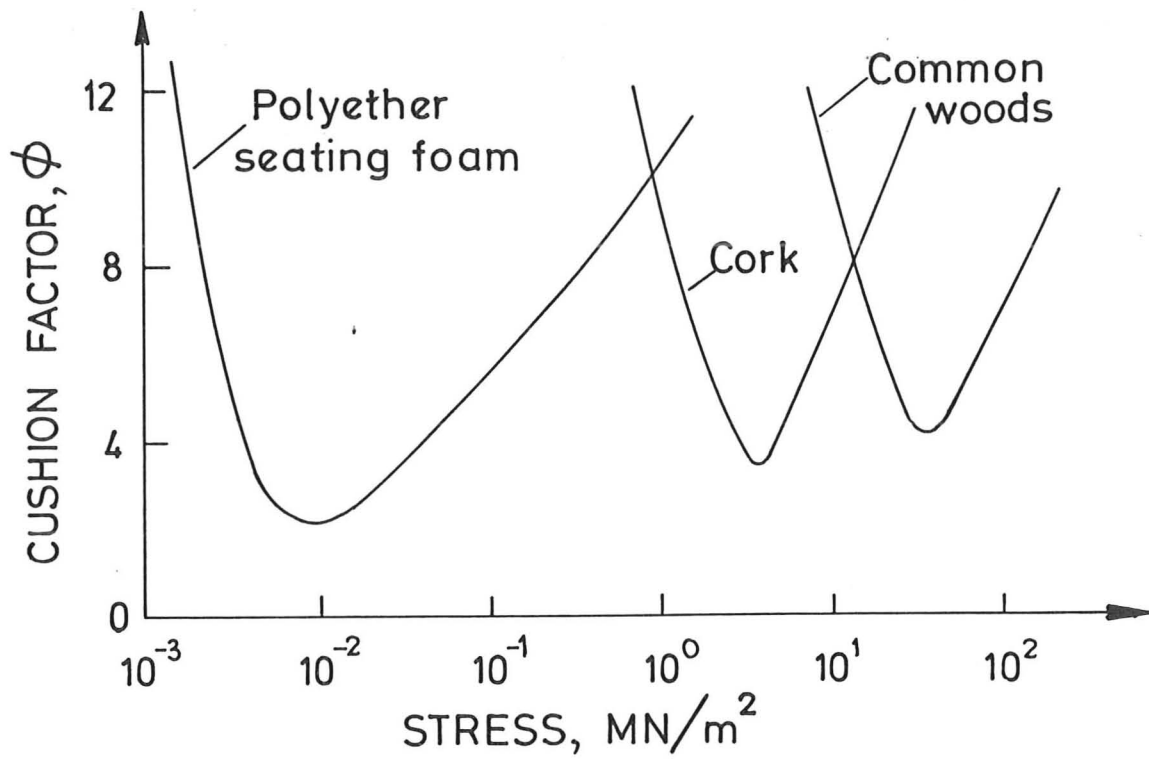
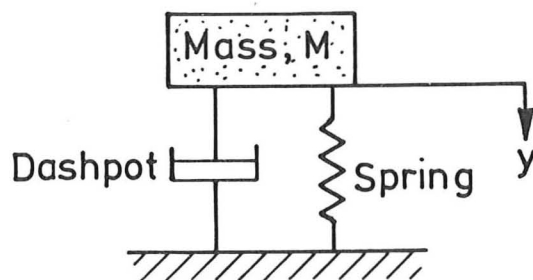Fig. 8.1 Cushion factor for various cellular materials.

Fig. 8.2 Mass-spring-dashpot model of a packaged object.

To solve this equation, $f(y)$ must be specified. The stress-strain curves of cellular solids (foamed polymers, cork, balsa wood and so forth) all look more or less like that shown in Fig. 8.3. It can be idealised in one of two ways. At small strains ($\varepsilon < 0.1$) it is *linear elastic* (Fig. 8.4a) when $f(y) = Ky$ where K is a spring constant (units: N/m). But at larger strains ($0.1 < \varepsilon < 0.6$) there is a *non-linear elastic* or *plastic* plateau extending to a limiting strain ε_{max}, above which the stress rises steeply (Fig. 8.4b); then $f(y) = K_o$ where K_o is constant (units: N).

(a) Linear-Elastic Response

When $f(y) = Ky$, the appropriate solution for eqn. (8.2), with $y = 0$ at $t = 0$ is:

$$y = \frac{V_o}{\omega} \exp\left(-\frac{Ct}{2M}\right) \sin\omega t \qquad (8.3)$$

where

$$V_o = \text{velocity on impact} = \sqrt{2gh} \qquad (8.4)$$

$$\omega = \text{frequency of vibration} = \left(\frac{K}{M} - \frac{C^2}{4M^2}\right)^{\frac{1}{2}} \qquad (8.5)$$

and t is the time after impact.

The log decrement of the peak amplitude of successive cycles, Δ, can be related to the *loss coefficient* η of the material (the most widely used measure of damping and hysteresis in engineering materials). Provided η is small ($\eta < 0.5$), the relation is:

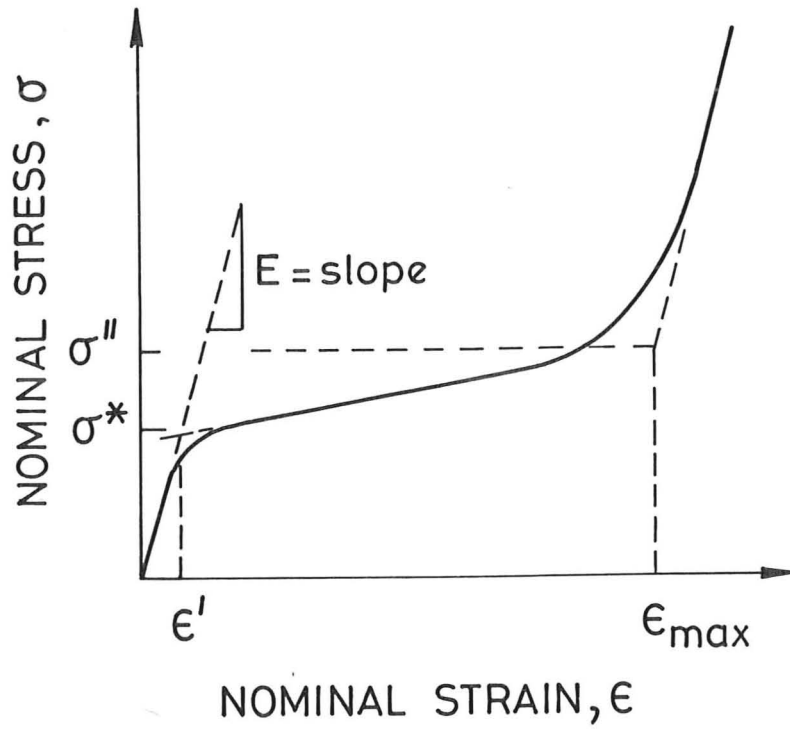$$\Delta = \frac{C\tau}{2M}$$

$$= \pi\eta$$

Fig. 8.3 Stress-strain curve for a flexible polyurethane foam.
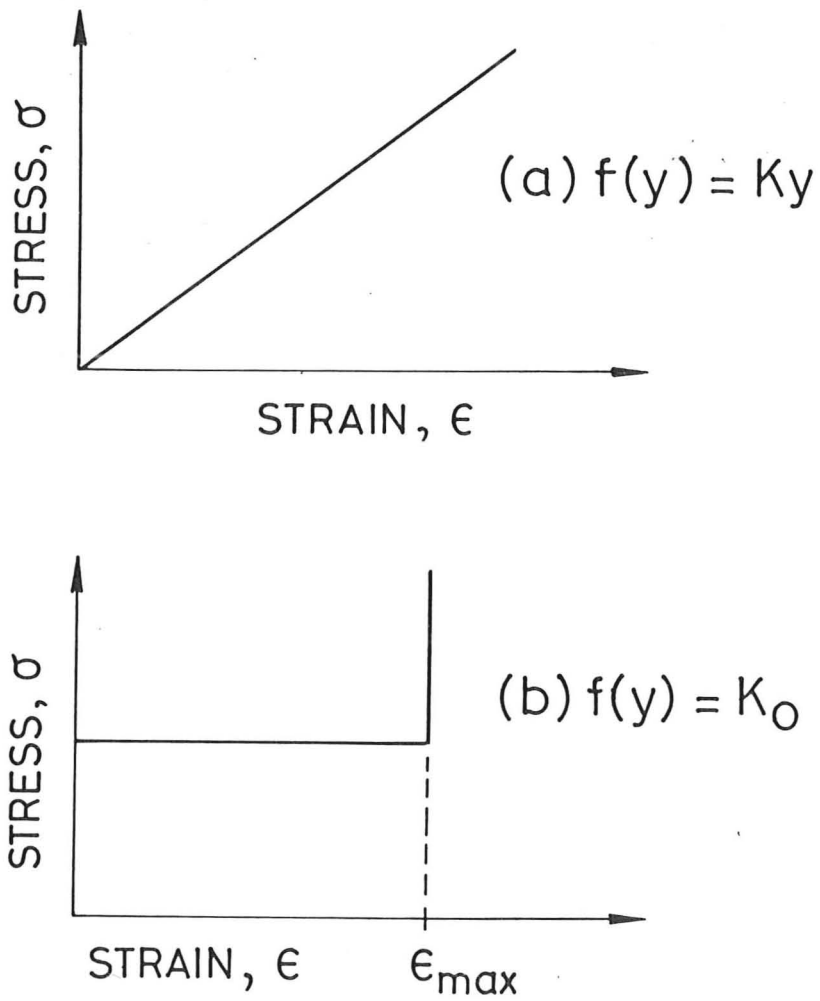
Fig. 8.4   Idealized stress-strain curves for cellular
           materials: (a) linear-elastic response and
           (b) constant stress response.

where τ is the period of oscillation. Putting $\tau = 2\pi/\omega$ we find:

$$C = M\eta\omega$$

The deceleration, $\ddot{y}$, of the component is a maximum when the curvature of y is a maximum, at $t = \tau/4 = \pi/2\omega$. The maximum value is then:

$$\ddot{y}_{max} = \frac{V_o}{\omega} \left(\frac{C^2}{4M^2} - \omega^2\right) \exp \left(- \frac{\pi C}{2M\omega}\right)$$

Substituting $C = M\eta\omega$ and $\omega = (K/M - C^2/4M^2)^{\frac{1}{2}}$ we find:

$$\ddot{y}_{max} = - V_o \left(\frac{K}{M}\right)^{\frac{1}{2}} \left(\frac{1}{1 + \frac{\eta^2}{4}}\right)^{\frac{1}{2}} \left(1 - \frac{\eta^2}{4}\right) \exp \left(- \frac{\pi\eta}{2}\right)$$

For most polymers η lies between 0.01 and 1.0 (Table 8.1), making the third and fourth terms of this expression approximately equal to one. Since the spring constant K is equal to EA/S for a linear-elastic material, we obtain:

$$\ddot{y}_{max} = V_o \left(\frac{EA}{MS}\right)^{\frac{1}{2}} \exp \left(- \frac{\pi\eta}{2}\right) \tag{8.7}$$

The maximum stress exerted by the packaging on the mass, σ_{max}, is:

$$\sigma_{max} = \frac{\ddot{y}_{max} M}{A} \tag{8.8}$$

This is also equal to the stress in the foam. Noting that the strain energy in the foam, per unit volume, is:

Table 8.1: Loss Coefficient Data for Polymers

Polymer	Frequency of vibration, f (Hz)	Loss coefficient η	Temperature ($^\circ$C)	Peak loss coefficient η_{peak}
Perspex (50 Leth, 66L)	0.0033 to 800	3.76×10^{-2} to 5.0×10^{-2}	25 $^\circ$C	6.36×10^{-2} at f = 10 Hz
Polyethylene (51 U)	12		30–80	0.23
Polyester (55 Be)	10 100 1000 10000	2.86×10^{-2} 2.00×10^{-2} 2.25×10^{-2} 2.60×10^{-2}	43	–
PMMA (54 Fine, 66L)	0.001 to 400	2.14×10^{-2} to 1.96×10^{-2}	25	2.4×10^{-2} at f = 50 Hz
Polypropylene (59 Boh)	10 100 1000	9.47×10^{-2} 1.31×10^{-1} 1.65×10^{-1}	20	–
Polystyrene (56 Maxω, 66L)	0.001 to 100	1.0×10^{-2} to 1.96×10^{-2}	–	1.96×10^{-2}

Data has been taken from Lazan (1968), p.234–238. See also Figs. 8.2 and 8.4 (Lazan, 1968). The brackets refer to Lazan's references.

$$U = \frac{Mgh}{AS} \qquad (8.9)$$

and using eqn. (8.4) we find:

$$\sigma_{max} = \sqrt{2UE} \exp \left(-\frac{\pi\eta}{2}\right) \qquad (8.10)$$

Note that as the loss coefficient, η, increases, the stress decreases: this happens for the following reason. The displacement time curve is sinusoidal (equation (8.3)) and its amplitude is related to η. As η increases, the amplitude decreases, and the maximum curvature, $\ddot{y}$, also decreases. Since $\ddot{y}$ is also the acceleration of the package, this also decreases, and thus the stress is reduced.

In Chapter 6 we found that:

$$E/E_s \propto (\rho/\rho_s)^2$$

where E_s is the modulus of the solid polymer of which the foam is made, and (ρ/ρ_s) is its relative density. The result describes well the measured moduli of a wide range of foamed plastics. Substituting into eqn. (8.10) gives:

$$\sigma_{max} = (\rho/\rho_s) \sqrt{2U} \exp \left(-\frac{\pi\eta}{2}\right) \qquad (8.11)$$

It is of interest to know the maximum deceleration possible while the foam remains linear-elastic. As a general rule, linear elasticity extends to a strain of roughly 0.1, when the stress reaches the collapse stress σ^* (Fig. 8.3). Thus:

$$(U_{max})_{linear} = \tfrac{1}{2} \sigma^* \varepsilon \qquad (8.12)$$
$$= 0.05 \sigma^*$$

Inserting the value for U gives:

$$\sigma_{max} = \sqrt{0.1 \sigma^*} (\rho/\rho_s) \exp \left(-\frac{\pi\eta}{2}\right)$$

We have also analysed and measured the elastic and plastic collapse stresses of foamed solids. The results from Chapter 6 (which again give a good description of a large body of experimental data) are:

$$\frac{\sigma_{el}^*}{E_s} = 0.05 \ (\rho/\rho_s)^2 \tag{8.14}$$

and

$$\frac{\sigma_{pl}^*}{\sigma_y} = 0.30 \ (\rho/\rho_s)^{\frac{3}{2}} \tag{8.15}$$

where (σ_y) is the yield strength of the solid polymer. Substituting into eqn.(8.13) gives the maximum stress exerted on the component by the package as:

$$(\sigma_{max})_{el} = 0.07 \ E_s \ (\rho/\rho_s)^2 \ \exp \ (-\frac{\pi\eta}{2}) \tag{8.16}$$

$$(\sigma_{max})_{pl} = 0.17 \ \sigma_y \ (\rho/\rho_s)^{\frac{7}{4}} \ \exp \ (-\frac{\pi\eta}{2}) \tag{8.17}$$

(b) *Non-Linear Elastic Response*

A mass, M, dropped from a height, h, onto a foam with a constant stress response $f(y) = K_o$ obeys the equation:

$$M\ddot{y} + C\dot{y} + K_o = 0$$

Solutions for this equation are given in the Appendix. If the plateau responsible for K_o (Fig. 8.3) is plastic in origin, or is non-linear elastic but heavily damped $(\eta > 0.5)$, the component is overdamped and is brought smoothly to rest. If η is small, an oscillating

solution results; but in all cases the maximum deceleration is:

$$\ddot{y}_{max} = \frac{V_o \, C + K_o}{M} \qquad\qquad (8.18)$$

where $\qquad V_o$ = velocity on impact = $\sqrt{2gh}$ $\qquad\qquad (8.19)$

$$K_o = (\frac{\sigma^* + \sigma''}{2}) \, A \qquad\qquad (8.20)$$

$$C \cong \frac{\pi \, K_o \, \eta}{V_o} \qquad\qquad (8.21)$$

where σ^*, σ'' and E are shown in Fig. 8.3. If $\sigma^* \approx \sigma''$ then substituting eqns. (8.20) and (8.21) into (8.18) gives:

$$\ddot{y}_{max} = \frac{\sigma^* A}{M} \, (1 + \pi\eta) \qquad\qquad (8.22)$$

The maximum stress exerted on the component by the package is again $\sigma_{max} = \ddot{y}_{max} \, M/A$ or:

$$\sigma_{max} = \sigma^* \, (1 + \pi\eta) \qquad\qquad (8.23)$$

Substituting eqns. (8.14) and (8.15) for the elastic and plastic collapse stresses, σ^*_{el} and σ^*_{pl} gives:

$$(\sigma_{max})_{el} = 0.05 \, E_s \, (\rho/\rho_s)^2 (1 + \pi\eta) \qquad (8.24)$$

$$(\sigma_{max})_{pl} = 0.30 \, \sigma_y \, (\rho/\rho_s)^{\frac{3}{2}} (1 + \pi\eta) \qquad (8.25)$$

8.3. CONCLUSIONS

We have shown that the maximum deceleration $(\ddot{y})$ or surface stress (σ_{max}) suffered by a packaged component when dropped, can be expressed in terms of certain properties of the packaging material. By using the results of our new analysis of the mechanics of cellular materials, the surface stress can be expressed in terms of the modulus E_s and yield strength σ_y of the bulk (un-foamed)polymer, its loss coefficient η, and the relative density of the foam ρ/ρ_s.

For light handling of the package, when the packaging material remains linear-elastic, the maximum stress (for a given drop height) scales as ρ/ρ_s (eqn. 8.11). But for a heavy drop, such that the packaging is compressed into the non-linear region, the maximum stress scales as $(\rho/\rho_s)^2$ or $(\rho/\rho_s)^{\frac{3}{2}}$, depending on whether the material is non-linear elastic or plastic. These results, and the associated dependencies on the properties E_s, σ_y and η of the solid polymer (eqns. (8.16), (8.17), (8.24) and (8.25)) should help in the rational choice of packaging materials.

APPENDIX 8A: Solution of the Differential Equation for Constant

Stress Response

For the constant stress response case, the first half cycle

(for which K_o is positive):

$$M\ddot{y} + C\dot{y} + K_o = 0 \tag{8A.1}$$

It is easily shown that by letting $z = dy/dt$:

$$\frac{dz}{dt} = -\frac{C}{M}(z + \frac{K_o}{C}) \tag{8A.2}$$

The solution to this is:

$$\ln(z + K_o/C) = -\frac{Ct}{M} + A'$$

$$\tag{8A.3}$$

or

$$z = \dot{y} = A \exp(-\frac{Ct}{M}) - \frac{K_o}{C}$$

If C is small, the solution oscillates, with K_o changing sign at

$y = 0$. But if K_o is caused by plastic collapse (not non-linear

elasticity), or η, and thus C, are large, $\dot{y}$ decays exponentially

to zero. Substituting the boundary condition that at $t = 0$, $\dot{y} = V_o = \sqrt{2gh}$

gives:

$$A = V_o + K_o/C$$

and

$$\dot{y} = \frac{V_o C + K_o}{C} \exp(-\frac{Ct}{M}) - \frac{K_o}{C}$$

Differentiating

$$\ddot{y} = -(\frac{V_o C + K_o}{M}) \exp(-\frac{Ct}{M}) \tag{8A.4}$$

At $t = 0$, this is a minimum of:

$$\ddot{y} = - \left(\frac{V_o C + K_o}{M}\right)$$

(8A.5)

It is difficult to relate C to the loss coefficient η in an exact way except by solving eqn. (8A.1) with an oscillating forcing function, giving very involved results. But since η varies by a factor of 2 between two samples of the same solid polymers, and since the magnitude of the loading, mgh, is usually not well known either, an approximate solution for C is adequate.

If a block of foam with a constant stress response $K_o = \sigma^* A$ is compressed by a displacement x at constant velocity, V_o, the maximum elastic strain energy stored is:

$$W_E = K_o x$$

The viscous force is $C\dot{y}$ and the energy dissipated in moving this force through a distance x is:

$$W_V = C V_o x$$

The loss coefficient is defined as:

$$\eta = \frac{D}{2\pi U_{max}}$$

where D is the specific damping energy, or the energy lost in one cycle of load and U_{max} is the maximum strain energy during the cycle This gives:

$$\eta = \frac{2C\, V_o\, x}{2\pi\, K_o\, x} = \frac{CV_o}{\pi K_o}$$

or
$$C = \frac{\pi\, K_o\, \eta}{V_o} \qquad\qquad (8A.6)$$

$$\eta = \frac{2C \, V_o \, x}{2\pi \, K_o \, x} = \frac{CV_o}{\pi K_o}$$

or
$$C = \frac{\pi \, K_o \, \eta}{V_o} \tag{8A.6}$$

CHAPTER 8 - REFERENCES

Allen D.C. (1972) J. Soc. Env. Eng., 21-28.

British Standard 1133 (1973) "The Packaging Code", Section 20, British Standards Institute.

Gordon, G.A. (1974) Testing and Approval, Impact Strength and Energy Absorption, PIRA.

Lazan, B.J. (1968) "Damping of Materials and Members in Structural Mechanics", Ch. 8, Pergamon.

Morton, D.H. (1978) Materials in Engineering Applications, Vol. 1, 66-73.

Pinkel, I.I. (1960) Mechanical Engineering, 60-63.

CHAPTER 9

CONCLUSIONS AND FURTHER WORK

The mechanical properties of foams can be successfully analyzed using beam theory. Both two- and three-dimensional cellular materials deform by the same sets of mechanisms: the elastic moduli E, and G, are governed by the bending stiffness; the elastic collapse stress σ^*_{el} by elastic buckling; and the plastic collapse stress, σ^*_{pl}, by the development of plastic hinges in the beam-like or plate-like members which make up the cell walls.

The way in which the properties of two-dimensional cellular materials depend on cell shape and density can be described exactly. Each of the exact equations derived can be rewritten so as to relate each property (normalized in terms of an appropriate cell wall property) to a geometric constant and to the relative density raised to the power two or three. We find that: $E/E_s = C_1 (\rho/\rho_s)^3$; $G/E_s = C_2 (\rho/\rho_s)^3$; $\sigma^*_{el}/E_s = C_3 (\rho/\rho_s)^3$; and $\sigma^*_{pl}/\sigma_y = C_4 (\rho/\rho_s)^2$, where C_1 to C_4 are geometric constants which can be evaluated for a given cell shape. Poisson's ratio is independent of relative density and depends only on the cell shape. Here E_s is Young's modulus for the cell wall material, σ_y its yield strength and ρ_s its density.

Three-dimensional foams have much more complicated geometries which cannot be analyzed exactly. But we have found that a dimensional analysis (based on the results for two-dimensional cellular materials) gives results which describe well the dependence of material properties on relative density. This analysis gives: $E/E_s = C_5 (\rho/\rho_s)^2$; $G/E_s = C_6 (\rho/\rho_s)^2$; $\sigma^*_{el}/E_s = C_7 (\rho/\rho_s)^2$, and $\sigma^*_{pl}/\sigma_y = C_8 (\rho/\rho_s)^{3/2}$. Here C_5 to C_8 are

constants related to cell shape which must be evaluated experimentally. Poisson's ratio is again found to be independent of density, and depends only on cell shape. We have distinguished open and closed-celled foams in our analysis. But our experiments and analysis of published data show that the two types of foam often behave identically. This is because the cell faces of closed-cell foams are often very thin compared to the edges, and so do not contribute significantly to stiffness or strength; almost all the load is carried by the cell edges.

We have applied these results to the analysis of polymeric and natural cellular materials. The elastic and plastic properties of polymeric foams are well described by our analysis of three-dimensional cellular materials. The results are presented as a set of figures, showing how each normalised property $(E/E_s, \sigma^*_{el}/E_s$ and so forth) varies with the relative density (ρ/ρ_s) of the foam, and incorporating all the data available to us. These plots, and the equations which describe them, have application in engineering design: they provide a rational way of selecting foamed polymers for a given application. To illustrate this, we present a simple analysis of a packaging problem, and derive criteria for the selection of a foam to meet certain packaging requirements.

In a second case study, we relate the mechanical properties of a natural cellular material - cork - to its structure. Cork has a quasi-two-dimensional structure: its cells are shaped like hexagonal prisms. We found that the two-dimensional analysis described its elastic moduli and collapse stresses well.

There is a further application of this work to natural materials: it can be used to explain some of the mechanical properties of wood. We have recently studied the structure and mechanics of balsa wood (Easterling et al., 1981), and find that both the magnitude and the large anisotropy in the Young's modulus of balsa can be explained in terms of the theory developed here. When loaded across the grain, the cell walls bend, and behave according to the rule $E/E_s = C_1 (\rho/\rho_s)^3$. But when balsa is loaded along the grain, the cells are in simple axial compression, so that $E/E_s = \rho/\rho_s$. Since the relative density, ρ/ρ_s, of balsa is about 0.10, this explains the enormous difference in modulus in the two directions. An initial examination of data for other, denser, woods suggests that, as in balsa, the moduli measured across the grain are governed by the bending of cell walls, while the modulus along the grain reflects the axial compression of the cell wall material. These findings, when coupled with an understanding of the anisotropic properties of the cell wall itself (due to the lay-up of the cellulose fibres within it) give a promising approach to the analysis of the mechanics of woods.

CHAPTER 9 - REFERENCES

Easterling, K.E., Harrysson, R., Gibson, L.J. and Ashby, M.F. (1981) The Structure and Mechanics of Balsa, Cambridge University Engineering Department Report CUED/C/MATS/TR.81.